CHALMERS

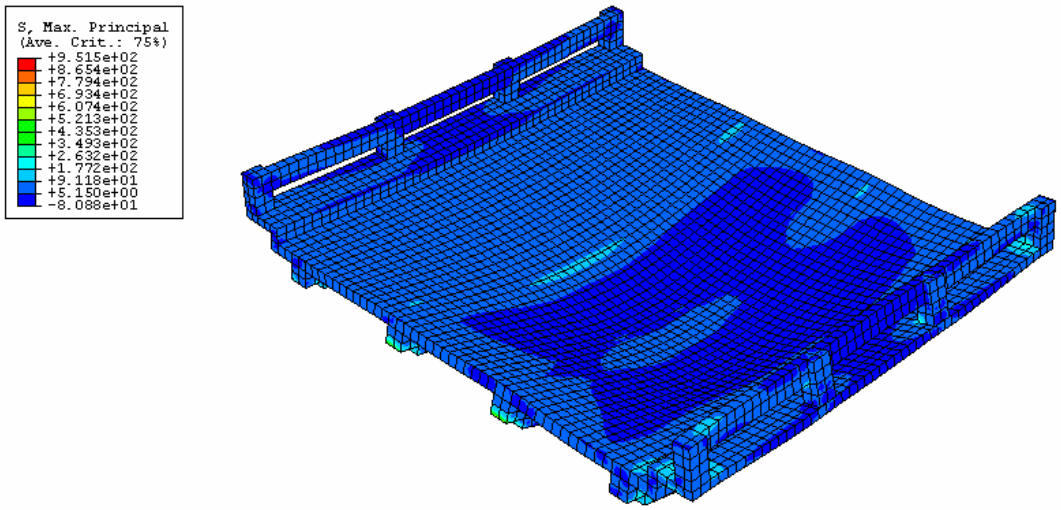

FE Modeling of FRP Strengthening Systems on the White Bayou Bridge

Master's Thesis in the International Master's Programme in Structural Engineering

JOSÉ ALBERTO ANCA PEREIRA

Department of Civil and Environmental Engineering
Division of Structural Engineering
Concrete Structures
CHALMERS UNIVERSITY OF TECHNOLOGY
Göteborg, Sweden 2005
Master's Thesis 2005:89

MASTER'S THESIS 2005:89

FE Modeling of FRP Strengthening Systems on the White Bayou Bridge

Master's Thesis in the International Master's Programme in Structural Engineering

JOSÉ ALBERTO ANCA PEREIRA

Department of Civil and Environmental Engineering
Division of Structural Engineering
Concrete Structures
CHALMERS UNIVERSITY OF TECHNOLOGY
Göteborg, Sweden 2005

FE Modeling of FRP Strengthening Systems on the White Bayou Bridge

Master's Thesis in the International Master's Programme in Structural Engineering
JOSÉ ALBERTO ANCA PEREIRA

Master's Thesis 2005:89
Department of Civil and Environmental Engineering
Division of Structural Engineering
Concrete Structures
Chalmers University of Technology
SE-412 96 Göteborg
Sweden
Telephone: + 46 (0)31-772 1000

Cover:
Maximum principal stresses in the FE model of the concrete span of the White Bayou Bridge.

Chalmers Reproservice / Department of Civil and Environmental Engineering
Göteborg, Sweden 2005

FE Modeling of FRP Strengthening Systems on the White Bayou Bridge

Master's Thesis in the International Master's Programme in Structural Engineering

JOSÉ ALBERTO ANCA PEREIRA
Department of Civil and Environmental Engineering
Division of Structural Engineering
Concrete Structures
Chalmers University of Technology

ABSTRACT

A large number of reinforced concrete bridges throughout the United States are deteriorated and/or insufficient to carry modern loads. Structural strengthening of a bridge is often necessary to extend the service life and increase the load-carrying capacity. External bonding of fiber-reinforced polymer strips can improve the structural performance of many of these bridges.

Louisiana has a large number of weight restricted bridges on US routes, state routes and parish routes. This situation can be attributed to the original design was based on lighter loads, reduction of the live load capacity or increase in dead load. The aim of this research was to analyze the behaviour of an existing reinforced concrete bridge to be strengthened with fiber reinforced polymer (FRP) materials. The existing bridge is weight restricted. As a consequence of the carrying out of the strengthening of the bridge, the load posting should be removed.

A finite element computer program called ABAQUS was used in this research. Unstrengthened and strengthened alternatives were studied. In the strengthened alternatives, different types of FRP materials were used. The finite element computer program provided deflections, stresses, strains and analysis of the behaviour in all the models. The data provided by the FEM analysis was examined. The results for the different strengthening systems were compared.

The results of the finite element method (FEM) analysis showed that all the strengthened models achieved a certain amount of reduction in deflection and stresses. Although the values were very similar for all the strengthening systems, one of the wet lay-up FRP systems appears to be the most effective one.

For the most effective strengthening system, a considerable extra moment capacity was achieved. With the extra moment capacity can be assured that the load posting can be removed. The bridge behavior has been improved due to the reduction in deflection achieved.

Key words: FE analysis, fiber reinforced polymers, reinforced concrete, bridge, strengthening.

Contents

Preface

In this study, an FE analysis of FRP strengthening systems on the White Bayou Bridge in the State of Louisiana has been carried out. The study has been carried out from September, 2004 to June, 2005. The work is a part of a research project concerning the FRP strengthening and short and long-term monitoring of a bridge in the State of Louisiana (US). This research project includes a literature search, hand calculations, basic computer modeling and finite element analysis. The project is carried out at the Department of Civil and Environmental Engineering, Structures & Structural Materials, Dr. Lamanna's research group, Tulane University, New Orleans (US). The project is financed through the Louisiana Department of Transportation and Development (LA DOTD), under the direction of Mr. Walid Alaywan.

This part of the project has been carried out with Professor Anthony J. Lamanna as supervisor. All research and models have been conducted in the laboratory of the Department of Civil and Environmental Engineering at Tulane University.

This Master thesis is a requirement to obtain the International Master Degree in Structural Engineering by Chalmers University.

Funding for this work was provided by the Louisiana Department of Transportation and Development through The Louisiana Transportation Research Center (LTRC) and the Louisiana State Board of Regents. The author would like to thank Dr. Paul H. Ziehl at the University of South Carolina for his initial work on this project. The author would also like to thank Mr. Walid Alaywan, P.E. of the LTRC for his guidance and advice regarding the White Bayou Bridge. The author is also thankful for the support given by the examiner and program director Björn Engström, without whom this research would not be possible. The help of the undergraduates and graduate students of the Department of Civil and Environmental Engineering at Tulane University has also been a aspect in the right development of this Master thesis.

Finally, it should be noted that this study could never have been completed without the sense of professionalism of the Department staff.

Göteborg, September 2005

José Alberto Anca Pereira

Notations

Roman upper case letters

E_c	Elastic Modulus of concrete
E_{ii}	Elastic Modulus in *i* direction
E_{tot}	Area under the load-deflection curve at ultimate failure (total energy)
E_y	Area under the load-deflection curve at yielding of tension steel
FS	Factor of safety
G_{ij}	In-plane shear modulus
I	Impact factor
IM	Dynamic load allowance percent
M_{dl}	Moment due to the dead load
M_{ll}	Moment due to live load
M_u	Moment capacity of the structure
P	Design wheel load
RF_{inv}	Inventory rating factor
RF_{opr}	Operating rating factor
W	Weight of the truck

Roman lower case letters

a_u	Midspan deflection at ultimate failure
a_y	Midspan deflection at yielding of tension steel
l	Tire contact length
w	Tire contact width
x	Distance from the right rear wheel to the support
y	Distance from the right rear wheel to the guardrail

Greek lower case letters

ε_{ii}	Strain in *i* direction
ϕ_u	Curvature at midspan section at ultimate failure
ϕ_y	Curvature at midspan section at yielding of tension steel
γ_{ij}	Shear strain
μ_Δ	Deflection ductility
μ_ϕ	Curvature ductility
μ_E	Energy ductility
υ_{ij}	Poisson's ratio
σ_{ii}	Stress in *i* direction
τ_{ij}	Shear stress

List of figures

List of tables

1 Introduction

The topic of deteriorating infrastructure has become an issue of critical importance in the United States, as well as in Europe and Japan. A considerable number of bridges in the US are deteriorated to such a degree that the allowable truck loading on the bridge must be reduced and notified by load posting. Structural strengthening may be necessary to extend the service life of the bridge (Klaiber et al. (1987)). Typical retrofitting techniques involve the use of: externally bonded steel plates, steel or concrete jackets, external post-tensioning, bonded fiber-reinforced polymer (FRP) lay-ups with fabrics, near surface mounted reinforcement (NSM) or externally applied FRP post-tensioned strands.

In recent years the development of the plate bonding procedures has been shown to be applicable to many existing strengthening problems in concrete structures. This technique consists of bonding composite sheets or plates of relatively small thickness with an epoxy adhesive to a concrete structure to improve its structural behavior and load bearing capacity. The plate bonding procedure has been attractive in recent years among the many strengthening techniques available, due to its simplicity and speed of installation, with minimum increases in structural self-weight and size.

Bonding of steel elements (plates, channels, angles or built-up members) to concrete structures was developed in the 1960s in Switzerland and Germany (Alkhrdaji et al. (2004)). It has since then become more and more popular in upgrading reinforced concrete structures. This technique consists of gluing steel elements to the concrete surface by a two-component epoxy adhesive to create a composite system. Bonding steel plates to concrete members can greatly increase the cracking load and ultimate load carrying capacity (Zhang et al (2001)). In addition to the epoxy adhesive, mechanical anchors typically are used to ensure the steel element will not detach in case of adhesive failure.

Although the steel plate bonding procedure has been successful in practice, it also presents some disadvantages:

- Heavy weight of the steel plates makes them complicated to install on-site.
- Corrosion of the steel plates that produces deterioration of the bond.
- Plate debonding.
- Limited use in certain locations due to the special response of the steel to environmental loadings such as fire or extreme cold.

Due to the drawbacks of the steel plate bonding technique, FRP materials are becoming the primary solution for strengthening concrete structures. The main advantages of using FRP materials are their resistance to electrochemical corrosion, high strength-to-weight ratio, and versatility of fabrication. Among techniques using FRP materials to strengthen concrete structures, external bonding and NSM procedures are becoming increasingly popular in bridge engineering and maintenance. Since 1982, externally bonded FRP sheets and strips have been successfully applied to strengthen concrete structures (Meier (1992)). The main drawbacks are higher

material costs and possible brittle failure of the strengthened structure. Ductile failure is desirable versus brittle failure, as ductile behavior allows a structure to undergo large plastic deformations with little decrease in strength. Ductility provides possible redistribution of load and moment. In the design of any kind of structures, safety is the most important issue. Plastic deformations are small in the case of brittle failure, which could limit warning time. If the structure posses ductile behavior, it will be able to experience large deflections while still holding near ultimate loads (Carlin (1998)).

There have been several experiments showing the effectiveness of using FRP in repairs. Most of the models developed for bridge retrofitting have used linear elastic finite element method (FEM) to validate both experimental and analytical results. The FEM has demonstrated it is a good tool for these uses. The finite element computer programs mainly used have been ADINA and ANSYS 7.0, such as those carried out by Tedesco et al. (1999) and Galati et al. (2004), and ABAQUS (Malek et al. (1998), Hormann et al. (2000)). In most of the research, beams and slabs have been modeled more often than the entire bridge (Malek et al. (1998), Hormann et al. (2000)).

The White Bayou Bridge is a weight restricted bridge located in the state of Louisiana. The current situation of the bridge can be attributed to the original design were based on lighter loads, reduction of the live load capacity or increase in dead load. The aim of this research is to analyze the behaviour of the White Bayou Bridge to be strengthened with fiber reinforced polymer (FRP) materials. This study should lead to chose a strengthening technique among various options.

Three-dimensional finite element models of the White Bayou Bridge should be developed to accurately represent the structure. In this study, ABAQUS is the computer program provided by Tulane University to carry out the FEM analysis on an entire span of the bridge. Unstrengthened and strengthened models should be studied. In the strengthened models, different types of FRP materials should be used. Static analyses should be conducted for representative spans of the bridge in both the existing and strengthened state. The finite element computer program should provide deflections, stresses, strains and analysis of the behaviour in all the models. The results for the different strengthened systems should be compared between them.

An unstrengthened bridge span and the same span with different strengthening systems should be analyzed with the finite element program. The following systems for strengthening the bridge should be analysed:

- The near surface mounted system (NSM)
- The externally bonded techniques.

Different types of carbon FRP strips were used in all models. The strips were applied at the bottom surfaces of the bridge girders as will be explained in Section 5.1. Design truck loads as requested by the LA DOTD should be applied at discrete locations to the finite element models and the predicted effects of the trucks on the bridge models have been quantified.

When the strengthening of the bridge were carried out, it will be loaded with similar loads than the used in this analysis. Stresses, strains and deflection should be measured in certain locations and these results should be compared with the data obtained from the FE analysis.

As a consequence of the carrying out of the strengthening of the bridge, the load posting should be removed.

2 Objectives and Scope

Louisiana has a large number of weight restricted bridges on US routes, state routes and parish routes. This situation can be attributed to a number of different factors:

- The original designs were based on lighter loads compared to loads in use at present.
- Reduction of the live load capacity as a result of aging, deterioration or damage to structural elements.
- Increase in dead load due to the placement of numerous layers of asphalt or concrete on top of the existing structural system.

If the bridge is unable to safely carry a given load, then the bridge is restricted to carry only reduced loadings and load posted. This leads to a loss of commerce in the state and a hindrance to the public.

The flexural capacity of the bridge girders is frequently the weakest link in the system.

2.1 Objectives

The principal aim of this research was to analyze how the behavior of an existing reinforced concrete bridge could be improved by strengthening. The strengthening of the bridge should lead to the removal of the actual load posting. The bridge is going to be strengthened with FRP materials, thus models of the unstrengthened and strengthened bridge were to be studied. A finite element computer program called ABAQUS should be used to model the bridge. The following models should be established and analyzed:

- Unstrengthened bridge.
- Bridge strengthened with FRP strips attached with the near surface mounted (NSM) procedure.
- Bridge strengthened model with wet lay-up FRP systems.

The finite element program should provide deflections, stresses and strains to be analysed and compared with the collected data, which will be obtained after strengthening the bridge. The data provided by the FE analysis should also help in selecting the locations for sensor placement when the strengthening system chosen was applied.

A literature search and review of the current use of FRP in bridge engineering for strengthening purposes should also be conducted.

The viability of externally attached fiber reinforced polymer (FRP) materials for the strengthening of concrete bridge structures should be prove as a result of this study.

2.2 Scope

Static analyses should be conducted for the bridge in both the existing and strengthened state. The models included non-linear effects where necessary to produce realistic results, as is often the case for conventionally reinforced concrete bridge girders.

The stresses and the deflections were to be examined at midspan of the bridge. Only the bridge girders and span were to be studied. The pier caps, foundations and other elements of the bridge were not within the scope of this study.

This study does not include:

- dynamic analysis
- fatigue analysis
- thermal analysis
- creep analysis
- effects from environmental causes
- effects from extreme overloading
- blast analysis
- impact analysis
- analysis of the substructure
- failure analysis

3 Strengthening of Bridges

A considerable number of bridges in the US are deteriorated to such a degree that many of them need to be repaired, reconstructed, or strengthened. About 35 % of all bridges in 1992 were either structurally deficient or functionally obsolete. Although the condition of bridges in the US has improved significantly since 1990, in year 2002 14 % of the nationwide bridges were functionally obsolete and another 14 % were structurally deficient. The Federal Highway Administration defines structurally deficient bridges as those that are restricted to light vehicles, require immediate rehabilitation to remain open, or are already closed (US Department of Transportation (2004)). The Bureau of Transportation Statistics (US Department of Transportation (2004)) defines that functionally obsolete bridges as those with deck geometry, load carrying capacity, clearance or approach roadway alignment that no longer meet the criteria for the highway network to which they belong.

It is here necessary to clarify some terms regarding the use of FRP on concrete structures. "Strengthen" means to make a structure stronger by increasing the load carrying capacity beyond the initial design capacity. "Stiffen" means to make the structure more rigid by reducing deflections. "Repair" means to restore a structure by replacing a part or fixing what is damaged. "Retrofit" means to install new or modified parts in the structure previously constructed to change the overall response to applied loads. The term repair implies that the structure was damaged. "Strengthen" and "stiffen" imply an improvement in the mechanical properties of the structure (from here on "strengthen" will be the term used for referring to the use of FRP on concrete structures).

The strengthening of existing reinforced concrete structures may be needed for different reasons: to reduce the vertical deflection at service (stiffening criterion), increase the maximum load capacity (strengthening criterion), or limit the width and the distribution of cracks in concrete (durability criterion) (Arduini et al (1997a)). Crack control of reinforced concrete structures is fundamental for serviceability and durability. Crack openings expose reinforcing steel to oxygen and moisture, making it susceptible to corrosion which causes structural problems, such as those affecting the rigidity, and energy absorption capacity of structural elements. They can also damage the appearance of the construction. The ACI Manual of Concrete Practice (1983) reviews the principal causes of cracking and discusses crack control procedures. Colotti et al. (2005) proposed a rational model for design with regard to crack control of reinforced concrete structures.

Corrosion is one of the problems present in reinforced concrete structures. When chloride ions from de-icing salts or seawater enter reinforced concrete structures they destroy the passivity of the steel, causing it to corrode. Structural deterioration is an effect of corrosion combined with design and construction deficiencies, inadequate protection and lack of systematic approaches to inspection and maintenance. Structural deterioration leads to loss of serviceability and functionality, as well as a reduction in safety.

Several procedures have traditionally been used to strengthen many types of structures. In case of concrete bridges, these techniques include introducing additional beams, strengthening existing bridges with externally post-tensioned tendons, and

attaching steel plates to the beams. The attachment of steel plates has been the most successful of these procedures. Attachment can be done either by gluing the plates with a two-component epoxy adhesive with mechanical anchors as a safety precaution. The plates are usually applied to the tension face of a flexural member, but can be applied in the compression or shear zones. This technique was first developed in the 1960's in Switzerland and Germany and has been proven to be reasonably effective in improving strength and stiffness (Mckenna and Erki (1993)). It has also shown many disadvantages, such as corrosion and debonding of the steel plate and complex installation procedures due to the excessive weight of the steel.

External bonding of fiber reinforced polymer (FRP) laminates or plates is becoming increasingly popular in bridge engineering and maintenance, as FRP is lighter than steel and does not corrode in most environments. Certain environments, such as alkalinity, salt water, chemical, ultraviolet light, high temperatures, high humidity and freezing and thawing cycles can degrade the mechanical properties of some FRP systems. FRP materials are attractive for strengthening concrete structures due to their high tensile strength, low weight, and resistance to corrosion (ACI 440.2R-02, (2002)).

The main drawbacks in the use of FRP are high material costs and possible brittle failure. Structures should be designed to fail in a ductile manner, meaning that the structural member can sustain inelastic deformation preceding a possible collapse without significant loss in resistance, consuming a substantial amount of energy. Ductility can be defined as the capability of a structure to deform while still carrying the load, even when the maximum load bearing capacity is reached. Meanwhile, brittle failure can be defined as the lack of this capability. There are many reliable devices to predict brittle failure. The use of externally bonded FRP reinforcement for flexural strengthening will reduce the ductility of the original member. The loss of ductility is negligible, although in some cases, sections that experience a significant loss in ductility, should be examined more closely. The ACI 440.2R-02, (2002) recommends the use of a strength reduction factor to brittle sections in the design of bonding FRP reinforcement for flexural strengthening. Ritchie et al (1991) tested a series of under-reinforced beams to study the effectiveness of external strengthening using FRP plates. The specimens showed a considerable increase in stiffness and strength. Many beams exhibited a very noticeable deflection and also a considerable increase in stiffness and strength. In spite of its brittleness, with suitable design, structural members strengthened with FRP materials can develop sufficient ductility (Ritchie et al (1991)).

Arduini et al. (1997a) state that increased stiffness is always attainable. The higher the FRP stiffness, the greater is the increase in stiffness of the structure. A stiffened repaired structure may become brittle depending on several parameters, such as existing member conditions as well as repair parameters (e.g., bonded length/half span of the beam ratio). Arduini et al. also state that in a strengthening system some limitations should be taken into account: shear strength of the existing member, mode of failure of the repaired system and deflection at new service load.

An increasing number of research studies concerning concrete structures strengthened with FRP materials have been conducted since many of the structures constructed in the first half of the 20th century are inadequate for today's traffic demands. A significant improvement in flexural strength, between 100 – 150 % compared to the

unstrengthened structure, has been demonstrated by Kachalakev (2001) and Sheikh (2002) depending upon FRP strengthening system.

3.1 Materials and Construction

In this section, various FRP materials for use in strengthening RC structures are presented. A short summary of the main procedures of installation is described. This is followed by a brief discussion about adhesives in FRP strengthening systems. The adhesives have a large importance in the systems overall behavior. Recent research on FRP materials, their uses and the different manufacturing procedures are also described.

3.1.1 FRP Materials

FRP materials are made of fibers embedded in a polymer resin matrix (ACI 440.2R-02 (2002). The fibers are the main load-carrying element. The wide range of strengths and stiffnesses of the different types of fibers make them ideal for construction uses. Carbon, glass and aramid fibers are the common types used in the production of FRP composites for construction. Their stress-strain relationship up to failure is linear. The typical mechanical properties of the most common types of fibers are given in Table 3.1.

Table 3.1 Typical properties of glass, carbon and aramid fibers (from Holloway et al. (2001).

Material	Elastic Modulus GPa (ksi)	Tensile Strength MPa (ksi)	Ultimate Strain %
Glass	70 - 85 (10150 - 12500)	2500 - 4500 (362 - 650)	3.5 - 6
Aramid	80 - 125 (11000 - 18000)	2750 (399)	2.5 - 4
Carbon	220 - 240 (32000 - 34800)	3790 - 4820 (550 - 700)	1.4 - 1.5

The resin matrix connects the fibers together, protects them from damage and from the environment, and maintains their alignment, and allows distribution of load among them. Thermosetting resins are almost exclusively used in civil engineering. Epoxy, vinylester and polyester are the most common matrices of the thermosetting resins. Epoxy has a pot life around 30 min at 20 ˚C but can be changed with different

formulations. Pot life is defined as the time available for use of the epoxi system after the resin and curing agent are mixed. The curing goes faster with increasing temperature. Epoxies have good strength, bond, creep properties and chemical resistance. The typical mechanical properties of the most common types of thermosetting resins are given in Table 3.2.

Table 3.2 Typical properties of thermosetting resins (from Holloway et al. (2001).

Material	Elastic Modulus GPa (ksi)	Tensile Strength MPa (ksi)	Ultimate Strain %
Polyester	2.5 - 4 (362 - 580)	45 - 90 (6.5 - 13)	1.0 – 6.5
Vinylester	4 (580)	90 (13)	-
Epoxy	3.5 - 7 (507 – 1015)	90 - 110 (13 – 16)	1.5 - 9

FRP materials are a new option to enter the construction industry. It is currently being used in many areas of civil engineering. The use of FRP in repair, strengthening and upgrading of bridge decks using the externally bonding procedure, and column wrapping has been highly developed. Also the application of FRP materials in the construction of new bridges and bridge decks is currently growing. The first FRP superstructure on a state highway in the US was constructed in October 1998 (Alampalli (2000)). Besides strengthening of concrete structures, FRP materials are being used in rehabilitation of masonry and brick structural wall systems. Holloway and Head (2001) summarize some of the constructions developed using FRP materials.

Alkhrdaji et al. (2004) reviewed the current techniques in structural repair and strengthening of concrete facilities. Their study identifies how FRP materials are now becoming a spread technology for the structural upgrade of concrete structures due to its characteristics, such as non-corrosive properties, speed and ease of installation, lower cost and aesthetic appearance.

FRP materials are available in forms of rebars, prestressing tendons, pre-cured laminates/shells and fiber plates of sheets for concrete reinforcement. FRP rebars and tendons are normally used for internal concrete reinforcement. FRP pre-cured plates or sheets are generally used for external concrete reinforcement. FRP plane laminates have been used to replace bonded steel plates (Ross et. al. (1999). FRP shells have been used as jackets for columns (Monti and Spoelstra (1997)).

3.1.2 Fiber Reinforced Polymer Strips

In this study, from all FRP materials, FRP strips are the chosen to analysed in strengthening the White Bayou Bridge. FRP strips are composites of high modulus fibers with a polymer matrix. The fiber strips exhibit anisotropic behavior because of the anisotropic intrinsic characteristics of the fibers. This principal characteristic allows the engineer to design the composite to suit the required shape and specification.

Typical composite materials' properties include: ease of transportation and handling, high strength and stiffness and resistance to corrosion. FRP composites present linear elastic strain-stress curve to failure due to the elastic behavior of the fibers since matrix materials deform plastically. Brittle failure is the typical mode for FRP composites under excessive stresses. Lately some research has been conducted in order to avoid the loss of ductility in concrete structures retrofitted with FRP. Some new fabrics such as a hybrid of carbon and glass fibers have been researched and these tests showed no significant loss in beam ductility (Grace et al. (2002)). Continuous research shows how FRP materials are showing a promising future for structural strengthening.

3.1.2.1 Resins

Resins are used in the FRP strips to create the matrix in which the fiber reinforcement will be embedded. Resins are at least an order of magnitude weaker than the fibers embedded in them. For the FRP systems, resins with the following characteristics should be used:

- Compatibility with and adhesion to both the concrete substrate and the reinforcing fiber.
- Resistance to environmental effects.
- Workability.
- Development of appropriate mechanical properties of the FRP composite.

The most common types of resins used in the FRP materials are epoxies, vinylesters, phenolics and unsaturated polyester. Holloway and Head (2001) summarize the properties and characteristics of the most common types.

The coefficient of thermal expansion of polymers is generally much higher than that of other materials, such as steel or concrete. At high temperatures, all the polymers will soften and/or decompose. The upper temperature limit for the use of most common thermoplastic polymers lies between 100 and 200 ˚C.

The environmental conditions have a great importance for the behaviour of the resins. Temperature extremes or fluctuations, high humidity, direct contact by rain or dust, excessive sunlight can retard or accelerate the resin curing time.

3.1.2.2 Fibers

The traditional reinforcement for FRP systems are continuous glass, aramid and carbon fibers. The fibers give the FRP systems their strength and stiffness. For the three systems studied in this project, carbon fibers were chosen. The mechanical properties of carbon fibers are shown in Table 3.3.

Table 3.3 Carbon fiber properties from manufacturer's data (Sika, Version 3.0).

	Density g/cm^3 ($lb/in.^3$)	Elastic Modulus GPa (10^3 ksi)	Tensile Strength MPa (ksi)	Elongation %
Carbon	1.8 (0.065)	220-240 (32-34)	3790-4820 (550-700)	1.4-1.5

Carbon fibers may be manufactured from polyacrylonitrile (PAN), pitch, or rayon precursor materials by high-temperature (1000 to 18000 ˚C) carbonization or graphitization processes. Carbon fibers manufactured from the pitch precursor are used to reinforced metal matrices, carbon-carbon composites, thermosetting and thermoplastics polymers. Carbon fibers are in general not affected by moisture, atmospheric conditions, solvents, bases and weak acids.

3.1.3 Procedures of Manufacturing FRP

FRP composites can be produced by different manufacturing procedures in many shapes and forms. The different techniques influence the mechanical properties of the final material. Holloway and Head (2001) classified the procedures of manufacture of FRP materials in the following categories:

- manual process: wet lay-up, spray-up, pressure bag moulding and autoclave mouldings
- semi-automated process: compression moulding and resin injection
- automated process: pultrusion, filament wound and injection moulding

Pultrusion and wet lay-up are the processes used to manufacture the FRP materials used in this research. In this section these process will be briefly explained in general. In Section 3.3.1 the procedures of strengthening reinforced concrete structures by attaching FRP materials are thoroughly explained.

3.1.3.1 Wet Lay-up Manufacture Process

The wet lay-up process is a manual procedure to manufacture FRP materials. Most of the FRP products fabricated with this procedure are FRP laminates. It consists of dry fibers impregnated by hand with a saturating resin. The fibers are in the form of woven, stitched or bonded fabrics or sheets. The fibers may be randomly orientated or directionally orientated. The saturating resin is used to provide a binding matrix for the fiber. Rollers and brushes are used with impregnators for forcing resin into the fabrics. Laminates are left to cure under standard atmospheric conditions or at elevated temperatures in controlled conditions such as a factory.

A modified wet-lay up system uses "prepreg" fibers, which are impregnated with resin at the manufacture's facility (ACI Committee 440 (2002)).

Holloway and Head (2001) provide an introduction to the wet lay-up manual process. Their book also gives information about the important commercial procedures available to manufacture FRP materials by this technique.

3.1.3.2 Pultruded Fiber Reinforced Polymer Strips

In the beginning pultrusion was a continuous molding process for manufacturing long, straight structural members of constant cross-sectional area. The pultrusion is comparable to a continuous press. It consists of ''pulling'' resin impregnated reinforcing fibers and fiber fabrics through a heated curing die (Bakis et al. (2002)). In recent years curved sections and members with different cross-sectional areas have also been pultruded. FRP materials such as solid rods, hollow tubes, flat sheets, various types of beams and strips are common pultruded products (Mallick 1988). The pultrusion process closely controls some critical variables such as fiber placement, resin formulations, catalyst level, die temperature and pull speed. Holloway and Head (2001) showed that during the design and manufacture of the FRP materials these variables should be established to guarantee the specific properties of the product.

The FRP strips manufactured using the pultrusion process are produced with various dimensions of thickness and widths. The strips are normally unidirectional; the fibers oriented in the longitudinal direction. Correspondingly, the strip strength in this direction is related to the fiber strength and, thus, very high.

3.1.4 Adhesives in FRP Strengthening

Adhesives are used to produce a continuous bond between FRP strips and concrete to ensure that composite action is developed by the transfer of shear stress through the thickness of the adhesive layer. An excellent degree of adhesion to the involved surfaces must be achieved. Two-part ambient curing structural epoxy adhesives, which have been specially developed for use in the construction industry and specifically for bonding external plates work the best for structural applications (Sika

Carbudur design guidelines 3.0). The properties needed by an adhesive for suitable strengthening behavior are:

- It should present adequate adhesion to both the FRP and the concrete structure.
- It should present compatible thermal properties with both concrete and FRP.
- It should present low creep.
- It should not be sensitive to normal variations in the moisture content of prepared surfaces (both concrete and FRP).
- It should be resistant to the alkaline nature of concrete.
- It should possess gap-filling properties and be easy to mix, apply and cure. It should exhibit sufficient adhesion to enable FRP materials to be attached directly to overhead or vertical surfaces with minimal need for temporary fixings while the adhesive cures.

The environmental conditions have a great influence in selecting an adequate adhesive. These conditions include concrete surface temperature, air temperature, relative humidity and dew point. The temperature of the adhesive must not be greater than the Safe Working Temperature, which is 10˚C to 20˚C below the glass transition temperature of the adhesive. The value of the Safe Working Temperature is provided by the manufacturer. If this value is exceeded, the adhesive changes from a hard and relatively brittle condition to a viscous condition. High ambient temperatures can cause the adhesive to creep. The adhesives should not generally be applied to damp or wet surfaces. The bond between FRP strip and the concrete can be altered due to the transmission of moisture vapour from a concrete surface through the uncured adhesive (ACI 440.2R-02 (2002).

In a fire, the adhesive will commence to soften and will lose its load-carrying capacity. If the concrete surface temperature is below a minimum level specified by the manufacturer, the integrity of the adhesive and the resin can be altered.

3.2 Strengthening by Steel Strip Bonding

Strengthening concrete structures by steel plate bonding was developed in the 1960s in Switzerland and Germany, although the first use reported was in 1964, when a strengthening of a beam in a basement was done. A report by Mckenna and Erki (1993) summarizes some of the strengthened concrete members using steel plates realized from the 60's to the 90's all around the world. Such projects as the strengthening of Shelly Bridge in Perth (Australia) and strengthening of over 200 bridges in Japan have been quite successful. This procedure presents the advantage of minimal interruption of the normal use of the structure during strengthening and less cost than replacing the existing structure.

The procedure consists of gluing steel plates with an epoxy adhesive to the concrete surface creating a composite system. The surfaces in both the concrete and the steel

plate must be clean, and the operation itself must be executed with great care. The epoxy's bond strength to the concrete should at least match the concrete's tensile strength. Adhesive anchors can be used to compress the concrete and steel together. Supplemental anchors at the end of the plate should be provided in case of adhesive failure; in addition, false work is needed to maintain the steelwork's position during bonding. The steel must be protected against corrosion and aggressive environment. Fire protection should also be taken into account when using steel elements. Mechanical anchors, gypsum boards or spray-on materials are some of the procedures of protecting bonded steel elements from the effect of fire. In case of epoxy failure because of fire mechanical anchors must be installed. Gypsum boards are good insulating materials. The most economical form of passive protection for steel elements is the cement-based spray-on materials with some form of fiber reinforcement.

Steel can be a good choice for externally strengthening structural elements, due to its stiffness, strength, low cost and ductile behavior. Both short and long-term experience indicate that steel plate bonding suffers from a number of drawbacks:

- Difficult handling, the heavy weight of steel plates.
- Frequent joints due to the limited delivery lengths of steel plates.
- Intensive scaffolding to meet required labor safety.
- Deterioration of the bond at the interface of steel and concrete, due to electrochemical corrosion of the steel plates.
- Plate debonding either at the plate end or in the cracked concrete zone.
- Limited use in certain "sensitive" structures due to the magnetic and electrical characteristics of steel plates.

Although steel is appropriate for enhancing the strength of structural members, it is generally not recommended for use, since adequate surface preparation for bonding is difficult and steel plates exhibit poor durability characteristics.

Raithby (1980) analyzed the response of a strengthened bridge with bonded steel plates. The report describes the strengthening and load testing of the bridges at Quinton (U.K). Laboratory tests were conducted. The beams were 5 m (16.4 ft) long with different types of adhesive and dimensions of the plates. The results of the laboratory tests showed that the post-cracking stiffness of these beams increased between 35 to 105 % depending on the type of adhesive and the dimensions of the plates. The possibility of deterioration of the bond between steel and concrete was also studied. Small samples of plain concrete having a strip of steel bonded to one surface were exposed to weather conditions. After two years of exposure the specimens showed a slight loss in strength but still the mean strength exceeded the original strength, determined four months after casting the concrete. The steel plates exposed to weather showed corrosion between the plate and the adhesive. Local debonding also was present in the weathered sample.

Experimental investigations show that the flexural failure load for bonding with epoxy adhesives is 45 – 60 % greater than the flexural failure load for bolting the steel plates. Sirju and Sharma (2001) compared different procedures for strengthening concrete members subjected to compression and flexure. Square concrete columns with a cross section of 200 x 200 mm (7.9 x 7.9 in.) were loaded up to failure. The different procedures analyzed were: wrapped columns with ferro-cement mix, wrapped columns with fiber cement mix, strengthened columns with externally bonded steel plates and strengthened columns with externally bolted steel plates. The increase in strength presented in the specimens with externally bonded steel plates was 125 % and it was the largest of all the different models analyzed. The steel strengthened specimens showed sudden and brittle failure. The columns wrapped in ferro-cement mix and in fiber cement mix showed ductile failure.

Oh et al. (2003) identified the local failure of strengthened concrete members with steel plates. Blocks of concrete of 150 x 150 x 400 mm (5.9 x 5.9 x 15.75 in.) with a steel plate bonded to it were loaded up to failure by displacement control method. Specimens with different plate and adhesive thickness were tested. Only one end of the steel plates was bonded to the concrete to perform half-beam test to confine the premature failure region to that location. The half-beam test members showed rip-off failure, which means that part of the concrete with a strengthened plate is taken off the main body of the test members. Increasing the plate thickness increased the shear strength at the interface. Increasing the adhesive thickness did not have a direct relationship with the failure, as the specimens failed by rip-off. A study in failure of reinforced concrete beams strengthened by bonded steel plates by Oehlers (1990) showed that the flexural peeling failure depended on the flexural rigidity of the plated reinforced concrete beam, the tensile strength of the concrete and the plate thickness. The increasing of the plate thickness reduced the moment at the end of the plate at which debonding due to flexural peeling occurs. This is the reason why it is not always good to increase the thickness of the plate.

3.3 Strengthening with FRP Systems

In recent years, the number of concrete structures strengthened using FRP strips has increased considerably. Compared to steel plate bonding, FRP is typically more economical. Although the FRP is between 4 and 20 times as expensive as steel in terms of unit volume, the ultimate strength of FRP is generally from 5 to 15 times the ultimate strength of steel (Holloway and Head (2001)). In addition to material costs installation of FRP is less expensive than installation of steel, due to the heavy weight and difficult handling of steel. In strengthening bridges, FRP shows its great advantages when corrosion, traffic management costs, and length of the required strengthening should be taken into account. These advantages are:

- FRP materials are easy to transport and handle, which means that they require less falsework than steel plates and may be used in areas with difficult access due to their lightweight.

- The fibers can be introduced in a certain position, volume fraction and direction in the matrix to obtain maximum efficiency.

- FRP materials are noncorrosive and exhibit high tensile strength.

The principal disadvantage compared to steel plate bonding is that concrete structures strengthened with FRP sometimes exhibit brittle failure while the structures retrofitted with bonded steel plated present ductile failure (Aprile et al. (2001)). The brittle behavior can be prevented with proper design. A report by Spadea et al. (2001) showed that with an effective design of an anchorage system the strengthened structure can regain some part of the lost ductility of the unstrengthened structure.

A general classification of FRP systems forms can be made upon how they are delivered and installed:

- Externally bonded strips: The strip is adhesively bonded to the concrete surface by means of epoxy adhesive.

- Near surface mounted procedure: The strips are placed in a groove made on the concrete surface.

- Mechanically fastened systems: The strips are attached to the concrete surface by means of fasteners.

The three procedures are explained in the following sections.

3.3.1 Externally Bonded Strips

In the externally bonding procedure a wide range of materials besides the fibers are used. Resins, primers, putty fillers, saturating resin, adhesives and protective coatings are used to achieve a better behavior of the bonded FRP system.

There are several ways of bonding the FRP strips to the concrete. The most common types are wet lay-up and precured systems. ACI Committee 440 (2002) defines the wet lay-up system as a procedure in which the dry fibers are prepared and applied on-site. The strips are manufactured off-site for the precured systems.

Rizkalla et al. (2003) describe the uses of the primer and the putty. Primer and putty are surface preparation agents. The primer is used to penetrate the surface of the concrete, providing an improved adhesive bond for the saturation resin or adhesive. Later, the putty is used to fill small surface voids in the substrate and to provide a smooth surface to which the FRP can bond.

3.3.1.1 Wet Lay-up Systems

In his doctoral thesis, Carolin (2003) characterizes the wet lay-up systems by dry fibers and matrix that are systematically applied to a surface and the composite is built up and bonded at that time. The dry unidirectional or multidirectional fiber sheets of fabrics are impregnated with a saturating resin on-site. The saturating resin provides a binding matrix for the fiber and bonds the sheets to the concrete surface along with a compatible primer and putty.

The wet lay-up systems can be subdivided in two different common types. In the hand lay-up systems the dry fiber sheets are saturated on-site with the epoxy resin. When the composite is cured, it is bonded to the concrete surface over compatible primer and putty. In comparison with hand lay-up systems, prepeg systems include a saturating resin that is impregnated off-site, depending upon the system requirements. Prepeg systems are cured in place. (ACI Committee 440 (2002)).

3.3.1.2 Precured Systems

Precured FRP systems consist of a variety of composite shapes manufactured off-site. An adhesive along with the primer and putty is used to bond the precured shapes to the concrete surface. The system manufacturer should be consulted for recommended installation procedures. The most common types of precured systems are:

- Unidirectional laminates, delivered in the form of large flat stock or thin ribbon strips coiled on a roll.
- Multidirectional grid coiled on a roll.
- Precured shells in the form of shell segments cut so they can be opened and fitted around columns or other elements. Multiple shell layers are bonded to the concrete and to each other to provide seismic confinement or strengthening.

Rizkalla el. al. (2003) summarized the current state of knowledge of FRP materials and their different strengthening techniques. Externally bonded FRP sheets and strips have been applied to reinforced concrete beams since 1982. Externally bonded FRP sheets and strips are at present the most commonly used procedures for strengthening bridges and concrete structures. Still there is some concern about this procedure, such as failure due to debonding, it is unprotected against wear, impact loads, and the effect of harsh environmental conditions.

3.3.2 Near Surface Mounted Procedure

The NSM procedure has been used since the 1940´s, when steel bars where placed in grooves cut into the concrete structure surface. The drawbacks of using steel has led to the use of FRP materials. The NSM can be used with different types of FRP materials, such as rods and strips. Some research, such as that conducted by De Lorenzis et al. (2001), Pham et al. (2004) or Swamy et al. (1999), have shown how externally bonded reinforcement can present debonding failure. This type of failure can be prevented by means of the NSM FRP systems. When external reinforcement is going to be subjected to mechanical and environmental damage, the NSM becomes an attractive system as it provides protective concrete cover.

Strips normally are provided in rectangular cross-sections for the NSM procedure. The strips are precured in the factory and delivered to the job site. The strips are

placed into a groove made in the concrete surface by a saw. An epoxy adhesive or another kind of plaster is used to bond the strips into the surface.

The installation of the strips should be performed according to the following steps:

1. Cut groove: A groove should be made with help of a diamond blade saw. It should be wide enough to place the strip.

2. Prepare groove and FRP: The groove is completely cleaned using either a vacuum or compressed air. The FRP strip is cleaned by acetone. A masking tape or similar product is applied to prevent excess adhesive from adhering to the concrete surface.

3. Apply adhesive: The groove is carefully filled with a structural adhesive to prevent entrapped air hollows. The adhesive is usually applied with a cement mortar.

4. Place FRP strip into the groove: After application of the adhesive, the strip is inserted and slightly pressed into the groove to force the adhesive to flow between the FRP strip and the groove side.

5. Finish: The excess adhesive is removed. The adhesive surface is smoothen and any additional adhesive is added. General clean up and removal of the masking. Protective coatings are essential for long-term durability. The coating should be a non-vapor barrier, flexible, water proof, and compatible with the FRP material (Karbhari et al. (2004)).

Bonding the strip inside the groove provides a greater anchorage capacity in comparison with externally bonded procedure (Hassan et al. (2002) and (2003)). The NSM procedure requires no surface preparation work after cutting the groove, and requires minimal installation time compared to the externally bonded reinforcing technique (Sena Cruz et al. (2004)).

Hassan et al. (2002) investigated the feasibility of using externally bonded carbon fiber reinforced polymers (CFRP) strips and CFRP NSM strips for flexural strengthening of bridge slabs. For both systems, the same type with the same amount of cross sectional area of CFRP strips was used. One specimen was bonded with six CFRP strips. Another specimen had six CFRP strips cut into two halves and inserted into the grooves. Their research showed that the NSM reinforcement enhanced the ultimate load carrying capacity by 43 %; meanwhile the externally bonded procedure enhanced the ultimate load carrying capacity by 11 %. A cost analysis was also carried out. The efficiency of NSM FRP strips, defined as the ratio of the percentage increase in capacity to construction cost, was three times that of the externally bonded strips.

Täljsten et al. (2003) tested a series of concrete beams strengthened with CFRP NSM strips. The beams were strengthened with CFRP laminates and strips and also different types of adhesive were used. Four point bending tests were carried out. The results showed increases in the ultimate load up to 90 %. The effectiveness of the NSM procedure compared to the externally bonded procedure was confirmed.

Hassan et al. (2003) tested T-section concrete beams strengthened with CFRP NSM strips. The specimens had different embedment lengths. The results showed that the strips increased both stiffness and strength of concrete beams. The ultimate load carrying capacity increased as much as 53 %. An analytical model was proposed to validate the interfacial shear stresses. The model was validated by comparing the predicted values with test results and also with a nonlinear finite element model. Excellent agreement was established between the three models. A parametric study was carried out based on the results from the analytical model. The influence of the embedded length, concrete compression strength, reinforcement ratio and groove width was discussed. In case of rupture of the CRFP strips, increasing the reinforcement ratio increased the rupture load. Increasing the concrete compressive strength resulted in an increase in the maximum shear stresses.

3.3.3 Mechanically Fastened FRP Strips

The externally bonded procedure requires time and careful preparation for an ideal installation. The surface preparation and the saturation of the fibers, if the installation is on-site, are complex procedures. The adhesive full cure is attained in 24 h (Sika 3.0). Attaching FRP mechanically to the concrete surfaces might prevent these problems.

Debonding of an externally bonded FRP plate is in many cases catastrophic with brittle behavior and little ductility. This failure has been shown by Swamy et al. (1999) and Ritchie et al. (1991). A number of researchers, such as Holloway et al. (2001) or Swamy et al. (1999), have claimed that the brittle failure of the strengthened beam by strip debonding might be prevented by mechanical anchorage to the composite strip at its ends. In recent years, researchers have studied strengthened concrete structures by FRP using the mechanical anchorage without any bonding (Lamanna et al. (2001)).

The University of Wisconsin-Madison has developed a procedure of strengthening structures based on mechanical anchorage. The procedure is known as the mechanically fastened (MF) FRP procedure. The MF-FRP procedure uses simple hand tools, lightweight materials and unskilled labor. The strengthening is obtained by attaching FRP materials by means of fasteners and, if necessary, steel expansion anchors. A number of different pultruded FRP strips were used in the MF-FRP investigation carried out at University of Wisconsin-Madison. Lamanna et al. (2001a) recommended the concrete and the strips to be predrilled at the required fastener spacing with holes to receive the fasteners. The drilled holes should be the same size as the fasteners diameters. The fastener is driven into the concrete by means of a powder actuated system. The surface of the fastener becomes deformed and generates friction with the surrounding material. The heat generated in this process causes sintering and creates a bond between the concrete and fastener. These two factors give the fastener its holding capacity. In Figure 3.1, a schematic of the MF-FRP system is shown.

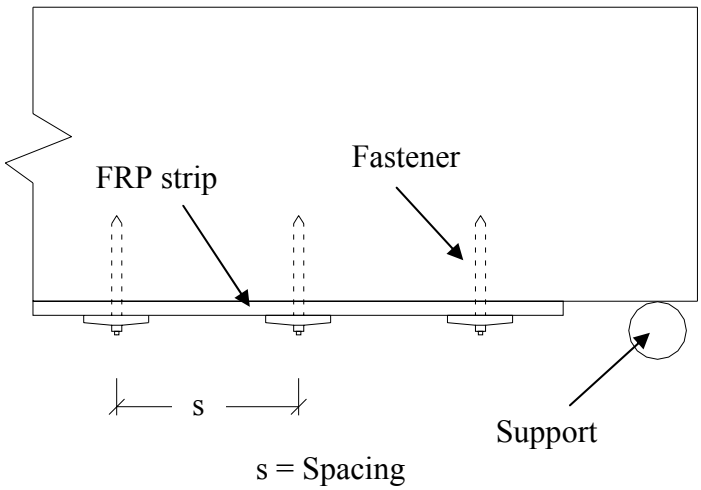

Figure 3.1 Sketch of the MF-FRP system (adapted from Lamanna (2002)).

Some investigations concerning the feasibility of the procedures have been carried out. Lamanna et al. (2001b) tested concrete beams with a rectangular cross section of 305 mm x 305 mm (12 in. x 12 in.) and a length of 3,658 mm (144 in.). Unstrengthened specimens and strengthened specimens with externally bonded FRP strips and with mechanically fastened (MF) strips were tested. The FRP strips were attached at the bottom face of the beams. For the MF-FRP systems, the strips were fastened with different type of fasteners and different spacing. All the beams were loaded until failure. The ultimate moments of the MF-FRP systems were 163.8 kNm (1450 kip-in.) and 159.4 kNm (1411 kip-in.) for the systems depending on the spacing of the fasteners. An increase of the ultimate moment of 20 % and 17 % over the unstrengthened specimens was achieved. The beams with externally bonded strips presented an increase in the ultimate moment of 20 % with respect to the control beams. The results showed that, with the correct fastener layout and strip properties, the same strengthening capacity as the beams with externally bonded strips could be achieved. Although the strengthening capacity of both procedures was the same, the MF-FRP provided a pseudo ductile failure. These beams failed at the average failure deflection that the control beams, meanwhile the beams with externally bonded FRP strips showed much less deflection capacity than the control beams.

As a summary the principal advantages of this procedure are the little surface preparation of the concrete needed and the ductile failure mode obtained in the strengthened members. These advantages made the MF-FRP procedure very attractive for rapid strengthening applications where time is critical or where the externally bonded procedure cannot be applied. The type of mechanical fasteners can be varied, from powder activated fasteners to expansion bolts to concrete screws, depending on the characteristics needed.

3.3.4 Failure Mechanisms

It has been shown in the literature that different failure mechanisms, from ductile to very brittle, could occur when externally bonded FRP reinforcement was added to a

flexural member. Many researchers, such as Arduini et al. (1997b), Buyukozturk et al. (1998), and Holloway et al. (2001), have presented the wide variety of failure modes observed in the strengthened concrete members. The failures can be affected by different parameters. Yielding of steel and rupture of the laminate should better occur before compressive concrete failures. Existing shear reinforcement, crack configuration prior to strengthening, laminate length and relative laminate/adherent/concrete stiffnesses can affect the modes of failure. Arduini et al. (1997b) confirmed that it is possible to effectively strengthen beams, but the possibility of brittle unexpected failure mechanisms needs to be considered.

With reference to a simply supported RC beam strengthened with FRP materials and with a 4-point bending load, Arduini et al. (1997b) summarized four possible failure mechanisms. Figure 3.2 shows a sketch of these possible mechanisms.

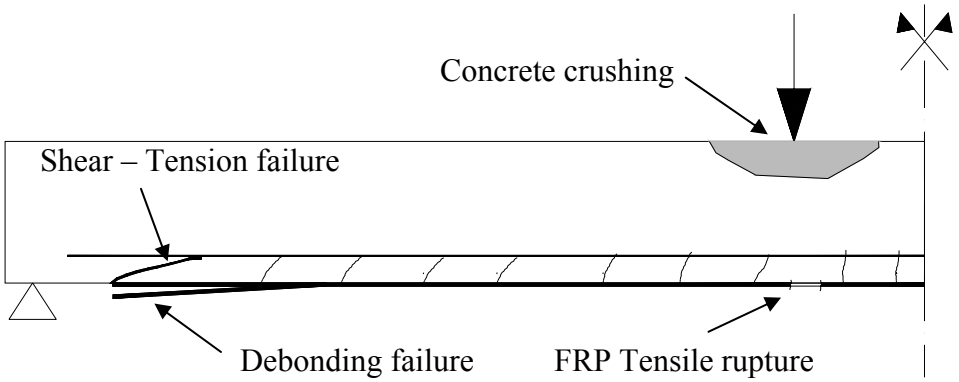

Figure 3.2 Failure modes for FRP systems.

1. FRP rupture when the FRP strain reaches its ultimate value in the zone of maximum moment. This occurs when the original beam is under-reinforced and the beam remains under-reinforced when strengthened with a composite plate. This kind of failure mode is very unusual due to the high ultimate strength of FRP materials.

2. Concrete crushing when the concrete compressive strain reaches its ultimate value in the zone of maximum moments.

3. Debonding failure which may involve any of a variety of debonding cases:

    a. Between FRP and concrete due to failure at the concrete-adhesive interface. This failure mechanism can initiate at any flexural shear crack and propagates to the end of the FRP reinforcement. In this type of failure three different mechanisms interact between them. In Section 3.3.5 these three mechanism along with systems to avoid them are explained. Figure 3.3 shows a sketch of how this failure could be triggered by a flexural shear crack.

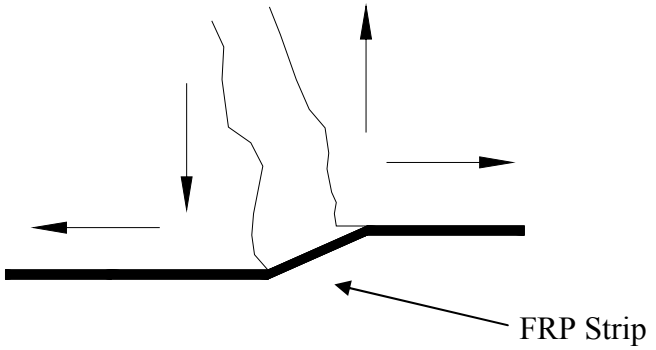

Figure 3.3 Debonding due to shear crack, adopted from Buyukozturk et al. (1999).

b. Between FRP and concrete due to failure at the FRP-adhesive interface.

c. Failure in the thin layer of concrete near to the adhesive. It occurs within a depth less than 1 mm (0.039 in.) from the surface. Stress concentrations occur at the laminate anchorage zone leading the concrete to failure (Buyukozturk et al. (1998)).

d. Failure in the adhesive. This can be prevented by using an adequate structural adhesive.

4. Shear-tension failure resulting from a combination of shear and normal tensile stress in the concrete in the plane of the longitudinal steel bars. This failure mechanism initiates at the ends of the FRP plate, results in the propagation of a horizontal crack, and causes separation of the concrete cover along the plane of the tensile rebars.

The failure mechanisms 1 and 2 occur following a large deflection of the member and that results in better structural performance than members failing in the other two modes. In the case of FRP rupture, the main steel reinforcement was past yielding in the beams tested by Arduini et al. (1997a). Moreover, from an economical point of view, the rupture of the FRP plate is preferred because all of the mechanical resources of the FRP (a costly material) are utilized.

Failure mechanisms 3 and 4 in beams tested by Arduini et al. (1997a) were brittle and occurred at values of the applied load lower than expected with conventional design equations. In both cases, the stiffening/strengthening resources of the FRP plate are of lesser advantage. The strengthened beams were still stronger, although they no longer failed in a ductile mode. Anchoring the FRP plate ends may help attain a higher ultimate load and an increase in ductility in cases where failure mode 3 occurs.

In the state-of-art review of FRP for construction Bakis et al. (2002) also reviews the different failure modes for the externally bonded FRP strengthening systems.

3.3.5 Debonding Failure and End Anchorage

The debonding of a bonded FRP strip is a brittle and catastrophic mechanism. The problem of preventing debonding failure is a particularly complicated problem. Researches have shown that there are three mechanisms of debonding that interact between them. These three mechanism are flexural peeling, shear peeling and axial peeling. Oehlers (2001) proposed a solution based on deriving a model for each mechanism separately and then their interaction.

The flexural peeling mechanism is shown in Figure 3.4. The flexural peeling crack starts at the plate end and propagates inwards. It is necessary to apply an axial force and moment in the plate in order to the deformation of the plate would be the same as if it had been attached to the beam. The stress resultants can be seen in the lower diagram of Figure 3.4. It is these stress resultants, which have to be transferred from the RC, beam to the plate that cause debonding.

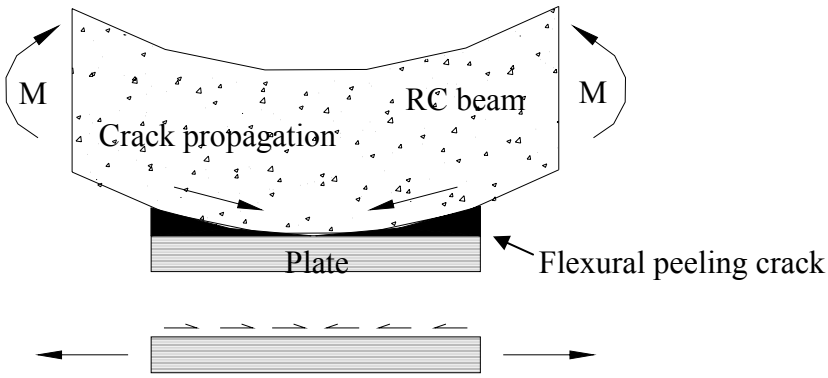

Figure 3.4 Flexural peeling mechanism adapted from Oehlers (2001)(Deflections exaggerated).

Figure 3.5 shows the shear peeling mechanism. Beams tested by Oehlers (2001) showed that the mechanism always occurs after the formation of diagonal shear cracks. The sliding or rotation of the critical diagonal crack causes the debonding crack to start at the base of the diagonal crack and propagates to the direction of the arrow.

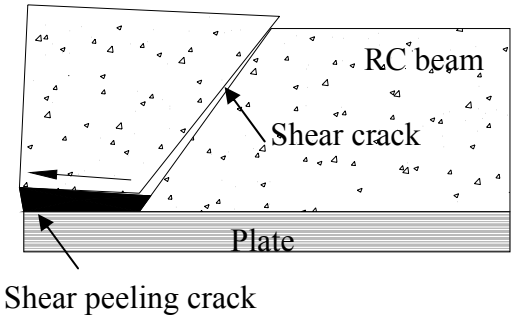

Figure 3.5 Shear peeling mechanism adapted from Oehlers (2001).

Figure 3.6 shows the proceeding of the axial peeling mechanism. A debonding crack along the edge of a plate occurs when a flexural crack touches the plate. The strains

that have to be accommodated where the plate crosses the crack induce debonding cracks that propagate away from the flexural crack.

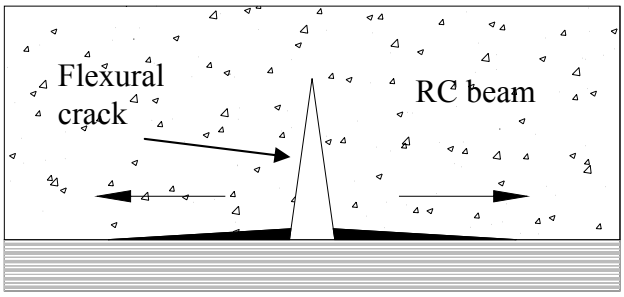

Figure 3.6 Axial peeling mechanism adapted from Oehlers (2001).

Some researchers, such as Swamy and Mukhopadhyaya (1999), showed that the laminate debonded suddenly prior to ultimate failure in rectangular cross section concrete beams. Analytical and numerical models developed by Arduini et. al (1997) showed that this type of failure could be initiated form a flexural crack in the shear span. Both models, analytical and numerical, were compared with experimental data obtained from strengthened RC beams. The models showed good agreement with the experimental data. The debonding begins at the point where the shear crack initiates. The debonding propagates form that point to the plate end. Another type of debonding failure initiates from the plate cut-off point near the end support (Ritchie et. al (1991). End anchorages become essential to resist and delay this type of debonding. End anchorages also increase the failure load.

The ultimate failure caused by the debonding of the FRP plate is always catastrophic with brittle behavior. The phenomenon leaves a significant amount of the load-bearing capacity of the FRP unutilized. This failure has been shown by Swamy and Mukhopadhyaya (1999) and Ritchie et. al (1991).

The use of anchorage in the strip ends will have no significant effect on the response of the structure in terms of stiffness, serviceability and yield loads; however, the main advantage of inclusion of anchorages is prevention of premature anchorage failures and increase of the ductility. All forms of anchorage do delay the occurrence of failure and increase the maximum load carried and the ductility in comparison to the corresponding un-anchored specimen, allowing higher maximum plate and concrete strains to be attained (Hollaway and Head (2001)).

Spadea et. al. (2001) investigated the strength and ductility aspects of reinforced concrete beams strengthened with an externally bonded carbon FRP. The failure behavior in unstrengthened beams and in strengthened beams with and without anchorage was studied. The anchorage consisted of steel plates bonded to the concrete with the same adhesive used with the carbon FRP. Spadea et al. (2001) defined the ductility failure based on ratios of deflection, curvature and energy:

- Deflection ductility:

$$\mu_{\Delta} = \frac{a_u}{a_y} \tag{3.1}$$

- Curvature ductility:

$$\mu_{\phi} = \frac{\phi_u}{\phi_y} \tag{3.2}$$

- Energy ductility:

$$\mu_E = \frac{E_{tot}}{E_y} \tag{3.3}$$

where a_u = midspan deflection at ultimate failure; a_y = midspan deflection at yielding of tension steel; ϕ_u = curvature at midspan section at ultimate failure; ϕ_y = curvature at midspan section at yielding of tension steel; E_{tot} = area under the load-deflection curve at ultimate failure (total energy); and E_y = area under the load-deflection curve at yielding of tension steel. Ductility can be defined as the capacity of a material to deform, which means to absorb energy. Ductility is very important and desirable for impact and earthquake design.

The unstrengthened beams failed in a conventional manner, in flexure, after extensive yielding of tension steel, and followed by crushing of the concrete in the compression zone. The energy ductility ratios of the unstrengthened beams range from 11.6 to 15.7. The strengthened beams without any external anchorages presented a sudden brittle failure with explosive debonding of the FRP laminate at failure, although significant increase in strength was obtained. The energy ductility ratios of the strengthened beams without any external anchorage range from 1.9 to 3.2. The strengthened beams with the end anchorages produced more ductile failures and carried still high failure loads than the strengthened beams without external anchorages. The strengthened beams with the end anchorages presented higher values in the ductility ratios than the strengthened beams without anchorage. The energy ductility ratios of the strengthened beams with the end anchorage range from 9.5 to 13.2. These results give emphasis to how important the anchorage systems are in designing strengthened systems in order to maintain ductile failures.

A very important aspect of interface behavior is that there exists an effective length beyond which an extension of the bonded length cannot increase the shear resistance. De Lorenzis et al. (2001) proved this statement with research in the bonding of FRP laminates to concrete. The factors affecting bond of FRP laminates to concrete, such as, bonded length, concrete strength, number of plies, ply width and surface preparation were studied. Three series of T-cross sections simply supported beams of plain concrete with three different bonded lengths, different concrete compressive strength and different number of plies were loaded under four-point bending. The failure occurred at the concrete-epoxi interface, which means that the concrete strength did not affect the ultimate load. The results also showed that the bonded length did not affect the ultimate load, so confirming the existence of an effective

length beyond which no stress is transferred. The use of end anchorage is particularly important when the length of the FRP system is restricted and the effective length is not sufficient to achieve the ultimate strength of the FRP reinforcement. Chen and Teng (2001) proposed a new rational model based on fracture mechanics analysis and experimental observations. The new model properly predicts the bond resistance and the effective bond length in FRP-concrete under shear. The knowledge of the bond resistance is fundamental in anchorage strength design.

The most typical type of anchorage is end bolts. The area of the FRP plate surrounding the drilled holes is very susceptible to local rupture and should be specially reinforced. Another typical anchorage system is the use of steel plates. The steel end anchorage normally consists of U-shape plates and is bonded with the same adhesive used to bond the FRP material. Although steel anchorage is effective in the laboratory, it presents some disadvantages as steel corrosion, stress concentrations and incompatibility between steel and carbon FRP.

In order to avoid the problems with traditional procedures of anchorage, an innovative anchoring system was developed using FRP materials only. The system has been called U-anchor. The U-anchor can be used with FRP sheets and precured laminates that are unbonded or fully bonded to concrete or masonry (Khalifa (1999)). The anchorage system consists of a groove perpendicular to the longitudinal axis of the fiber, located at the end of the FRP sheet, as shown in Figure 3.7. After the FRP sheet is attached to the concrete surface and in the groove, the groove is filled half way with epoxy paste. Then an FRP bar, with a length equal to the width of the sheet, is placed in the groove and slightly pressed in place, allowing the paste to flow around the bar and cover the inside of the groove. The groove is then filled with the same epoxy paste to improve the anchorage mechanism.

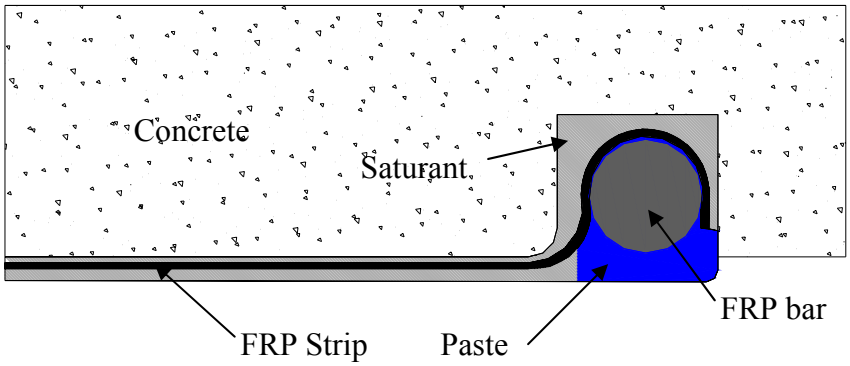

Figure 3.7 Detail of the U-anchor system (adapted from Gose and Nanni (2000)).

A viability study by Khalifa et al. (1999) showed that the U-anchor system increased the ultimate capacity of T-shape reinforced concrete beams strengthened in shear with CFRP. The CFRP is applied to the sides of the section in the form of strips with fibers perpendicular to the longitudinal axis of the beam. The RC beams were tested using four-point loading. An increase of 145% was shown over a beam with no shear reinforcement, and a 45% increase compared to a beam strengthened with CFRP but no anchor. The system provided an effective solution for cases in which the bonded length of FRP composites is not sufficient to develop its full capacity or where anchorage to adjacent members is required.

4 Assumptions in the Analysis

4.1 Description of Present Bridge and its Design

The bridge selected for strengthening was built in 1951 and is located on LA route 19 in East Baton Rouge parish. It consists of eleven 7.31 m (24 ft) simply supported spans with a deck width of 8.84 m (29 ft). Four reinforced concrete tee girders support the deck in each span. The bridge has a 7.31 m (24 ft) clear roadway width with two 3.2 m (10 ft 6 inches) traffic lanes and a 0.46 m (1 ft 6 inches) shoulder on each side, as shown schematically in Figure 4.1. Appendix A also shows some pictures of the current state of the bridge.

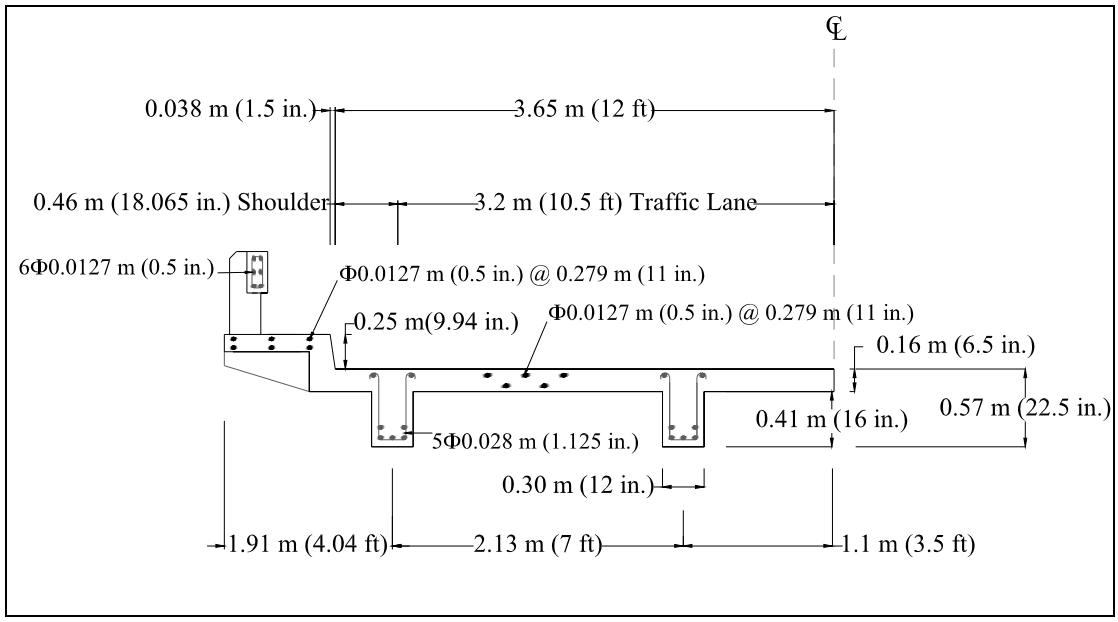

Figure 4.1 Bridge cross section with girder details.

The bridge was originally designed for an American Association of State Highway and Transportation Officials (AASHTO) H15 design loading. A schematic layout of the H15 design truck is shown in Figure 4.2. The White Bayou Bridge is weight restricted. Louisiana has a large number of weight restricted bridges. This situation can be generally attributed to different factors:

1. The original design was based on lighter loads (H15), compared to loads in use at present (HS44). The H truck load is a vehicle with two axles with a rear to front weight ratio of four (4) to one (1). The HS truck load is a vehicle with three axles and rear to front weight ratio of 4:4:1.

2. The original designs were based on codes, specifications, or stress levels that are no longer applicable.

3. Reduction of live load capacity as a result of aging, deterioration, or damage to structural members. In this case, aging was the cause of the reduction of live load capacity.

4. Increase of the dead load due to the placement of numerous layers of asphalt or concrete on top of the existing structural system.

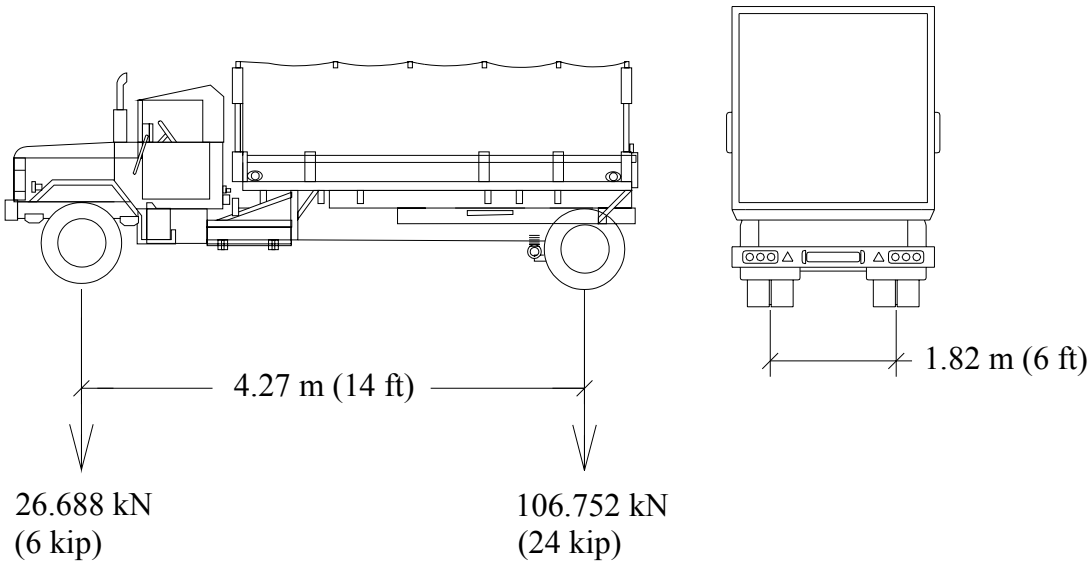

Figure 4.2 H15 design truck layout.

Concerning the situation with the White Bayou Bridge, the load restriction and load posting result in a loss of commerce and represent a nuisance to the public. These problems lead to the corresponding need of strengthening the bridge and removing the load posting. Figure 4.3 shows a lateral view of the current state of the bridge.

Figure 4.3 Lateral view of the White Bayou Bridge.

4.2 Investigated Strengthening Systems

In order to determine the optimum strengthening of the bridge, three different types of FRP strips were studied. The behavior of the bridge with one and two layers of each type of strip was modeled.

Two different systems for strengthening of the bridge were studied. The Near Surface Mounted (NSM) procedure was used with the Sika CarboDur S512, meanwhile the externally bonded procedure was used either with the Sika Wrap 103C or with the MBrace CF 530 strips. The manufacturer will provide the Sika CarboDur S512 in 50 mm (1.97 in.) wide strips, which were assume to be cut in half. Thus, three strips were cut in 2 pieces and then inserted into six grooves. Although the grooves had a width of 3.18 mm (0.125 in.) wide and 25.4 mm (1 in.) deep, only the FRP strips were modeled in ABAQUS because a perfect bond between concrete and FRP was assumed. In Figure 4.4, a schematic of the NSM system can be seen.

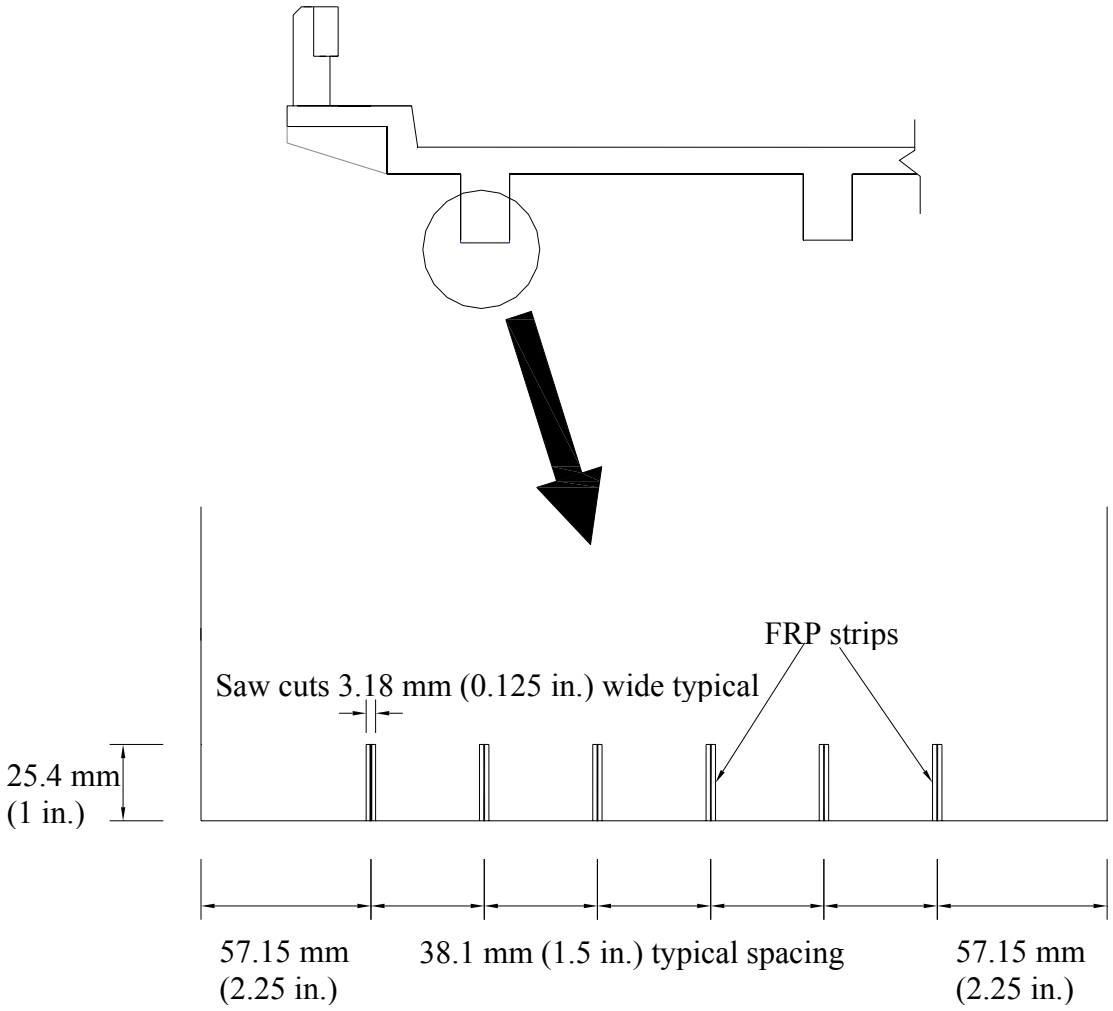

Figure 4.4 Schematic of the assumed NSM FRP system.

For the externally bonded procedure, the strips were assumed to be bonded to the bottom face of the beams across the full width of the web width and from support to

support. In Figure 4.5 their positions at the bottom of the girders can be seen. Figure 4.6 shows a layout of the different systems considered.

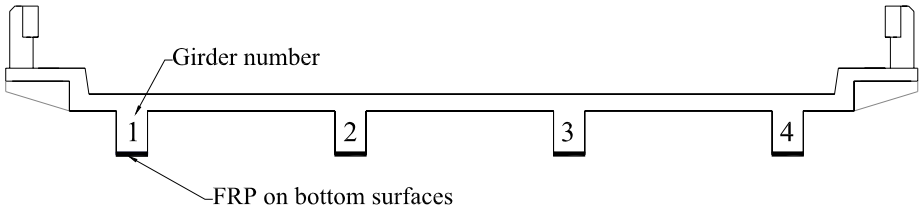

Figure 4.5 Location of FRP and beam numbering.

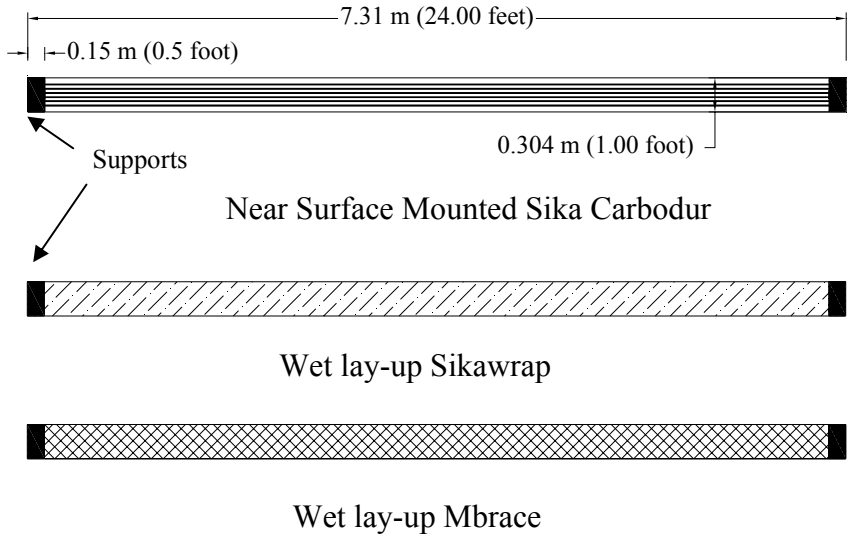

Figure 4.6 Bottom view of girders and FRP system details.

The supports have been considered as a surface 0.30 x 0.15 m (12 x 6 inch). The displacements in the vertical direction for all the supports have been restrained, meanwhile the displacement in the longitudinal direction was restricted just in one of the supports of each beam, to simulate actual conditions in the bridge.

4.3 Loading

The loads considered in this analysis were been dead and live loads. As dead loads the selfweight of the bridge and the weight of the asphalt were taken into account. Two types of trucks were considered for the live loads. A more complete explanation of the load cases and their modeling is presented in the following sections.

4.3.1 Truck Loads

Louisiana Department of Transportation and Development (LA DOTD) requires two different design truck loads to be applied as live loads. The design trucks applied are Type 3 truck with a load of 182 kN (41 ksi) and H-20-44 truck with a load of 178 kN (40 ksi). Schematic layouts for each type of design truck are shown in Figure 4.7 and Figure 4.8.

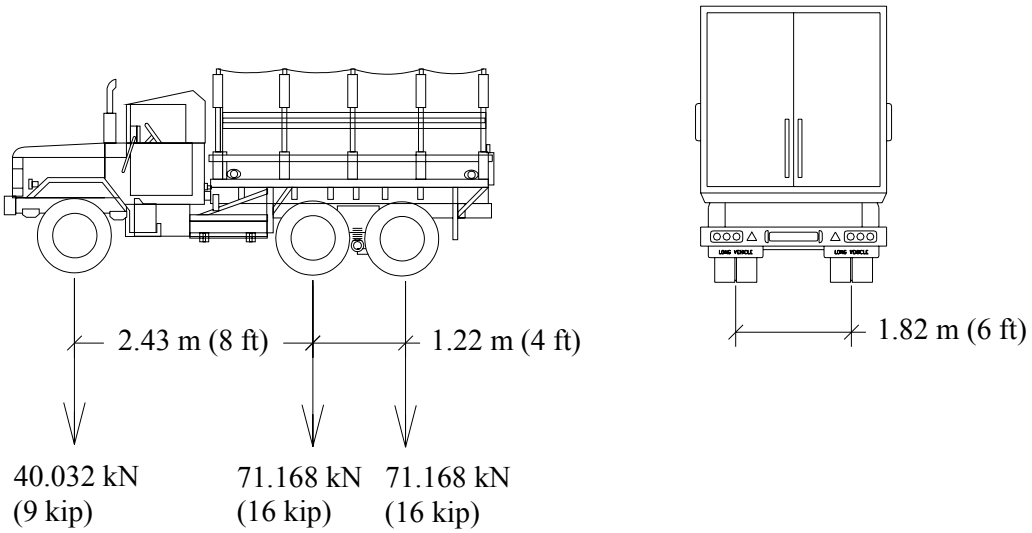

Figure 4.7 Type 3 truck load.

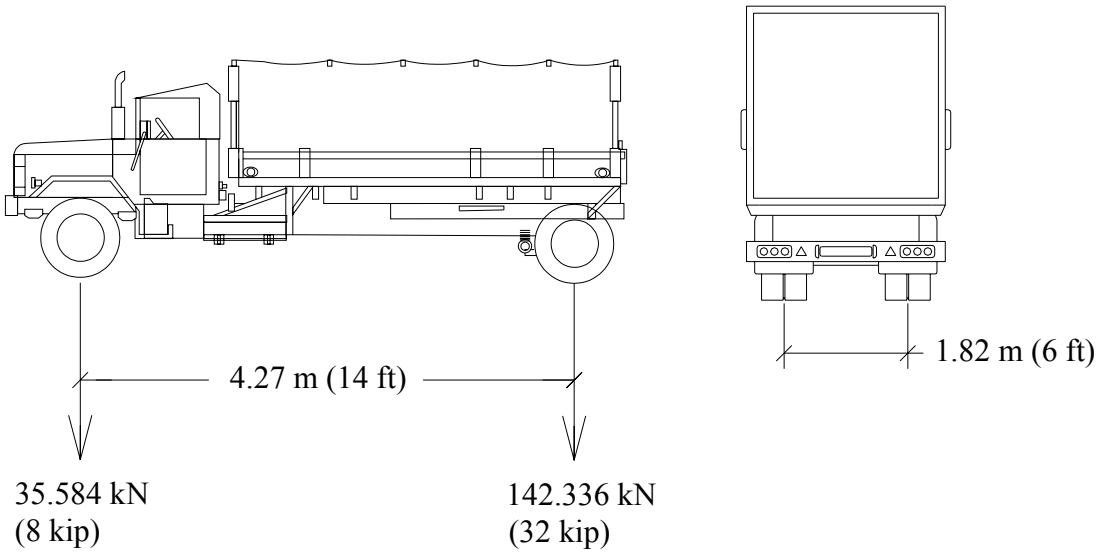

Figure 4.8 H20-44 truck load.

4.3.2 Load Pattern in ABAQUS

The weight of the asphalt was applied in the FE model as a surface load. Considering a thickness of the asphalt of 0.127 m (5 in.), the density of the asphalt is 2306 kg/m^3 (144 lb/ft^3), which made a load of 2.87 kN/m^2 (0.416 psi). It was applied on the entire slab surface.

To find the trucks' positions that create the maximum moment, as the bridge is simply supported, the loads were positioned at a certain distance from the supports and the moment was computed for different positions of the load with help of the Microsoft Excel Program. In Figure 4.9 and Figure 4.10 a sketch of the systems can be observed.

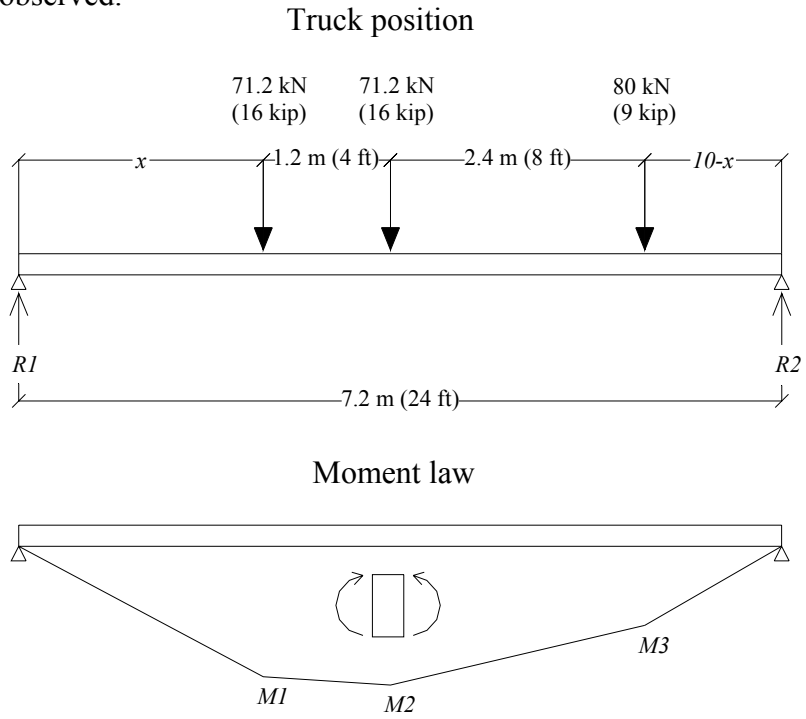

Figure 4.9 Load position and moment law for Type 3 truck load.

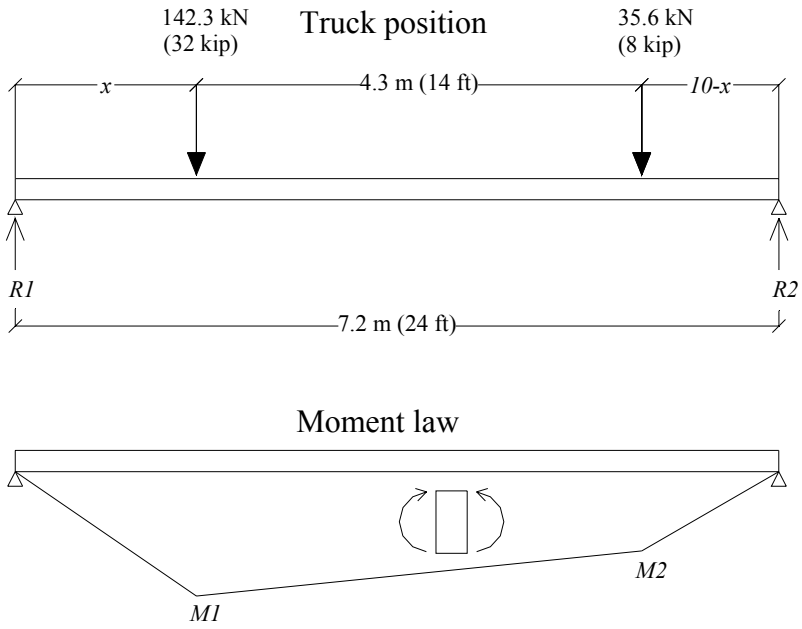

Figure 4.10 Load position and moment law for H20-44 truck load.

For the Type 3 truck load, the maximum moment is *M2* and it appears when the load is located at x = 7.9 ft. For H-20-44 truck load, the maximum moment is *M1* and it appears when the load is located at x = 10 ft.

According to the American Association of State Transportation Highway Officials (AASHTO) load-and-resistance factor design (LRFD) Bridge Design Specifications (AASHTO (2004)), the wheel load can be applied over a finite surface area of the deck in computing the load effects on a bridge deck. This area is defined as "the tire contact area". The guideline for the truck loads (area in in.^{2}) may be calculated using equations 4.1 and 4.2.

- Tire width:

$$w = \frac{P}{0.8} \tag{4.1}$$

- Tire length:

$$l = 6.4 \cdot \gamma \cdot \left(1 + \frac{IM}{100}\right) \tag{4.2}$$

Where P is the design wheel load in kip, γ is the load factor, IM is the dynamic load allowance percent. The load factor γ is 1.35 following the AASHTO specifications for live loads. The static effects of the design truck shall be increased by the dynamic load allowance percentage which, following the AASHTO specifications for components besides deck joints, was assumed to be 33 %. Table 4.1 and Figures 4.11 and 4.12 show the loads and the contact areas for both types of trucks.

Table 4.1 Loads and contact areas for Type 3 and H-20-44 trucks.

	Load P kN (kip)	Tire contact Width w mm (in.)	Tire contact length l mm (in.)	Tire contact area mm^2 (in.^{2})	Surface load (MPa) (psi)
Type 3 Truck	20.02 (4.5)	143 (5.6)	292 (11.5)	41756 (64.69)	0.48 (69.56)
	35.59 (8)	254 (10)	292 (11.5)	74168 (115)	0.48 (69.56)
H-20-44	17.80 (4)	127 (5)	292 (11.5)	37084 (57.5)	0.48 (69.56)
	71.17 (16)	508 (20)	292 (11.5)	148336 (230)	0.48 (69.56)

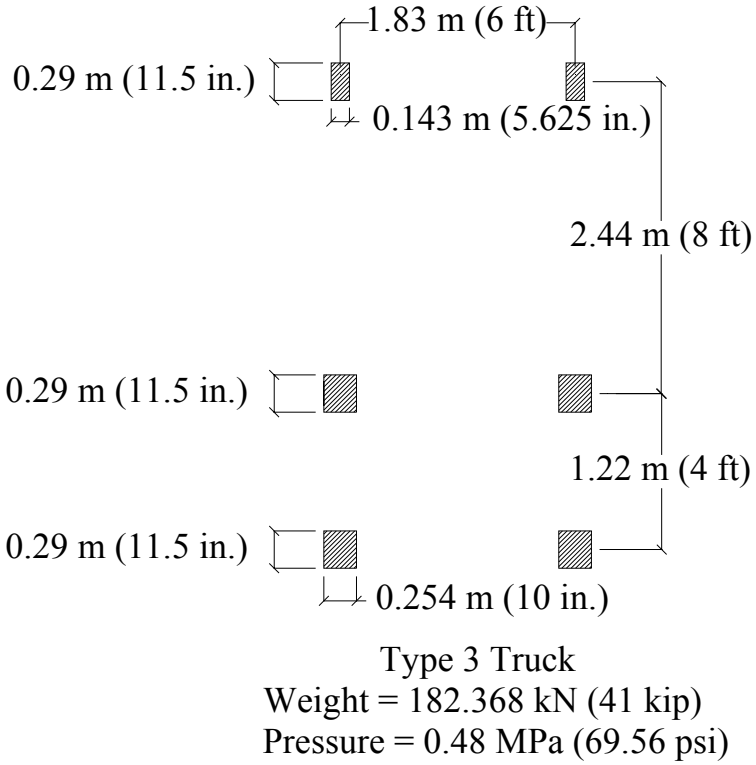

Figure 4.11 Contact areas and pressure for Type 3 truck.

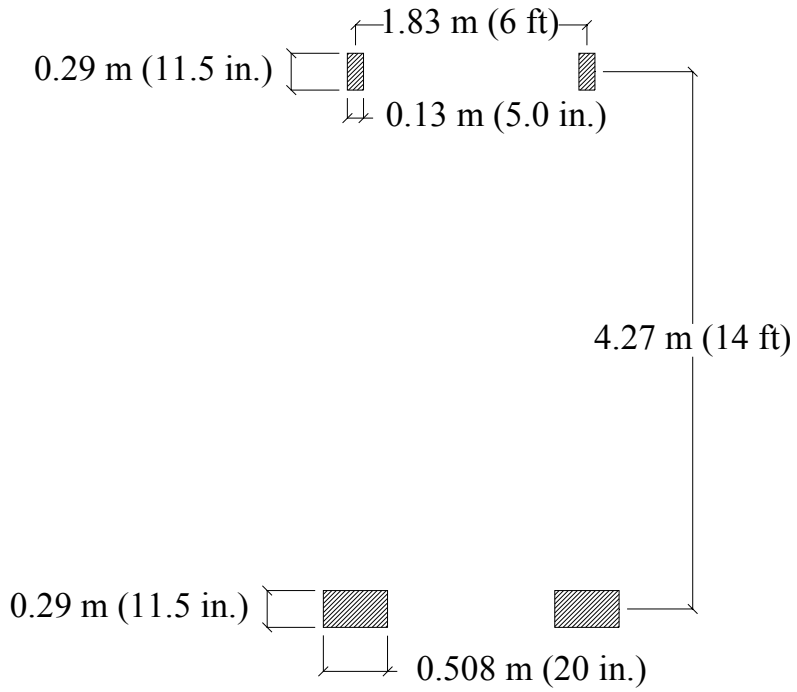

Figure 4.12 Contact areas and pressure for H-20-44 truck.

To find the final critical positions, the model was analyzed with the load in several positions. These positions can be observed in Figure 4.13.

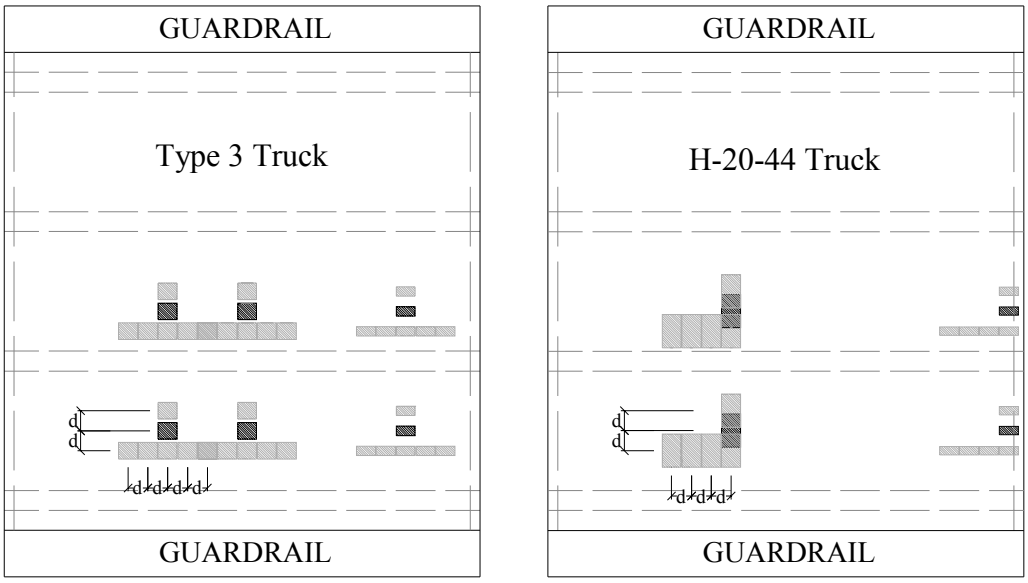

Figure 4.13 Different positions for both trucks (d = 0.30 m (1ft)).

As the supports in the bridge are modeled as a surface 305 mm x 152.5 mm (12 x 6 in.) and also the contact areas of the truck-bridge, the final critical positions are shown in Figure 4.14 and Figure 4.15. For H-20-44 since the maximum moment is reached when the truck load is located at x = 3 m (10 feet), the front axle position would be located at the deck joint. To avoid this situation, the truck load was assumed to be located at x = 2.7 m (9 feet).

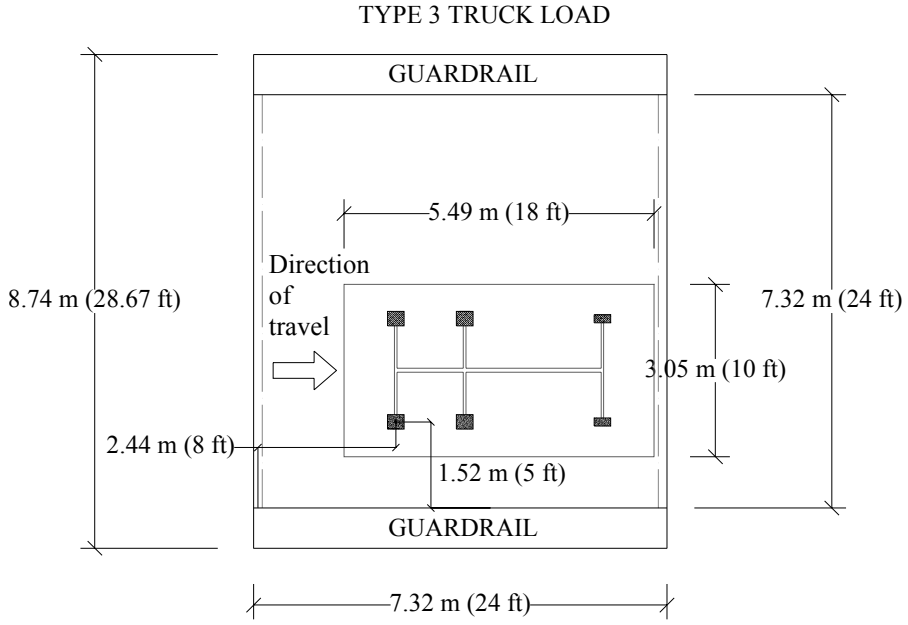

Figure 4.14 Loads positions for Type 3 truck that cause maximum deflection.

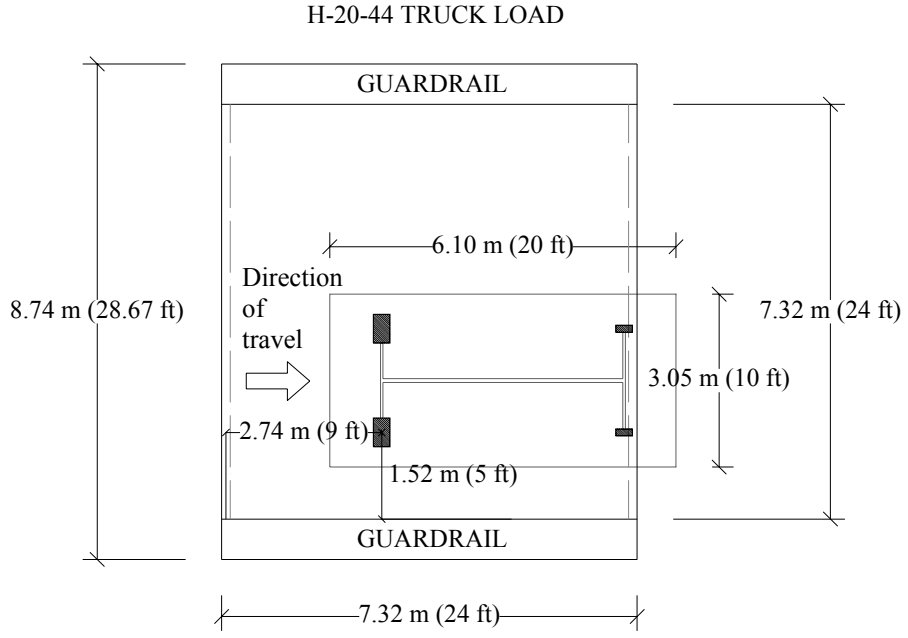

Figure 4.15 Loads positions for H-20-44 truck that cause maximum deflection.

It was necessary to analyze the bridge in the most adverse situations concerning loading. These situations were created moving the truck load over the upper surface of the deck bridge. In comparison with fixed load positions, a better overall understanding of the bridge behavior was achieved.

The specified loads were applied in critical locations to produce the maximum load effect. These situations occur when two truck loads are in the same span at the same time. Since the truck lengths are 5.5 m and 6.1 m (18 and 20 feet) long and the span length is 7.3 m (24 feet) long, it was necessary to analyze two adjacent spans in order to fit both trucks in the same model. Different positions for the trucks were analyzed, with the trucks in different lanes and opposite directions, with both trucks in the same lane and direction, with both trucks in the same lane and opposite directions.

The positions of the trucks will be defined by two distances: x = Distance from the right rear wheel to the support and y = Distance from the right rear wheel to the guardrail as shown in the figures in Appendix E. Figure 4.16 shows a sketch of the coordinate system and the positions of the trucks when the bridge is loaded with two Type 3 trucks. The coordinate system and the positions of the trucks are similar when the bridge is loaded with two H20-44 trucks. Table 4.2 and Table 4.3 show the values of the coordinates of the different positions for each truck load when the bridge is loaded with two trucks.

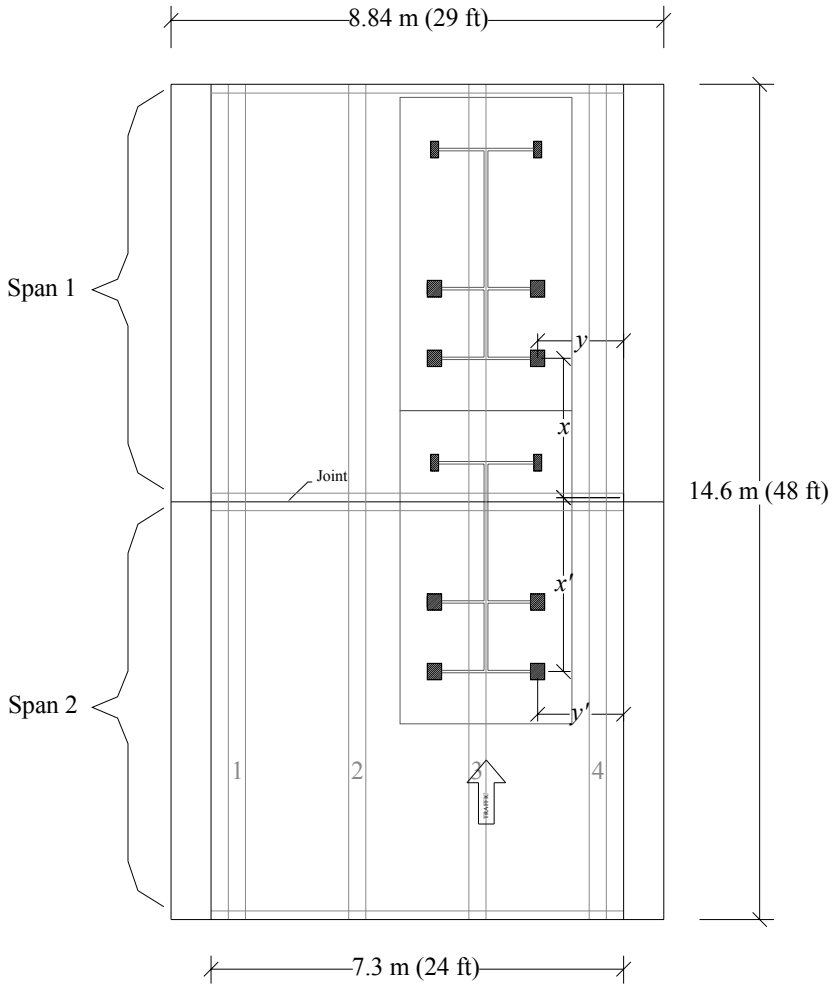

Figure 4.16 Coordinate system for loading with two trucks for Type 3 truck.

Table 4.2 Load positions for loading with two trucks for Type 3 truck.

Type 3 Truck	Position 1st Truck		Position 2nd Truck	
	x m (in.)	*y* m (in.)	*x'* m (in.)	*y'* m (in.)
Case A	2.440 (96)	1.524 (60.00)	3.048 (120.00)	1.524 (60.00)
Case B	2.440 (96)	1.524 (60.00)	0.610 (24.00)	1.524 (60.00)
Case C	2.440 (96)	1.524 (60.00)	4.724 (186.00)	4.572 (180.00)
Case D	2.440 (96)	1.524 (60.00)	3.658 (144.00)	4.572 (180.00)

Table 4.3 Load positions for loading with two trucks for H20-44 truck.

H20-44 Truck	Position 1st Truck		Position 2nd Truck	
	x m (in.)	*y* m (in.)	*x'* m (in.)	*y'* m (in.)
Case A	2.743 (108)	1.524 (60.00)	3.354 (132.05)	1.524 (60.00)
Case B	2.743 (108)	1.524 (60.00)	0.914 (36.00)	1.524 (60.00)
Case C	2.743 (108)	1.524 (60.00)	2.743 (108.00)	4.572 (180.00)
Case D	2.743 (108)	1.524 (60.00)	4.419 (174.00)	4.572 (180.00)
Case E	2.743 (108)	1.524 (60.00)	2.743 (108.00)	4.572 (180.00)

As a summary, two different types of analyses were carried for each of the strengthened and unstrenghtened cases. In the first type of analyses, one span of the

bridge was loaded with one truck of each type in different positions. In the other type of analysis, the bridge was loaded with two trucks in different positions. In this situation two spans were modeled in order to fit both truck loads.

5 FE Modeling

The finite element method is a general procedure useful to conduct a structural analysis. In the FEM, the solution of a problem in continuum mechanics is approximated by the analysis of an assembly of finite elements. The finite elements are interconnected at a finite number of nodal points and represent the solution field of the problem.

A range of engineering problems, such as stress analysis of solids to the solution of acoustical phenomena, neutron physics and fluid dynamic problems, have been solved using FEM as a powerful procedure for numerical solution of these problems. Partial differential equations can be also solved by the FEM when initial and boundary conditions are known. A brief review of previous studies on the application of the finite element method to the analysis of strengthened reinforced concrete structures is presented in this section.

Meyer et al. (1985) presented an excellent description of the theory and application of the FEM to the analysis of linear and nonlinear reinforced concrete structures. Kwak et al. (1990) also revised the FEM application to the analysis of reinforced concrete structures until 1990.

Most of the models that have been developed for strengthened bridges utilized linear elastic FEM (finite element model). Many of the FEM analyses in bridge retrofitting have been conducted through implementation of the ADINA and ANSYS 7.0 finite element computer programs, such as those carried out by Tedesco et al. (1999) and Galati et al. (2004). Some models have used the ABAQUS finite element computer program, but these have modeled beams and slabs rather than the entire bridge (Malek et al. (1998), Hormann et al. (2000)).

Ross et al. (1999) conducted a nonlinear FE analysis to confirm the results from an experimental study. Twenty-four reinforced concrete beams strengthened with CFRP plates bonded to the tension face of the beams were tested during the experimental study. All of the beams had a rectangular cross section of 200 mm x 200 mm (8 in. x 8 in.) and a length of 3.05 m (10 ft). The beams had different reinforcement ratios. The heavily reinforced beams failed by crushing of the concrete in the compression zone accompanied by horizontal cracking in the tension zone. The lightly reinforced beams failed by debonding of the CFRP plate due to failure at the CFRP-adhesive interface (failure mode 3.b). The FE analysis predicted the response of the more lightly reinforced beams very accurately. For the more heavily reinforced beams, the prediction of the response by the FE analysis was not so accurate.

Arduini et al (1997) have demonstrated the similarity between the experimental results and the numerical results obtained by finite element analysis carried out using ABAQUS. Arduini et al. (1997) focused in simulating the failure of reinforced concrete beams strengthened with FRP plates and flexible sheets with analytical and numerical problems. The numerical simulation was conducted in accord with the theory of the smeared crack approach. The numerical results showed good accordance to the experimental results in terms of load-deflection response, load-FRP strain response and evolution of cracks.

Although FRP has been modeled as a linear elastic material in most of the models using FEM, few models considering the nonlinearity of the FRP in their in-plane shear stress-strain relation have been developed. Hu et al. (2004) used the finite element program ABAQUS to examine rectangular reinforced concrete beams strengthened by FRP. A failure analysis was performed simulating non linear behavior of reinforced concrete and FRP. The beams were modeled with different beam lengths and reinforcement ratios. Analyses with the unstrengthened beams and with the FRP attached to the bottom face of the beams were carried out. Also beams strengthened by FRP on both sides were modeled. The results showed that the length of the beam did not affect the behavior of the beams with high reinforcement ratio and strengthened with FRP at the bottom; however, the length affected beams with low reinforcement ratio that were strengthened with FRP on the bottom.

Concerning cracks, the FE analysis by Hu et al. (2004) showed how the reinforcement ratios affect the location of the cracks for the beams strengthened with FRP at the bottom. The beams with high reinforcement ratios would have more cracks at the central region than those with low reinforcement ratios. Meanwhile beams with low reinforcement ratios would have more cracks at the support area than those with high reinforcement ratios.

Hu et al. (2004) verified the dependence of the ultimate load on the fiber angle for short beams strengthened by FRP on both sides, with different fiber angle θ. The fiber angle of the lamina was measured counterclockwise from the midsurface of the beams. The optimal fiber angle seems to be 0° not depending on the reinforcement ratio and the numbers of FRP layers. On the other hand, increasing the ultimate load in long beams strengthened by FRP on both sides, when the FRP layer numbers is small, seems to be less dependent on the fiber angle θ.

The interaction at concrete-FRP interface has become an important issue in the study of externally bonded FRP materials to reinforced concrete beams. An approximation of the interfacial stresses can be modeled as spring reactions. Ascione et al. (2005) performed an FE analysis using a mechanical model where the FRP plate was assumed to be bonded to the concrete core by continuous distributions of bilateral elastic springs. A simplified procedure for verifying the interfacial stress state was also presented. The FE model accurately predicted the stress state at the interface between concrete core and reinforced plate.

In this section the model used in the FE analysis is explained. After explaining the assumed properties of the materials involved in the FE analysis, the models used in the FE analysis for each material are expounded. Following this, the structural model of the FE analysis and a convergence studied carried are explained.

5.1 Materials and construction

Reinforced concrete was the material used in the construction of the White Bayou Bridge. In this chapter the assumed properties of all the materials involved in the strengthening of the bridge are exposed, as well as the materials involved in the construction.

In Table 5.1 the guessed properties of the concrete and reinforcing steel used for the analysis are shown:

Table 5.1 Guessed materials properties of concrete and steel for the FEM model.

Material	Elastic Modulus MPa (ksi)	Ultimate Strength MPa (ksi)	Ultimate Strain
Concrete	29165 (4230)	37.9 (5.5)	0.0028
Steel	200000 (29000)	207 (30.0)	0.0090

5.1.1 Concrete

As the bridge was built in 1951 there is not much information regarding the concrete material properties in the bridge.

For the FE anlysis, the concrete was assumed to have an elastic modulus of 29,2 MPa (4,230 ksi) and a compressive strength of 37.9 MPa (5.5 ksi). In Figure 5.1, the assumed stress-strain relationship in the concrete is shown. It was assumed that the concrete has a bi-linear behavior.

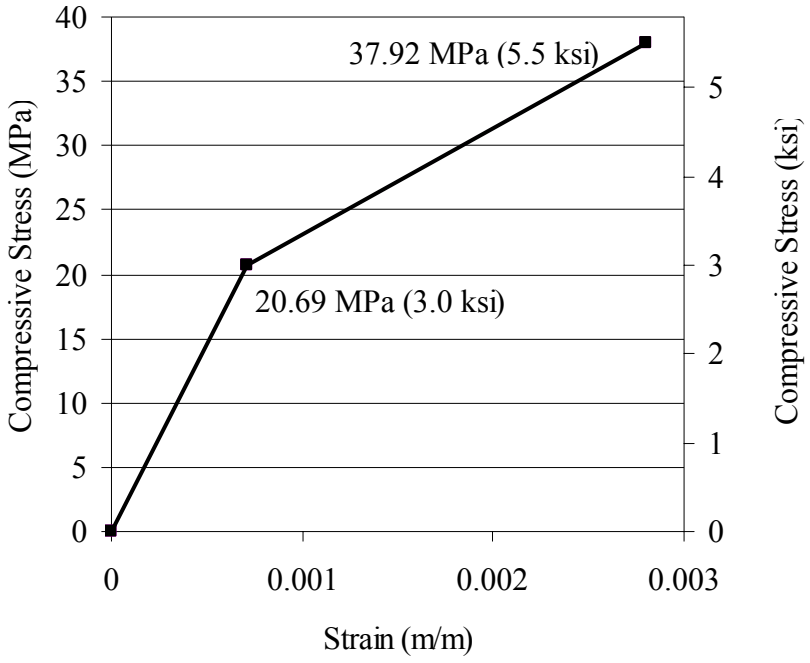

Figure 5.1 Assumed stress-strain curve for the concrete in compression used in the FEM analysis.

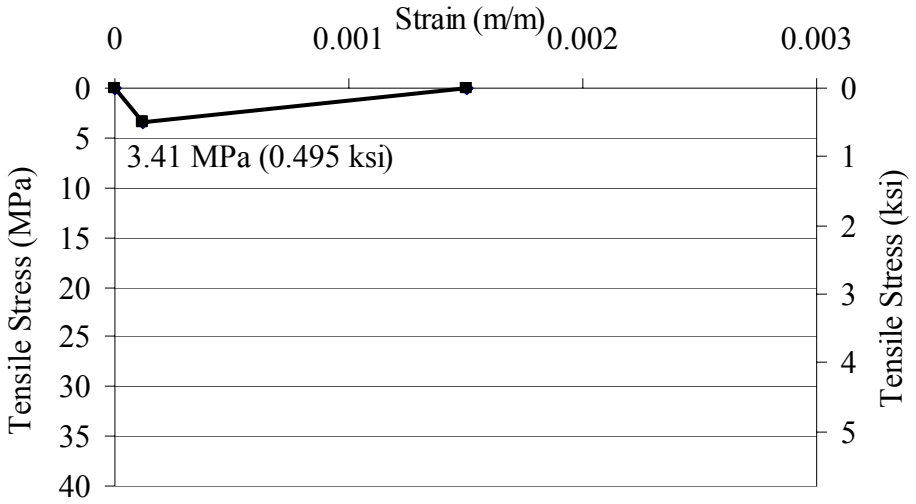

Figure 5.2 Assumed stress-strain curve for concrete in tension used in the FEM analysis.

5.1.2 Steel

As for the concrete, there was very little information regarding properties of the reinforcement material in the bridge.

For the FE model, the material constituting the internal steel rebars was assumed to behave ideally elastic-plastic, as shown in Figure 5.3. The steel was assumed to have an elastic modulus of 200000 MPa (29000 ksi) and a tensile strength of 200 MPa (29 ksi). Futhermore, the steel was assumed to be a strain hardening plastic material.

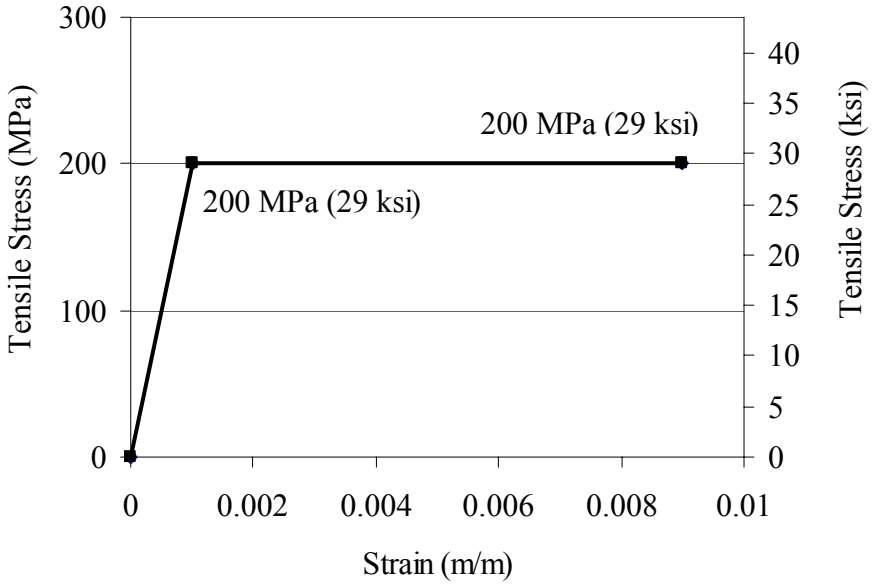

Figure 5.3 Assumed stress-strain curve for reinforcement bars used in the FEM model.

5.1.3 Fiber Reinforced Polymer Strips

FRP materials are microscopically inhomogeneous and anisotropic. Thus, their mechanics are more complex than conventional materials'. Mallick (1988) presents two different approaches in the mechanics or FRP materials:

1. The micromechanics approach, in which the interaction of the constituent materials is examined on a microscopic scale.

2. The macromechanics approach, in which the interaction of the constituent materials is examined on a macroscopic scale.

In this research, a simple macromechanics approach was followed. The FRP material was assumed to be homogeneous, linearly elastic and orthotropic. 2-D analysis was considered because the FRP strips have two dimensions much larger than the third one. It was assumed that the FRP strips do not present bending stiffness and the stresses in the out of plane direction were neglected. Figure 5.4 shows a sketch of the stresses in an orthotropic lamina under a plane stress condition. Equations of orthotropic elasticity are used to define the materials properties:

$$\varepsilon_{xx} = \varepsilon_{11} = \frac{\sigma_{xx}}{E_{11}} - \nu_{21} \cdot \frac{\sigma_{yy}}{E_{22}} \tag{7.1}$$

$$\varepsilon_{yy} = \varepsilon_{22} = \frac{\sigma_{yy}}{E_{22}} - \nu_{12} \cdot \frac{\sigma_{xx}}{E_{11}} \tag{7.2}$$

$$\gamma_{xy} = \gamma_{yx} = \gamma_{12} = \gamma_{21} = \frac{\tau_{xy}}{G_{12}} \tag{7.3}$$

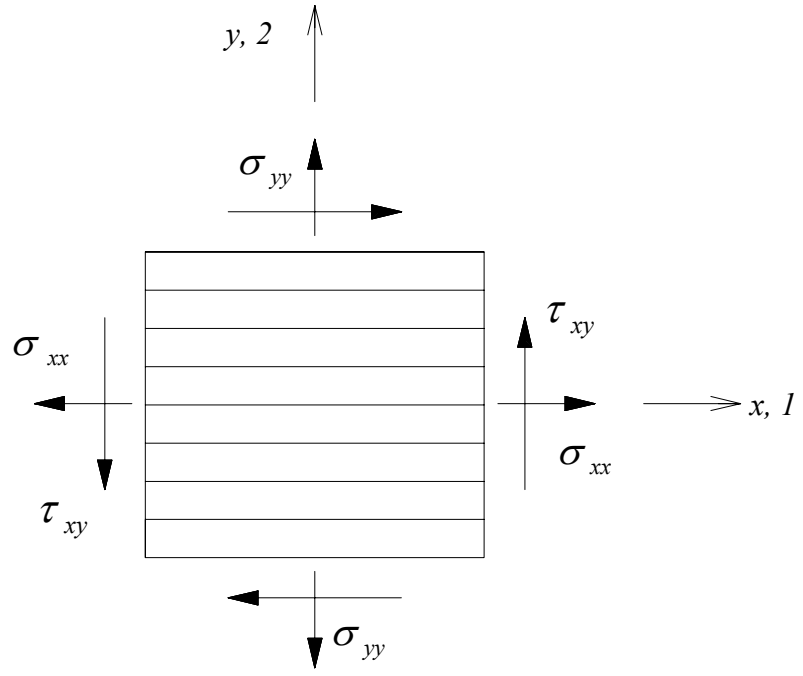

Figure 5.4 Stresses in an orthotropic lamina under a plane stress condition.

Three different types of strengthening have been considered in the analyses.

- Carbodur: NSM procedure for installing SIKA Carbodur S512 strips.
- SikaWrap: Wet lay-up procedure with SikaWrap 103 C fiber fabrics embedded in a matrix of Sikadur Hex 300 Epoxy. The fabrics embedded in the epoxy matrix will form what will be named the SikaWrap strips.
- Mbrace: Wet lay-up procedure with Mbrace CF 530 fiber fabrics.

Two of them are manufactured by SIKA and the other one is manufactured by Degussa Construction Quemicals (Sika, Version 3.0). The Near Surface Mounted (NSM) procedure is used to install the SIKA Carbodur. The SikaWrap 103 C and the MBrace CF530 are fabrics of fibers for wet lay-up systems

The Carbodur strip has an elasticity modulus of 165 GPa (23900 ksi) and a tensile strength of 2.8 GPa (405 ksi). The SikaWrap strip has an elastic modulus of 65 GPa (9447 ksi) and a tensile strength of 0.7 GPa (104 ksi). The Mbrace fabric has an elastic modulus of 372 GPa (54000 ksi) and a tensile strength of 3.5 GPa (510 ksi). The properties of strips used in the FE analysis are given in Table 5.2 and Figure 5.5.

Table 5.2 Strip properties from manufacturer's data (Sika, Version 3.0).

Commercial Material	Width mm (in.)	Thickness mm (in.)	Elastic Modulus GPa (ksi)	Tensile Strength GPa (ksi)	Ultimate Strain m/m
Carbodur strips	50 (1.97)	1.15 (0.047)	165 (23900)	2.8 (405)	0.0169
SikaWrap strips	30.5 (12)	1.01 (0.040)	65 (9447)	0.7 (104)	0.0110
MBrace fabrics	30.5 (12)	0.16 (0.0065)	372 (54000)	3.5 (510)	0.0094

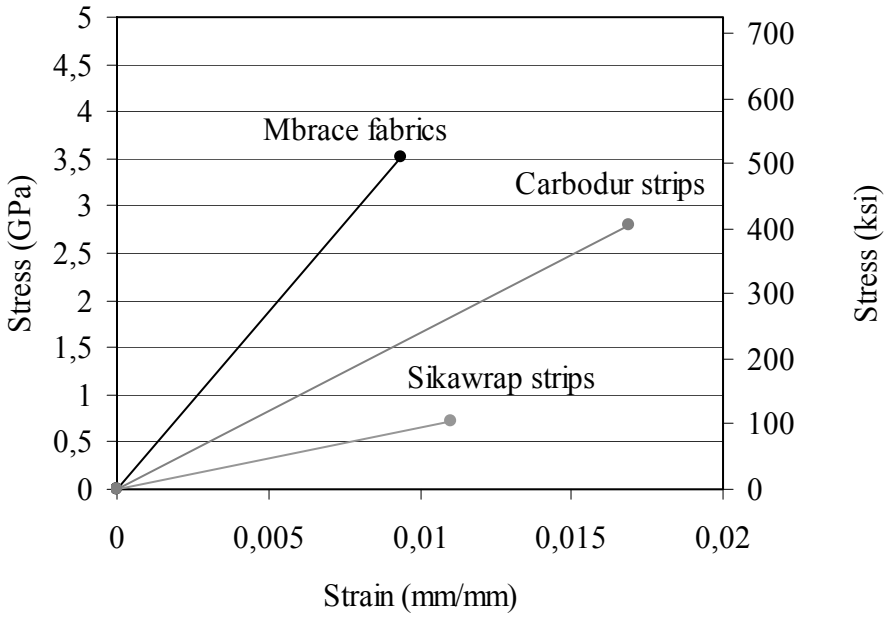

Figure 5.5 Stress-strain diagrams for the strips.

5.2 Analytical Model in ABAQUS

In this section the element types used for modeling the different materials used in the analysis are explained, followed by a brief explanation of how a FE analysis is defined in ABAQUS

5.2.1 Element Types

The materials used in the analyses involved reinforcing steel, concrete and FRP. Reliable constitutive models for strengthening steel and concrete are available in the ABAQUS material library

5.2.1.1 Concrete

The smeared crack concrete model in ABAQUS was used. It provides a general capability for modeling concrete in all types of structures, and it was intended primarily for the analysis of reinforced concrete structures. It uses concepts of oriented damaged elasticity (smeared cracking) and isotropic compressive plasticity to represent the inelastic behavior of concrete (ABAQUS Version 6.4).

ABAQUS uses a type compression surface together with a crack detection surface to model the failure surface of concrete. Figure 5.6 shows the concrete failure surface in plane stress. When the principal stress components of concrete are predominantly compressive, the response of the concrete is modeled by an elastic-plastic theory with

an associated flow law and an isotropic hardening rule. The crack detection surface defines when a crack is going to form in tension. When the first crack is detected, then ABAQUS uses the damaged elasticity theory to model the crack.

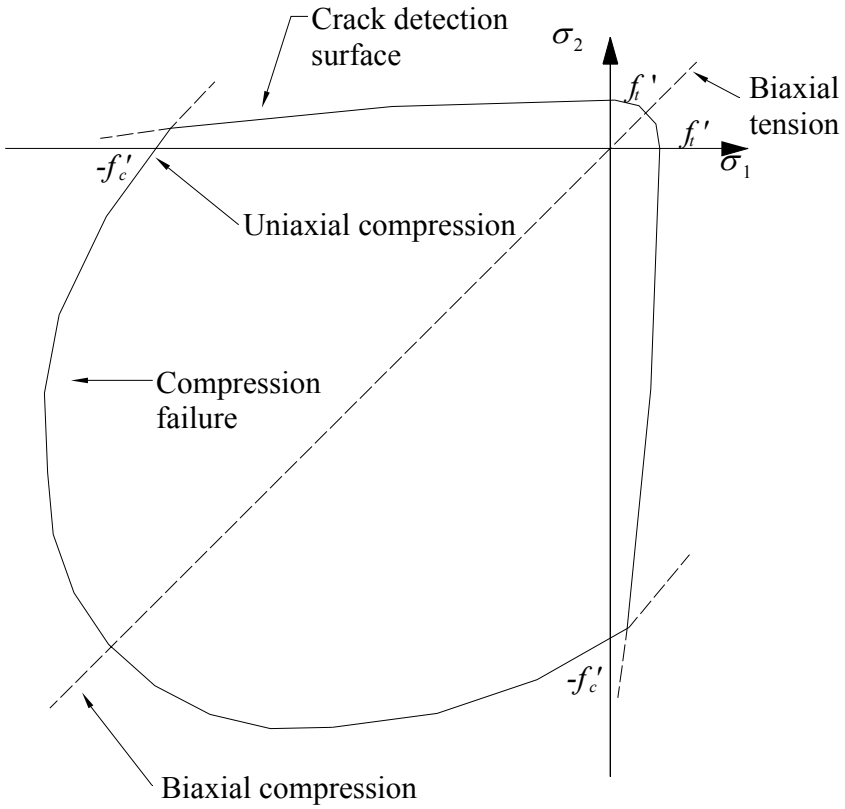

Figure 5.6 Concrete failure surface in plane stress (adapted from ABAQUS Version 6.4).

Hu et al. (2004) give a complete explanation of the damaged elasticity model. When cracking of concrete takes place, a smeared model (smeared crack approach) was used to represent the discontinuous macrocrack behavior. The behavior of the crack is "smeared out" over the elements and the material behavior is modeled by continuum constitutive relations for the material including cracks. The smeared crack approach is based in the non-linear fracture mechanics models generally used for concrete.

The smeared crack model represents spaced cracks perpendicular to the principal stress direction. The effect of a discontinuity is smeared out to a strain over a certain width. The crack spacing was computed following Eurocode 2, see Appendix B. The crack spacing in the structure was 6 in. (152.4 mm) and the element length chosen was also 6 in. (152.4), thus this led to the assumption that length of one crack is distributed over the element.

The concrete option in ABAQUS requires the "tension stiffening" option. This option was used to model the behavior of the cracked regions. The average stiffness of a cracked region exceeds that of a cracked section. Furthermore, a crack can transfer stresses during its formation. This effect is called tension stiffening. The tension stiffening effect was taken into account by increasing the strain values in the traction-

strain relations for the concrete. Figure 5.7 shows a graph of the tension stiffening effect used to model the concrete. The value of the strain ε^* at which the tension stiffening stress reduced to zero was 0.0015.

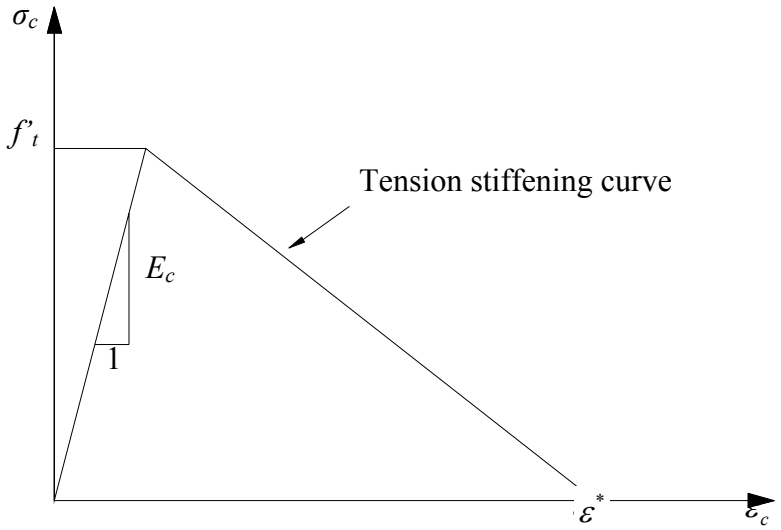

Figure 5.7 Tension stiffening model (adapted from ABAQUS Version 6.4).

5.2.1.2 Reinforcing Steel

ABAQUS material library recommends embedded surface elements in the model used with concrete to model steel reinforcement. Each layer of reinforcement was modeled as a surface element. In these surfaces, the reinforcement was defined by the cross-sectional area of each rebar, rebar spacing in the plane of the surface element, position and orientation of each layer of steel rebars.

The surface elements were embedded in the concrete model by means of the 'Embedded Element option". With this modeling approach, the reinforcement does not have separate degrees of freedom and complete interaction was assumed. In the cracked element the forced in the reinforcement is transferred to the concrete in the next element. The elements along a reinforcement bar show a stiffness that corresponds to a cracked section. As explained before, the average stiffness of a cracked region exceeds that of a cracked section (tension stiffening effect). With the embedded reinforcement concept, the whole cracked tensile region has the lower stiffness, corresponding to the crack sections, which results into a some extent too low overall stiffness of the structure (Plos (2000)). The tension stiffening effect was taken into account through the "tension stiffening" option in the implementation of the properties of the concrete.

The surface elements containing the beam reinforcement have been placed 66.7 mm (2.625 in.) and 142.9 mm (5.625 in.) from the bottom surface. The deck reinforcement has been placed 320 mm (1.25 in.) from both upper and bottom deck surfaces, with a distance between bars of 280 mm (11 inches). The beam and deck reinforcement location in the FE model can be observed in Figure 5.8.

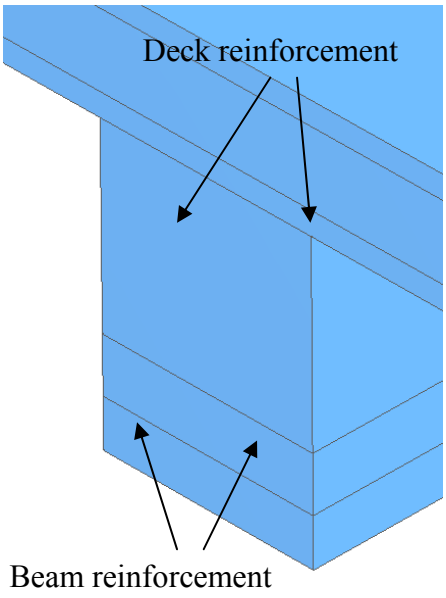

Figure 5.8 Beam and deck reinforcement in FE model.

5.2.1.3 FRP

As the FRP material has been assumed to behave as a linearly elastic and orthotropic material, a "lamina" option for the elastic behavior of the material was chosen. Tests carried out by Lamanna (2002) proved these statements. For this type of material, ABAQUS requires the longitudinal, transverse and shear modulus of elasticity. All this data was provided by the manufacturer for the SikaWrap 103 C, meanwhile for the SikaCarboDur S512 the only data provided was in the longitudinal direction. In the case of MBrace CF530, the manufacturer provided the longitudinal and transverse modulus of elasticity, but not the shear modulus. As the "lamina" option requires all this data, the data finally assumed based on the average properties of carbon fibers is shown in Table 5.3.

For the near surface mounted system, the strips were modeled in the same way as the reinforcing steel was. Meanwhile the reinforcing steel was modeled with surface elements and the FRP strips were modeled using membrane elements. Membrane elements represent thin surfaces in space that offer strength in the plane of the surface, but have no bending stiffness.

An ABAQUS tool called "Skin Reinforcement" was used to model the FRP strips externally bonded to the beams. This tool defines a skin that is perfectly bonded to the surface of an existing part and specifies its engineering properties. Each skin is defined by a surface, a section name and material orientation.

Table 5.3 Elastic properties of FRP strips assumed in the FE analyses.

Commercial Material	Longitudinal Elastic Modulus MPa (ksi)	Transverse Elastic Modulus MPa (ksi)	In-plane Shear Modulus MPa (ksi)	Out-of-plane Shear Modulus MPa (ksi)	Poisson's Ratio
Carbodur strips	164790 (23900)	6895 (1000)	3448 (500)	6895 (1)	0.2
SikaWrap strips	65137 (9447)	3973 (577)	2394 (347)	6895 (1)	0.2
MBrace fabrics	372330 (54000)	6895 (1000)	3448 (500)	6895 (1)	0.2

Each skin is defined by a surface and a section. The properties of the FRP strips are defined in the section. As long as only one skin can be placed on a surface of an element (skins cannot overlap), to model the cases for 2 layers of strips, the same section used for 1 layer cases was applied, but doubling the value for the thickness of the section.

5.2.2 Steps

A Finite Element (FE) analysis is defined in ABAQUS by:

- dividing the problem history into steps;
- specifying an analysis procedure for each step; and
- prescribing loads, boundary conditions, and output requests for each step.

The step sequence provides a convenient way to capture changes in the loading and boundary conditions of the model; it was defined as having two steps:

- Initial Step: When the boundary conditions and the dead loads (the selfweight and the weight of the asphalt) were applied. It was subdivided into 10 smaller steps in order to follow the response during the application of the load.
- Step One: The loads were applied. This step was defined as a general static step. It has also been subdivided into 10 smaller steps.

The "Step" tool in ABAQUS distinguishes between general nonlinear steps and linear perturbation steps. General nonlinear analysis steps define sequential events: the state of the model at the end of one general step provides the initial state for the start of the next general step. It can be used to analyze linear or nonlinear problems. Linear

perturbation analysis steps provide the linear response of the model about the state reached at the end of the last general nonlinear step and can be used only to analyze linear problems. The General nonlinear analysis steps were used in analyzing the bridge behavior in this study.

5.3 Structural Model

A three dimensional FE model was constructed for analysis of the bridge using a combination of finite elements. An isometric view of the FE model is shown in Figure 5.9. The FE analysis was conducted through implementation of the ABAQUS finite element computer program.

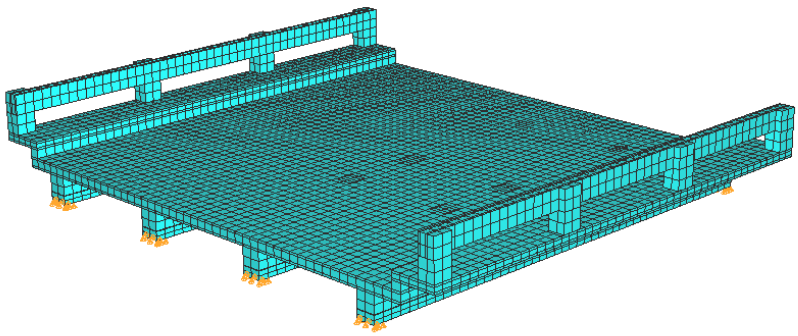

Figure 5.9 Isometric view of the finite element model of the bridge.

To create the composed sections of the bridge, three different models for the three materials were adopted from the ABAQUS library. A solid homogenous model was used for concrete. ABAQUS documentation recommended using surfaces to model the steel rebars. Each of the surfaces created contains one layer of reinforcement. This surface layer interacted with the concrete upon a tool called Embedded Element. A tool called "Skin reinforcement" was used for the FRP strips. These strips were modeled as surfaces, each with its respective thickness.

5.3.1 Assumptions

To model the bridge and the different strengthening systems some assumptions were made:

1) The concrete acts in a bi-linear behavior.

2) A linearly elastic and plastic behavior was chosen for the material constituting the internal steel rebars.

3) A linearly elastic model was used to model the three different types of FRP plates.

4) The concrete span is simply supported.

5) A perfect bond was assumed between the FRP strips and the concrete.

6) The bridge was not supposed to fail during the analysis.

5.3.2 Mesh

Three types of elements were used to mesh the bridge in all of the models: A 20-node quadratic brick with reduced integration (C3D20R) was used for modeling the concrete. The steel reinforcement was modeled using an 8-node quadrilateral surface element (SFM3D8). For the Near Surface Mounted system, the FRP strips were modeled using membrane elements (M3D8R). Membrane elements represent thin surfaces in space that offer strength in the plane of the surface, but have no bending stiffness. The externally bonded FRP strips were modeled with an 8 node quadrilateral doubly curved thick shell element (S8R). The shell elements were attached to the bottom surface of the concrete beam directly and perfect bonding between FRP and the concrete was assumed. In Figure 5.10 the elements used to mesh the bridge are shown.

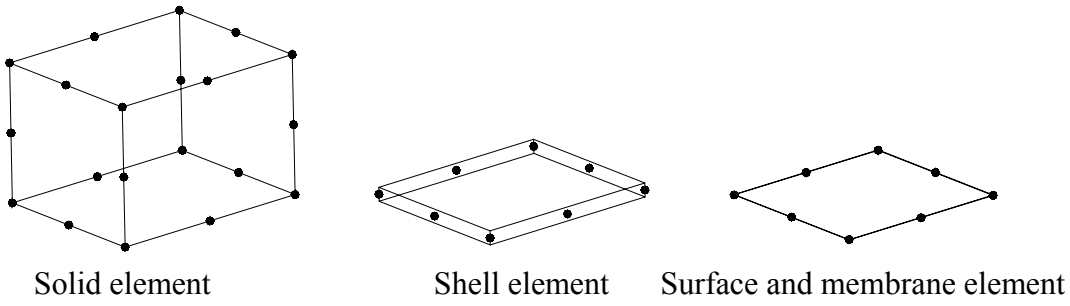

Figure 5.10 Isometric view of the elements used to mesh the bridge.

A total of 11344 elements were used in the FE analysis. 4412 elements were used to model the concrete. 6912 elements were used to model the reinforcing steel. The surfaces where the load was applied were modeled with 20 elements. The element length was considered to be 6 in. (152.4 mm).

5.4 Convergence Study

In order to verify the process and the calculations carried out with the Finite Element program ABAQUS, some hand calculations were made. It was assumed that Beam 3 and the corresponding portion of slab worked as a simply supported beam. Figure 5.11 shows a sketch of the corresponding section. A Type 3 truck load was applied (see Section 6.2 Truck loads). The position chosen for the convergence study was the one that cause maximum moment as explained in Section 6.2. Figure 5.12 shows the position where it was applied for the convergence study.

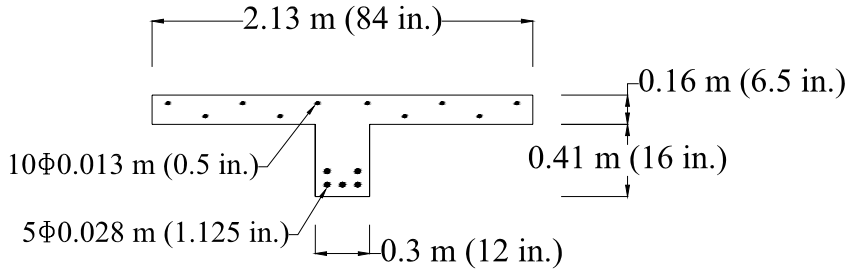

Figure 5.11 Slab and beam cross section assumed in the hand calculations.

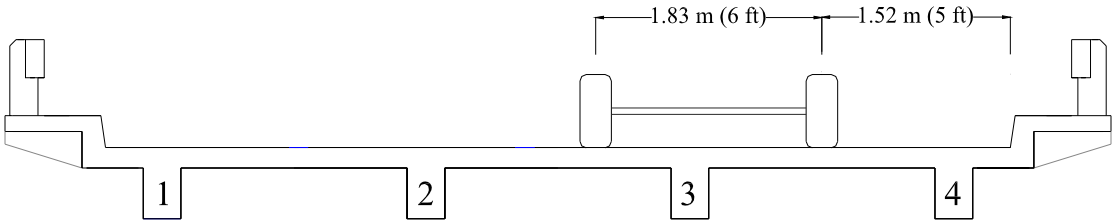

Figure 5.12 Cross section of the bridge deck and assumed load case in the hand calculations.

Assuming that the studied Beam 3 takes 30 % of the truck load, the hand calculations of midspan deflection are shown in the Appendix B (Leet (1989)). It gives a value of 1.27 mm (0.05 in.). The corresponding midspan deflection in the FE analysis was 1.123 mm (0.044 in.). Comparing the results, the deflection in the FE analysis was 0.17 mm (0.006 in.) less than the hand calculations; however, taking into account the difference between the models, it can be concluded that the ABAQUS FE analysis provides a reasonable result.

A convergence study was performed to determine if the mesh size of the final model was accurate enough with a convenient computational time.

Cases with different number of elements were studied (531, 911, 1436, 2710 and 11344 elements). The deflection at midspan on Beam 3 was compared in the different cases. Increasing the number of elements used in the model, an improved solution is reached, but the computational time also increases. A total of 11344 elements have been chosen to model the bridge, although the computational time increased in 150 % compared to the case with 2710 elements. Figure 5.13 shows the number of elements, the computational time, and also the result of the deflection at the center of Beam 3.

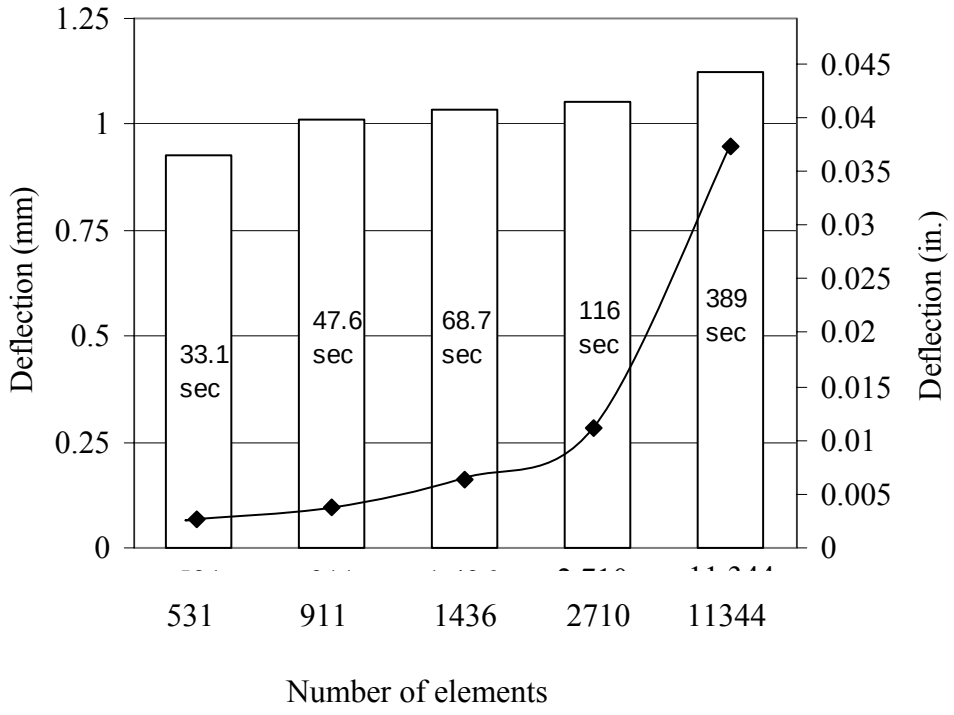

Figure 5.13 Convergence study comparison.

6 Analysis of Bridge Performance

6.1 Results from FE Analysis

Four different cases were analyzed to study the effects of various strengthening alternatives. An unstrengthened span of the bridge was the first case studied in order to provide a base to compare with. The other cases studied concerned the different strengthening procedures.

As explained in Section 6.2, two different types of analyses were carried for each of these cases. In the first type of analyses, one span of the bridge was loaded with one truck of each type in different positions. In the other type of analysis, in order to analyze a more realistic situation, the bridge was loaded with two trucks in different positions. In this situation two spans were modeled in order to fit both truck loads.

6.1.1 One Truck Loading

The models were run with the truck loads in the positions shown in Figure 6.7. The different positions were defined by two coordinates: x = distance between the rear axle and the left support and y = distance between right rear wheel and the guardrail. Figure 6.1 shows a sketch of a truck and definition of the coordinates. The methodology for Type 3 truck load and for H20-44 truck load was the same. As the results for Type 3 truck load and H20-44 truck load are quite similar, in this section only results for Type 3 truck load are shown. The maximum deflection at the midspan of the bridge was caused by the same load position for all the analyzed cases. Figure 4.14 and Figure 4.15 showed the positions that caused the maximum deflection.

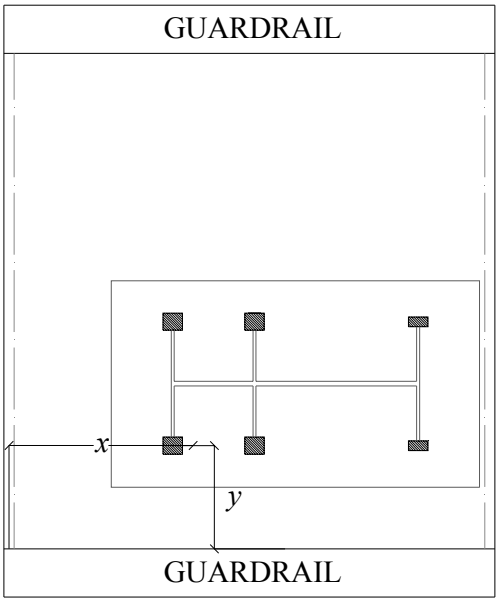

Figure 6.1 Coordinate system defining the load positions.

6.1.1.1 Unstrengthened Bridge

After running the model for the unstrengthened bridge with the loads in the different positions, the largest deflection appeared at midspan in Beam 3 when the Type 3 truck was applied at x = 2.44 m (8 feet) and y = 1.52 m (5 feet). The maximum deflection appeared at 3.352 m (132 in.) from the support in Beam 3 when H20-44 truck was applied at and x = 2.74 m (9 feet) and y = 1.52 m (5 feet) for H-20-44 Truck. The critical positions of the trucks are shown in Figure 6.8 and Figure 6.9. The corresponding maximum deflections of each beam are shown in Figure 6.2 for a Type 3 truck. The corresponding deflections for an H-20-44 truck are similar.

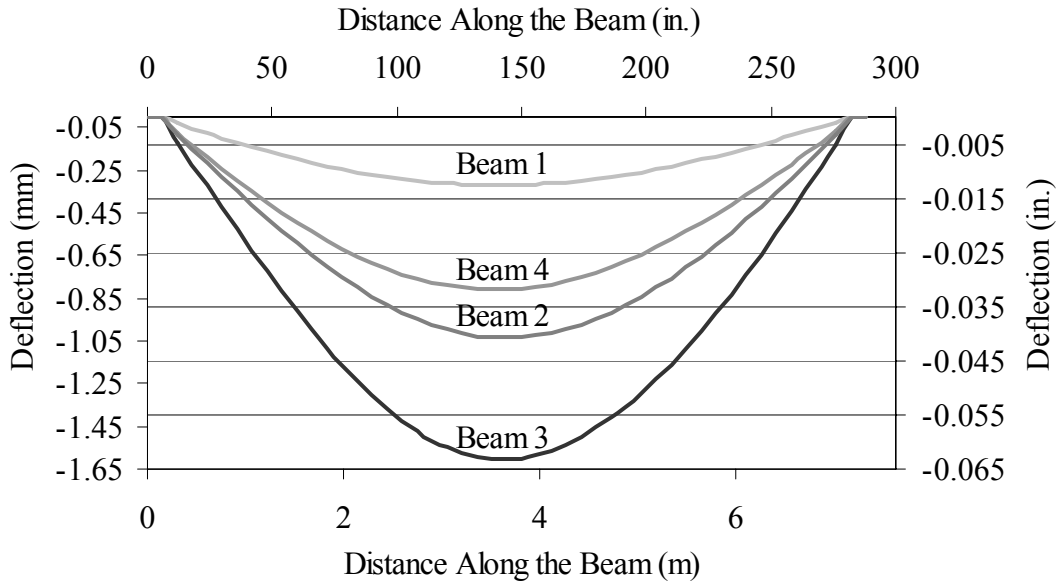

Figure 6.2 Deflection along the beams for Type 3 truck load.

Figure 6.3 shows the maximum principal stresses in the concrete for a Type 3 truck load. The maximum tensile stress in the concrete is 3.41 MPa (494.96 psi) and maximum compressive stress is 1.36 MPa (197.73 psi). The maximum stresses appeared in a section at a distance of 3.5 m (138 in.) from the left support of Beam 3. The maximum tensile stress in the steel elements was 21.47 MPa (3133.6 psi). The maximum stresses values are under the strength of concrete and steel. Table 6.1 shows the maximum values of the flexural stresses. Figure 6.4 shows an isometric view of the deflection of the bridge when the Type 3 truck load is applied.

Table 6.1 Concrete maximum stresses for Type 3 truck load.

	Maximum tensile stress MPa (psi)	Maximum compressive stress MPa (psi)
Flexural stresses in concrete	3.41 (494.96)	1.36 (197.73)
Stresses in reinforcing steel	21.47 (3133.6)	-

The maximum tensile stress in the concrete was below the tensile strength of concrete, 3.42 MPa (495 psi). This result leads to the conclusion that the concrete did not crack. This situation was possible because the model of the bridge was not loaded until failure.

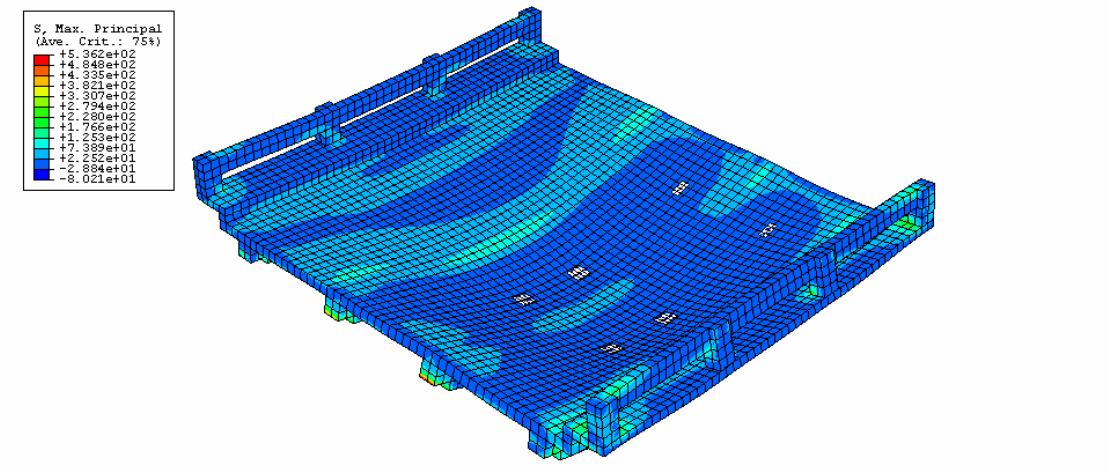

Figure 6.3 Maximum principal stresses in the concrete when the span is subjected to Type 3 truck and dead loads.

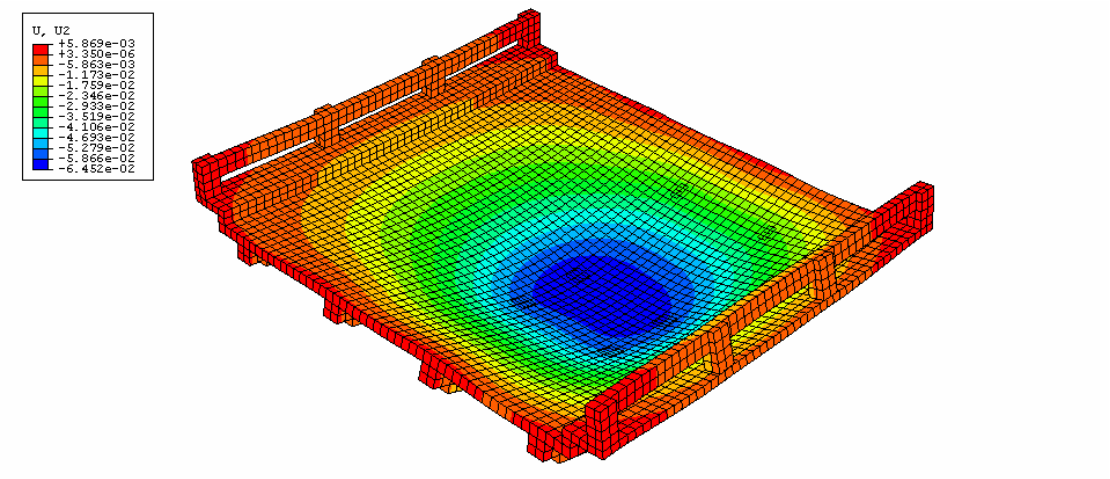

Figure 6.4 Vertical displacement of the span for Type 3 truck.

6.1.1.2 Strengthened Bridge

Two alternatives were analyzed for the SikaWrap 103 C and for the MBrace CF 530 systems respectively. The first alternative had one layer of FRP strips and the other alternative had two layers of FRP strips. The 'skin reinforcement' tool in ABAQUS does not allow overlapping skins; therefore, it required doubling the thickness of the strip to model the two layers correctly. Only one alternative was analyzed for the NSM procedure (SikaCarbodur S512).

A research by Arduini et al. (1997) showed good correlation between predicted and experimental results that justifies the assumption of perfect bond between both adhesive and concrete and adhesive and FRP. In this research the FRP strips were also modeled with a perfect bond to the concrete. This perfect bond to the concrete did not take into account the adhesive layer.

The maximum deflection for the three different types of strengthening was always located at the midspan of Beam 3 when the Type 3 truck was the load applied.

The results concerning stresses and deflections of the three different cases analyzed were very similar. The strengthening case of two layers of SikaWrap standed out because it presented the maximum reduction in deflection and stresses compared to the unstrengthened bridge. In this Section, only results from this case are presented.

For the bridge span strengthened with SikaWrap and loaded with Type 3 truck, the midspan deflection was found to be 1.595 mm (0.0628 in.) and 1.585 mm (0.0624 in.) for the cases of one and two layers of FRP strips respectively. A reduction in deflection of 1.4 % was achieved compared to the unstrenthened bridge span. Figure 6.5 shows the deflection along the beams when the bridge is loaded with Type 3 truck and strengthened with 2 layers of Sikawrap.

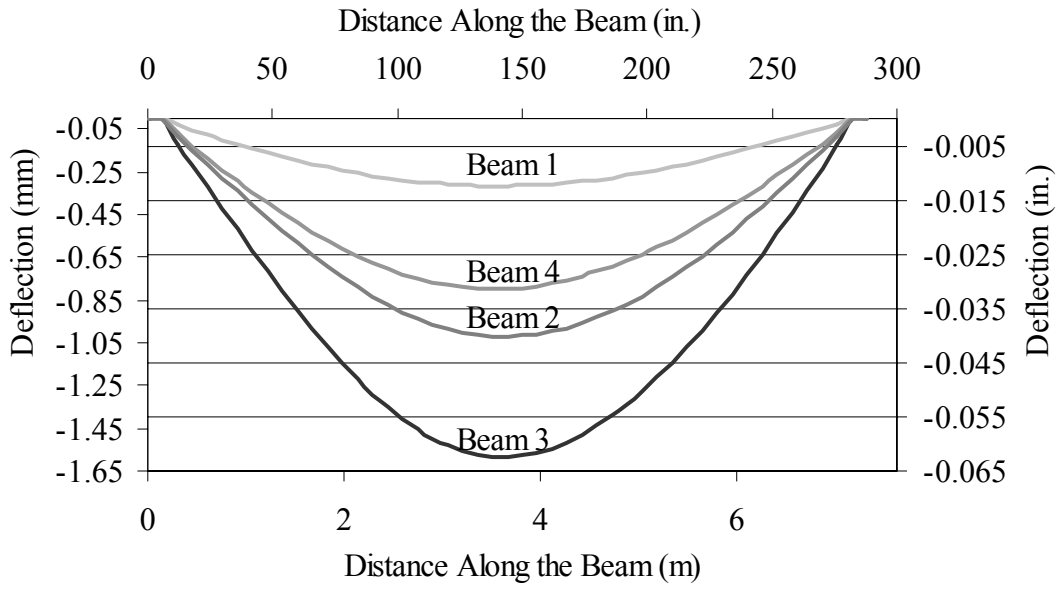

Figure 6.5 Deflection along the beams for Type 3 truck.

Concerning the stresses in the case of two layers of FRP material, the maximum flexural stresses for the three materials appeared in a section at a distance of 3.5 m (138 in) from the right support of Beam 3. In the concrete the maximum tensile stress was 3.41 MPa (494.96 psi). The maximum compressive stress had a value of 1.35 MPa (195.60 psi). The maximum tensile stress in the steel elements was 20.95 MPa (3038 psi). The maximum stresses values are well below the maximum stress of concrete and steel. The maximum tensile stress in the FRP strip is 8.31 MPa (1205 psi). This value is also below the ultimate strength in the FRP strip. Table 6.2 shows the values of the flexural stresses in the bridge.

The maximum tensile stress in the concrete was below the tensile strength of concrete, 3.42 MPa (495 psi). In this case, the concrete also did not crack.

Table 6.2 Concrete maximum stresses for Type 3 truck load.

	Maximum tensile stress MPa (psi)	Maximum compressive stress MPa (psi)
Flexural stresses in concrete	3.41 (494.96)	1.35 (195.60)
Stresses in reinforcing steel	20.95 (3038)	-
Stresses in FRP strips	8.31 (1205)	-

The values of the maximum stresses in the strengthened bridge were compared to the values of the maximum stresses in the corresponding unstrengthened bridge. Concerning the flexural stresses in concrete, there was no reduction in the tensile stresses and the compressive stresses reduced in 1 %. A reduction of 3 % was achieved for the maximum tensile stresses of the reinforcing steel.

6.1.2 Two Trucks Loading

In order to analyze the behavior of the bridge in a more unfavourable situation, the models were loaded with two trucks on different positions over the bridge. Two spans were modeled for all the systems in order to fit the two truck loads.

6.1.2.1 Unstrengthened Bridge

The two unstrengthened spans were studied with the same type of trucks (Type 3 truck and H20-44 truck) used in the one span study. For each type of truck the models were loaded with two trucks in different positions. The position of one of the trucks was the same that caused the maximum deflection in the one span study. The other truck was located in different positions. These positions studied are shown in Appendix E. The maximum deflection for both truck loads appeared in Beam 2 of span number 2. Figure 6.6 and Figure 6.7 show the cases that caused the maximum deflection for the two trucks.

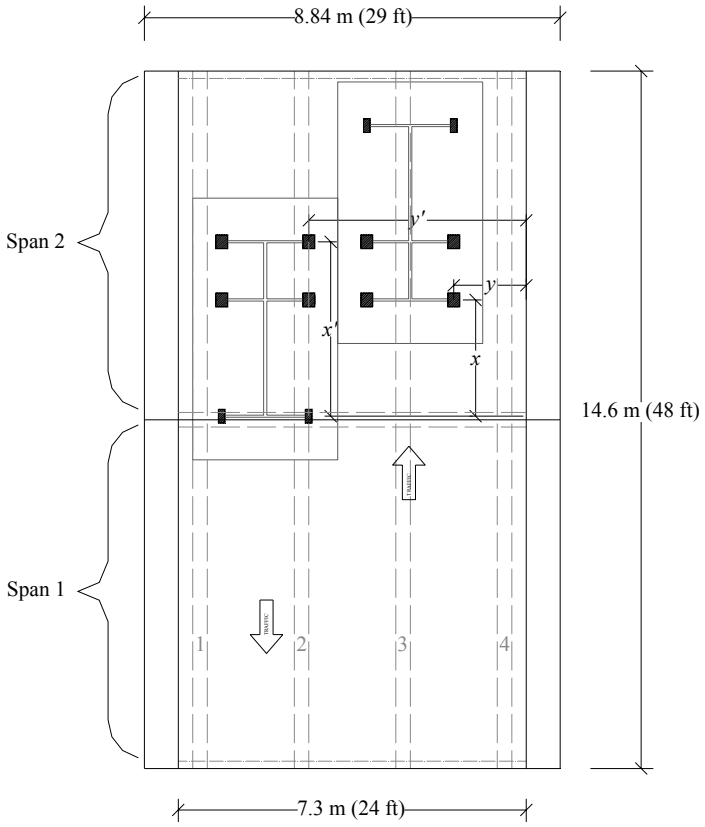

Figure 6.6 Position of Type 3 truck loads which caused the maximum deflection.

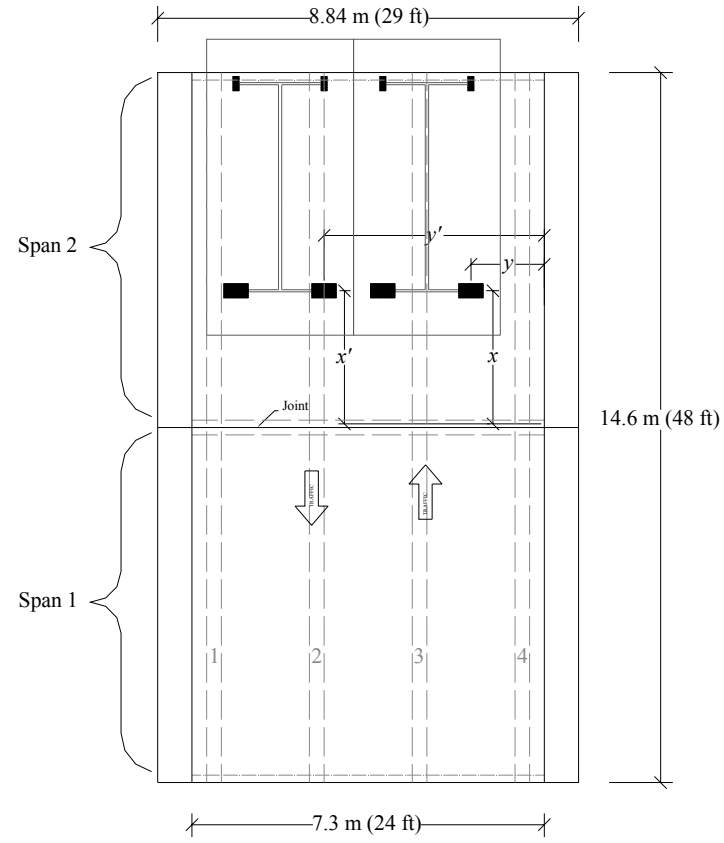

Figure 6.7 Position of H20-44 truck loads which caused the maximum deflection.

The maximum deflection for Type 3 truck load was found to be 2.286 mm (0.090 in.) at midspan of girder number 2. In the case of H20-44 truck load, the maximum deflection was 2.057 mm (0.081 in.). The behavior of the span for the two loadings was very similar. As the deflection and the concrete stresses for case D Type 3 truck load were larger than for the case C H20-44 truck load, in this section only, case D Type 3 truck load was exposed.

The maximum flexural stresses in the concrete were located in a section at Beam 3 at a distance of 3.5 m (138 in.) from the right support. The maximum tensile stress had a value of 3.41 MPa (494.98 psi). The maximum compressive stress had a value of 1.86. MPa (270.47 psi). The maximum tensile stress in the reinforcing steel appears at the bottom layer reinforcement at midspan of Beam 2. Table 6.3 show the values of the maximum stresses in the concrete and in the steel rebars for both truck loads.

Table 6.3 Maximum stresses for Type 3 truck load.

	Maximum tensile stress MPa (psi)	Maximum compressive stress MPa (psi)
Flexural stresses in concrete	3.41 (494.98)	1.86 (270.47)
Stresses in reinforcing steel	34.13 (4950.57)	-

6.1.2.2 Strengthened Bridge

In the case of two span strengthened bridge, the models used the same systems modeled in the one span study. All load cases studied are presented in Appendix E. For all of the strengthened bridges, only load case D for Type 3 truck is presented in this section. This case is the one that presented maximum deflection and stresses from all the cases analyzed.

For the bridge strengthened with SikaWrap and loaded with Type 3 truck, the midspan deflections were 2.261 mm (0.089 in.) and 2.235 mm (0.088 in.) for the cases of one and two layers of FRP strips respectively. It presented at midspan in Beam 2. A reduction in deflection of 2.2 % was achieved compared to the unstrenthened bridge. Figure 6.8 shows the deflection along the beams when the bridge was loaded with Type 3 truck and strengthened with 2 layers of Sikawrap.

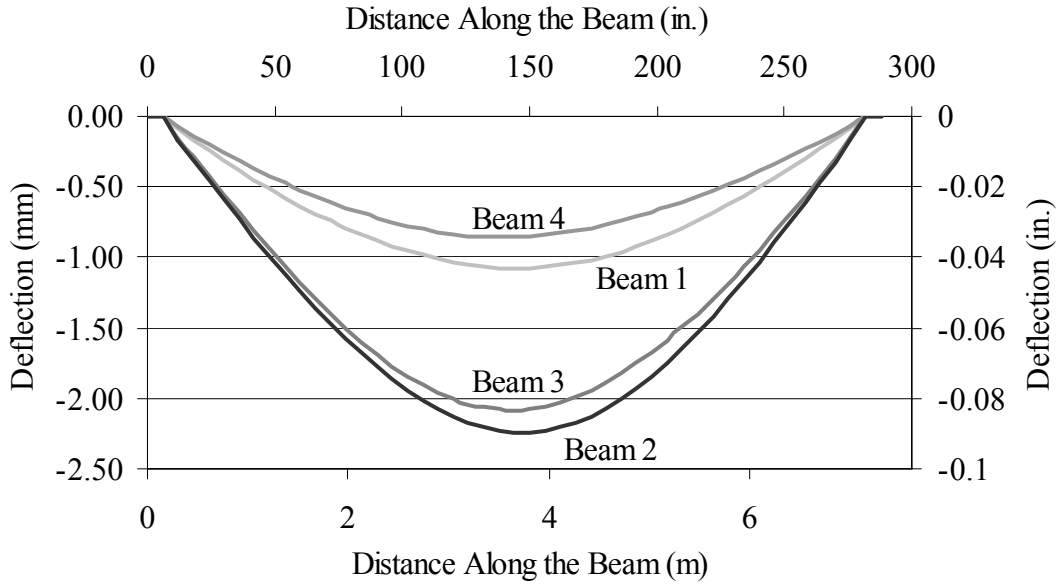

Figure 6.8 Deflection along the beams for two span case D load.

Concerning the stresses in the case of two layers of SikaWrap, the model of the strengthened bridge showed the following stresses. The maximum flexural stresses in the concrete were presented in a section in Beam 3 at a distance of 3.5 m (138 in.) from the right support. The maximum compressive stress had a value of 1.83 MPa (265.60 psi). The maximum tensile stress in the concrete was 3.41 (494.98 psi). The maximum tensile stress in the reinforcing steel appeared at midspan in Beam 2. The maximum tension in the steel elements is 32.73 MPa (4747.39 psi). The maximum stresses values are under the strength of concrete and steel. The maximum stresses in the SikaWrap strips also appeared at the midspan section of Beam 2. The maximum tensile stress was 12.97 MPa (1881.78 psi). This value was also under the ultimate strength in the FRP strip. Table 6.4 shows the values of the stresses in the strengthened bridge.

Table 6.4 Concrete maximum stresses for Type 3 truck load case D and SikaWrap strengthening system.

	Maximum tensile stress MPa (psi)	Maximum compressive stress MPa (psi)
Flexural stresses in concrete	3.41 (494.98)	1.83 (265.60)
Stresses in reinforcing steel	32.73 (4747.39)	-
Stresses in FRP strips	12.97 (1881.78)	-

In this case, also the maximum tensile stress in the concrete is below the tensile strength, 3.41 MPa (495 psi). It led to the conclusion that the concrete did not crack.

The values of the maximum stresses in the strengthened bridge were compared to the values of the maximum stresses in the corresponding unstrengthened bridge. Concerning the flexural stresses in concrete, there is no reduction in the tensile stresses and the compressive stresses reduced in 1.8 %. A reduction of 4.1 % was achieved for the maximum tensile stresses of the steel rebars.

6.2 Result Comparison Between Cases Analyzed

This section summarizes the results of the analyses. Deflections along the bridge girders and also stresses in the bridge are presented. The results of the one truck loading models are exposed followed by the results of the two truck loading models.

6.2.1 One Truck Loading Results

The bridge was analyzed with FRP attached, both one and two layers for the load positions selected which caused the largest deflection. The deflection at midspan in Beam 3 without any strip was 1.607 mm (0.0633 in.) for Type 3 truck load. The smallest deflection after attaching the layers and running all the different models was found to be 1.585 mm (0.0624 in.) for 2 layers of SikaWrap. When comparing the results using and not using strips, the biggest reduction in deflection was 1.4 % for 2 layers of SikaWrap. Observing the deflections between the unstrengthened bridge

and the strengthened bridge, it can be concluded that the stiffen resistance practically did not increase.

Table 6.5 and Table 6.6 show all the results for the different FRP systems for both loads and also the reduction in deflection achieved for each case.

Table 6.5 Comparison between strengthened and unstrengthened bridge for Type 3 truck.

Strips	Width m (in.)	Number of Layers	Deflection at Midspan Girder Number 3 mm (in.)	Deflection at Midspan (Without Strips) mm (in.)	Reduction in Deflection %
Sika Carbodur S512	0.025 (0.985)	-	1.592 (0.0627)	1.607 (0.0633)	0.9
SikaWrap	0.305 (12)	1	1.595 (0.0628)	1.607 (0.0633)	0.8
		2	1.585 (0.0624)	1.607 (0.0633)	1.4
MBrace CF 530	0.305 (12)	1	1.597 (0.0629)	1.607 (0.0633)	0.6
		2	1.587 (0.0625)	1.607 (0.0633)	1.3

The maximum deflection appeared at 3.352 m (132 in.) from the support in Beam 3 for H20-44 truck load. The maximum deflection without any strip was 1.477 mm (0.0581 in.). The smallest deflection after running the model with the FRP strips attached was 1.457 mm (0.0574 in.) for 2 layers of SikaWrap. Comparing the results of the strengthened bridge with SikaWrap strips with the unstrengthened bridge, the maximum reduction in deflection was 1.2 % for H20-44 load.

Table 6.6 Comparison between strengthened and unstrengthened bridge for H20-44 truck.

Strips	Width m (in.)	Number of layers	Deflection at Midspan Girder Number 3 mm (in.)	Deflection at Midspan (Without Strips) mm (in.)	Reduction in Deflection %
Sika Carbodur S512	0.025 (0.985)	-	1.463 (0.0576)	1.477 (0.0581)	0.9
SikaWrap	0.305 (12)	1	1.469 (0.0577)	1.477 (0.0581)	0.7
		2	1.457 (0.0574)	1.477 (0.0581)	1.2
MBrace CF 530	0.305 (12)	1	1.468 (0.0578)	1.477 (0.0581)	0.5
		2	1.459 (0.0574)	1.477 (0.0581)	1.2

Concerning stresses, in either the strengthened or unstrengthened bridge, the concrete stresses were always lower than the strength in concrete. The stresses in the strips were also lower than the maximum strength. Analyzing these results, it can be concluded that the bridge should be able to support bigger loads. Table 6.7 and Table 6.8 shows the values of the maximum stresses in the reinforcing steel and the FRP strips in the different strengthened alternatives and also the reduction in comparison with the unstrengthened bridge is shown. The concrete stresses are not presented because no significant reduction was achieved in the strengthened systems compared to the unstrengthened bridge.

Table 6.7 Maximum stresses for Type 3 truck load.

Strips	No. of layers	Max. tensile stress reinforcing steel MPa (psi)	Reduction. in stresses %	Max. tensile stress Strips MPa (psi)
Sika Carbodur S512	-	21.126 (3064.030)	1.7	20.921 (3034.230)
SikaWrap	1	21.206 (3075.650)	1.3	8.439 (1223.960)
	2	20.948 (3038.140)	2.5	8.308 (1205.030)
MBrace CF 530	1	21.234 (3079.690)	1.26	48.297 (7004.720)
	2	21.00 (3046.490)	2.2	47.728 (6922.190)

Concerning the Type 3 truck load, the FEM results showed that strengthening with two layers of SikaWrap appeared to be the more efficient system. The maximum stresses in the steel rebars were reduced by 2.5 % compared to the unstrengthened bridge. The deflections were also the lowest of all the alternatives studied. The maximum deflections were at the midspan of Beam 3. Figure 6.9 shows the longitudinal stresses in the two layers of SikaWrap strips.

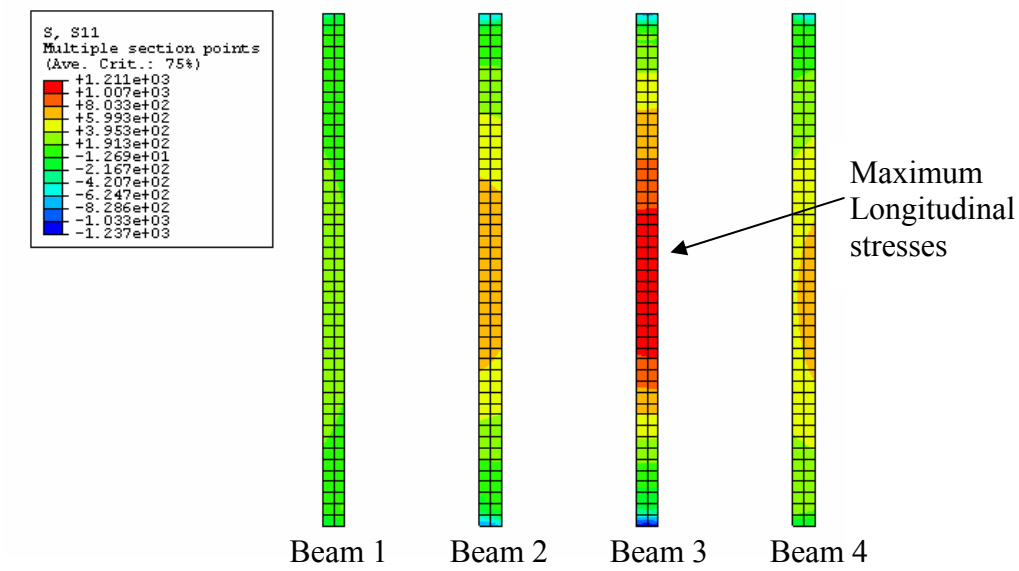

Figure 6.9 Bottom view of the strips for 2 layers of SikaWrap. Longitudinal stresses.

Table 6.8 Maximum stresses for H20-44 truck load.

Strips	No. of layers	Max. tensile stress reinforcing steel MPa (psi)	Reduction. in stresses %	Max. tensile stress Strips MPa (psi)
Sika Carbodur S512	-	21.522 (3121.350)	2	21.547 (3124.970)
SikaWrap	1	21.667 (3142.360)	1.3	8.750 (1269.120)
	2	21.362 (3098.160)	2.7	8.602 (1247.550)
MBrace CF 530	1	21.699 (3147.060)	1.2	49.993 (7250.610)
	2	21.421 (3106.820)	2.5	49.327 (7154.090)

In the case of H20-44 truck load, strengthening with two layers of SikaWrap also appeared to be the more efficient system. The maximum reduction in the stresses of the reinforced steel is 2.7 % and it is achieved for this case.

6.2.2 Two Trucks Loading Results

The results concerning deflections and stresses in the model of the strengthened bridge loaded with two trucks are exposed in this section. Case D for Type 3 truck load and case C for H20-44 truck load resulted in the maximum deflection and stresses of all the cases with two truck loads analyzed. This is the reason why only these cases are presented in this section.

The deflection at midspan in Beam 2 without any FRP strip was 2.294 mm (0.0903 in.) for case D of Type 3 truck load. The minimum deflection was found at midspan of Beam 2 for Type 3 truck load when the bridge was strengthened with 2 layers of SikaWrap. The maximum reduction in deflection was 2.2 %. Table 6.9 shows all the results for the deflection at midspan of Beam 2 for all the strengthened cases.

Table 6.9 Comparison between strengthened and unstrengthened bridge for Case D Type 3 truck load.

Strips	Width m (in.)	Number of Layers	Deflection at Midspan Girder Number 2 mm (in.)	Deflection at Midspan (Without Strips) mm (in.)	Reduction in Deflection %
Sika Carbodur S512	0.025 (0.985)	-	2.141 (0.0890)	2.294 (0.0903)	1.4
SikaWrap	0.305 (12)	1	2.267 (0.0892)	2.294 (0.0903)	1.2
		2	2.243 (0.0883)	2.294 (0.0903)	2.2
MBrace CF 530	0.305 (12)	1	2.272 (0.0894)	2.294 (0.0903)	1.0
		2	2.251 (0.0886)	2.294 (0.0903)	1.9

The deflection at midspan in Beam 2 without any strip was 1.977 mm (0.0778 in.) for case C of H20-44 truck load. The minimum deflection was found at a distance of 3.352 m (132 in.) from the supports of Beam 2 for Case C H20-44 truck load in the bridge strengthened with 2 layers of SikaWrap. The maximum reduction in deflection was 1.9 %. Table 6.10 shows all the results for the deflection at midspan of Beam 2 for all the strengthened cases.

Table 6.10 Comparison between strengthened and unstrengthened bridge for H20-44 truck.

Strips	Width m (in.)	Number of layers	Deflection at Girder Number 2 mm (in.)	Deflection (Without Strips) mm (in.)	Reduction in Deflection %
Sika Carbodur S512	0.025 (0.985)	-	1.953 (0.0769)	1.977 (0.0778)	1.1
SikaWrap	0.305 (12)	1	1.957 (0.0770)	1.977 (0.0778)	1.0
		2	1.939 (0.0763)	1.977 (0.0778)	1.9
MBrace CF 530	0.305 (12)	1	1.957 (0.0771)	1.977 (0.0778)	0.9
		2	1.942 (0.0764)	1.977 (0.0778)	1.8

Concerning stresses, either the strengthened or unstrengthened spans, the concrete stresses were always lower than the strength of the concrete. The stresses in the strips were also lower than the strength. Table 6.11 shows the maximum stresses in the different cases and also the reduction in comparison with the unstrengthened bridge. The largest reduction in stresses in the reinforcing steel was achieved for the case when the bridge was strengthened with 2 layers of SikaWrap. Figure 6.10 shows the longitudinal stresses in the SikaWrap material for the case of 2 layers of FRP strips. The concrete stresses are not presented because no significant reduction was achieved in the strengthened systems compared to the unstrengthened bridge.

Table 6.11 Maximum stresses for Type 3 truck load case D.

Strips	No. of layers	Max. tensile stress reinforcing steel MPa (psi)	Reduction. in stresses %	Max. tensile stress Strips MPa (psi)
Sika Carbodur S512	-	33.058 (4794.450)	3.1	32.347 (4691.340)
SikaWrap	1	33.289 (4828.000)	2.5	13.231 (1918.900)
	2	32.733 (4747.390)	4.1	12.975 (1881.780)
MBrace CF 530	1	33.410 (4845.540)	2.1	75.213 (10908.30)
	2	32.923 (4774.920)	3.5	74.096 (10746.30)

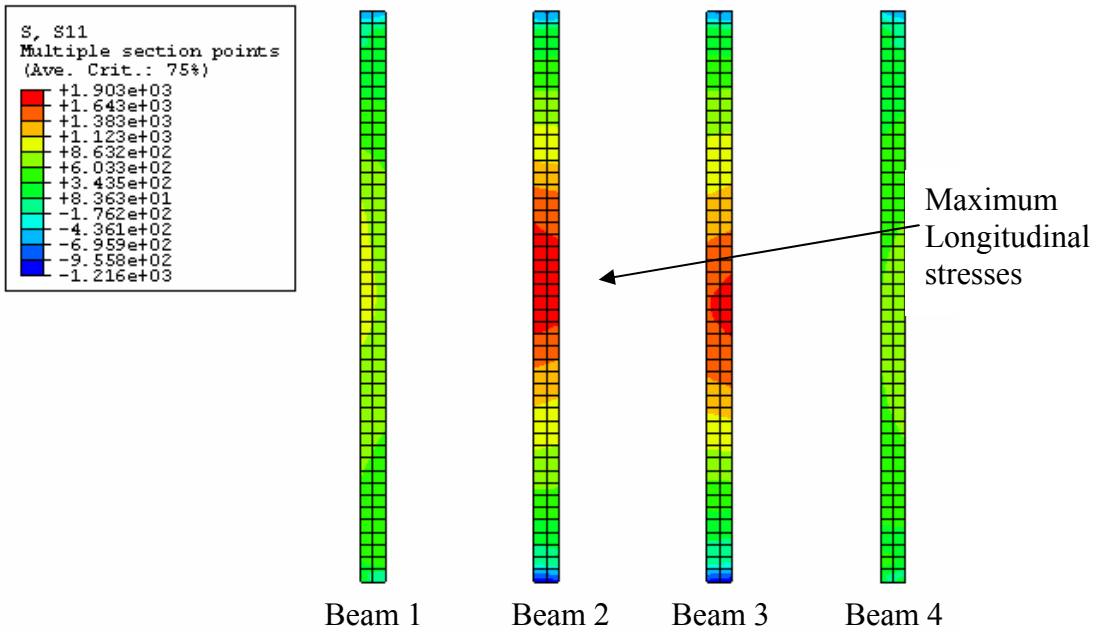

Figure 6.10 Longitudinal stresses for 2 layers of SikaWrap. Case D Type 3 truck load.

Table 6.12 shows the values of the maximum stresses in the different strengthening systems for case C H20-44 truck load. The reduction in comparison with the

unstrengthened bridge was also presented in Table 6.12. The largest reduction in stresses in the reinforcing steel was achieved when the bridge was strengthened with 1 layers of Mbrace CF530. Figure 6.11 shows the longitudinal stresses in the SikaWrap material for the case of 2 layers of strips.

Table 6.12 Maximum stresses for H20-44 truck load case C.

Strips	No. of layers	Max. tensile stress reinforcing steel MPa (psi)	Reduction. in stresses %	Max. tensile stress Strips MPa (psi)
Sika Carbodur S512	-	32.084 (4653.280)	2.3	31.342 (4545.57)
SikaWrap	1	29.271 (4245.360)	10.84	12.917 (1873.360)
	2	31.681 (4594.860)	3.5	12.636 (1832.60)
MBrace CF 530	1	25.145 (3646.920)	23.4	72.742 (10550.00)
	2	31.619 (4585.800)	3.7	71.439 (10361.00)

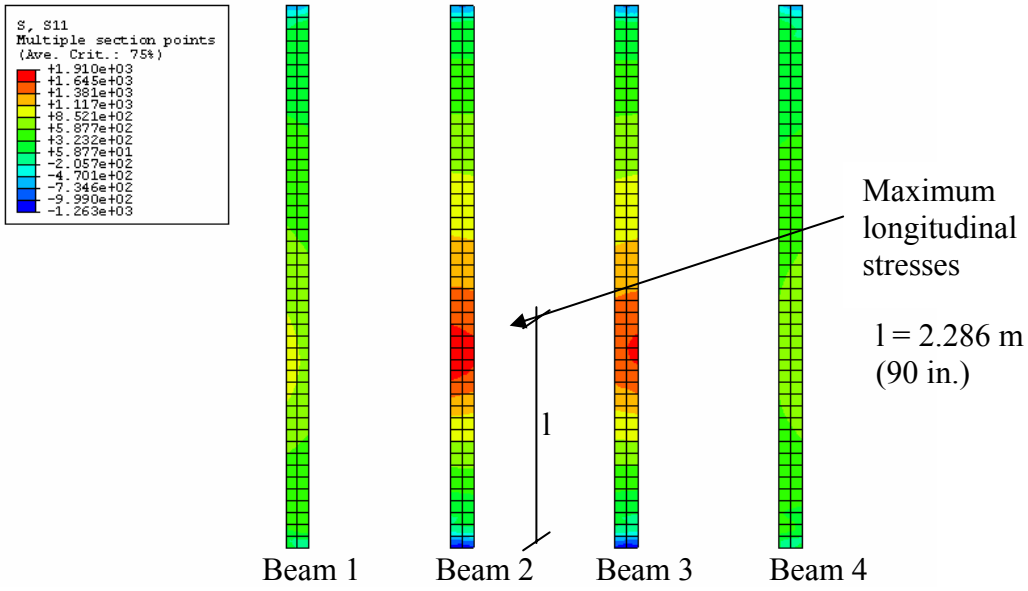

Figure 6.11 Longitudinal stresses for 2 layers of SikaWrap. Longitudinal stresses. Case C H20-44 truck load.

6.2.3 Summary of Result Comparison

All the cases with strengthening models achieved a certain reduction in deflection and stresses. Although the values were very similar for all the strengthened systems, the SikaWrap system appeared to be the most effective one. The SikaWrap system reached the largest reduction in deflection and stresses. Two layers of FRP material reduced the stresses in the concrete and in the reinforcing steel. The maximum stresses in the FRP material were found to be far from the ultimate strength of the FRP. The maximum stress in the FRP strip was 13.23 MPa (1918.90 psi) and the strength for SikaWrap is 717.08 MPa (104000 psi).

6.2.4 Potential for Higher Loads

It has been known that sometimes the standard trucks are overloaded. Considering this situation, an analysis for a more unfavourable situation was also carried out. The total weight of the truck was considered to be two times the normal weight of a Type 3 truck. The total load applied per truck was 360 kN (81 kip). The load case was Case D as can be seen in Appendix E. The unstrengthened bridge and the strengthened with 2 layers of SikaWrap were analyzed. Figure 6.12 and Figure 6.13 show the deflection in the beams for both systems

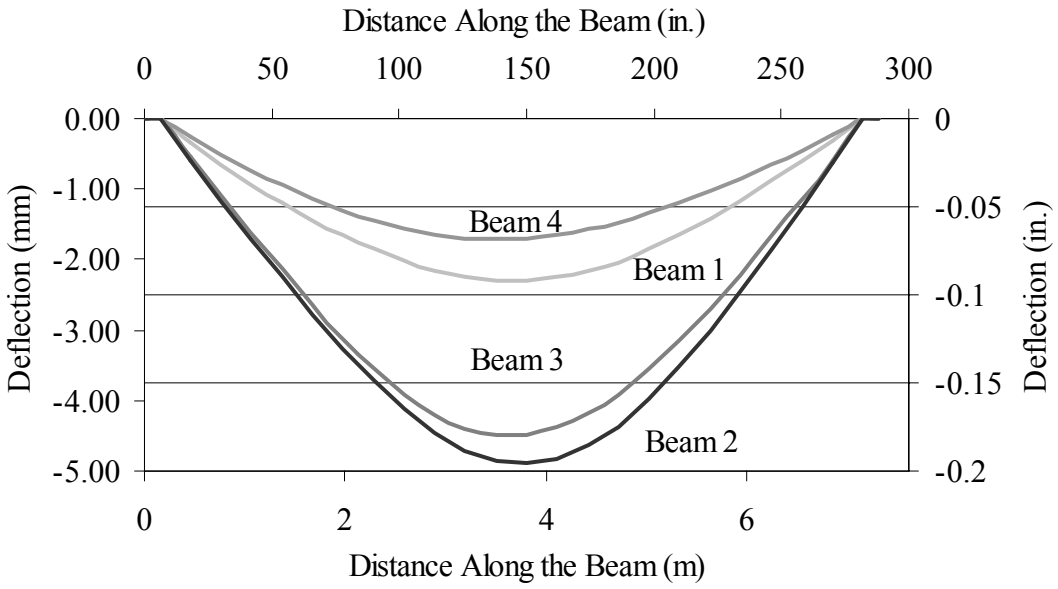

Figure 6.12 Deflection along the beams for case D and overweighted truck load (Unstrengthened bridge).

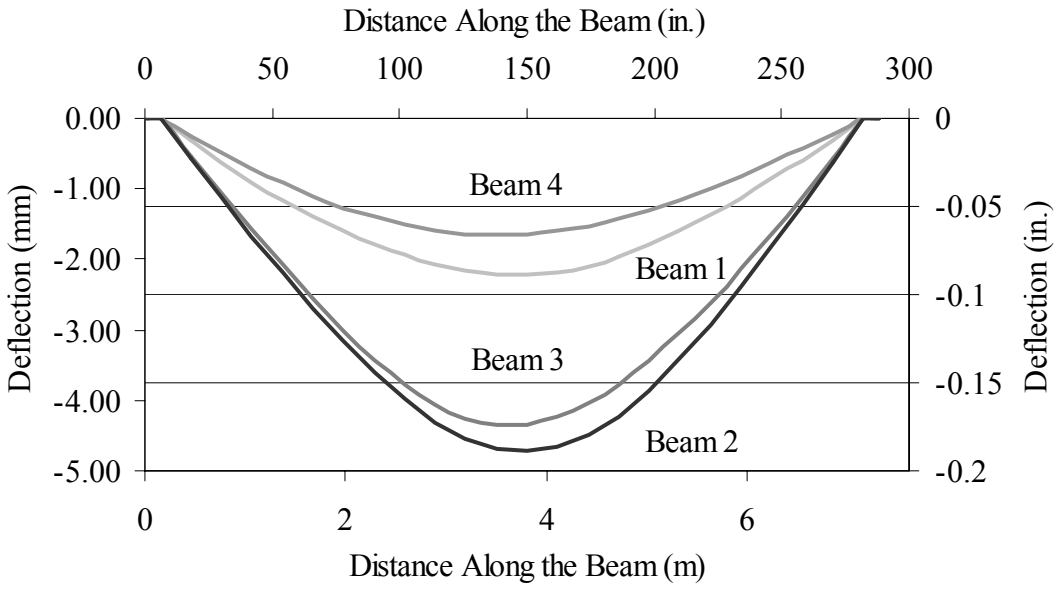

Figure 6.13 Deflection along the beams for case D and overweighted truck load (Strengthened bridge).

The maximum deflection for the unstrengthened bridge was 4.895 mm (0.193 in.). The maximum deflection for the strengthened bridge was 4.729 mm (0.186 in.). A reduction in deflection of 3.4 % was achieved.

Concerning stresses, Table 6.13 and Table 6.14 shows the maximum stresses in the unstrengthened and strengthened bridge respectively. A reduction of 1.66 % in the maximum compressive stress in the concrete was achieved. In the case of reinforcing steel a reduction of 6.4 % was achieved.

Table 6.13 Maximum stresses for case D and overweighted truck load (Unstrengthened bridge).

	Maximum tensile stress MPa (psi)	Maximum compressive stress MPa (psi)
Flexural stresses in concrete	3.39 (492.13)	0.92 (134.24)
Stresses in reinforcing steel	85.89 (12457)	-

Table 6.14 Maximum stresses for case D and overweighted truck load (Strengthened bridge).

	Maximum tensile stress MPa (psi)	Maximum compressive stress MPa (psi)
Flexural stresses in concrete	3.39 (491.94)	0.91 (132.01)
Stresses in reinforcing steel	80.43 (11664)	-
Stresses in FRP strips	32 (4640.64)	-

In both the unstrengthened and strengthened bridge, the maximum tensile stress in the concrete was below the tensile strength of concrete. Thus, also in these cases, the structure did not crack.

These results led to the conclusion that the bridge is able to support bigger loads than Type 3 and H20-44 trucks loads.

6.3 Moment Resistance and Load Posting

The bridge was originally designed for an American Association of State Highway and Transportation Officials (AASHTO) H15 design loading. Schematic layout for H15 design truck was shown in Figure 4.2.

Bridge load rating calculations provide a basis for determining the safe load carrying capacity of a bridge. All bridges should be rated at two load levels, the maximum load level called the Operating Rating and a lower load level called the Inventory Rating. The Operating Rating is the maximum permissible load that should be allowed on the bridge. Exceeding this level could damage the bridge. The Inventory Rating is the load level the bridge can carry on a daily basis without damaging the bridge.

At present days there is not any system for rating bridges strengthened with FRP strips. Although the LADOTD (2004) is a manual for typical reinforced concrete bridge design, it has been used to determine the load posting for the bridge. The LADOTD (2004) uses the following expressions in determining the load rating of a structure based on the moment capacity:

- Inventory Rating Factor:

$$RF_{inv} = \frac{\frac{3}{5}\left[\frac{M_u}{1.3} - M_{dl}\right]}{M_{ll} \cdot (1+I)} \tag{8.1}$$

- Operating Rating Factor:

$$RF_{opr} = \frac{\left[\frac{M_u}{1.3} - M_{dl}\right]}{M_{ll} \cdot (1+I)} \tag{8.2}$$

- Rating in tons:

$$RT = (RF) \cdot W \tag{8.3}$$

where M_u is the moment capacity of the structure, M_{dl} is the moment due to the dead load, M_{ll} is the moment due to live load, I is the impact factor to be used with the live load, and W is the weight (in tons) of the truck used in determining the live load effect. The calculations concerning the ultimate moment capacity of the structure can be found in Appendix D.

The rating evaluation vehicles are coded by a three digit number. The first digit is designated as the Rating Vehicle Code and is unique to the vehicle type. The second two digits are the gross vehicle weight to the nearest ton with the leading zeros.

The H15 truck load was used for inventory rating. The H20-44 truck load was used for operating rating. The Type 3 truck load was used for posting rating. Appendix F shows all the calculations for the load rating analysis. The load rating analysis gave the following results:

- Inventory: 114
- Operating: 123
- Posting: 425

With these values the need of load posting is established following the bridge weight limit requirements table (LADOTD (2004)). A type II posting sign is needed with the weight limits between 20 tons and 35 tons. Figure 6.14 shows a sketch of this sign.

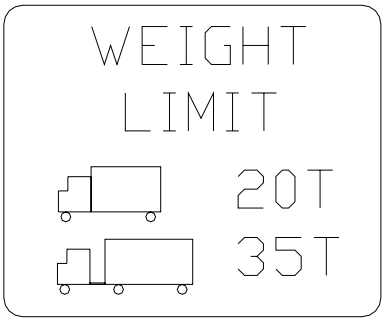

Figure 6.14 Load posting sign.

As explained before, the LADOTD (2004) is a manual for typical reinforced concrete bridge design. The moment-curvature relation was studied in both strengthened and unstrengthened situations to determine if it is possible to remove the load posting. Figure 6.15 shows the moment-curvature relationship in both systems.

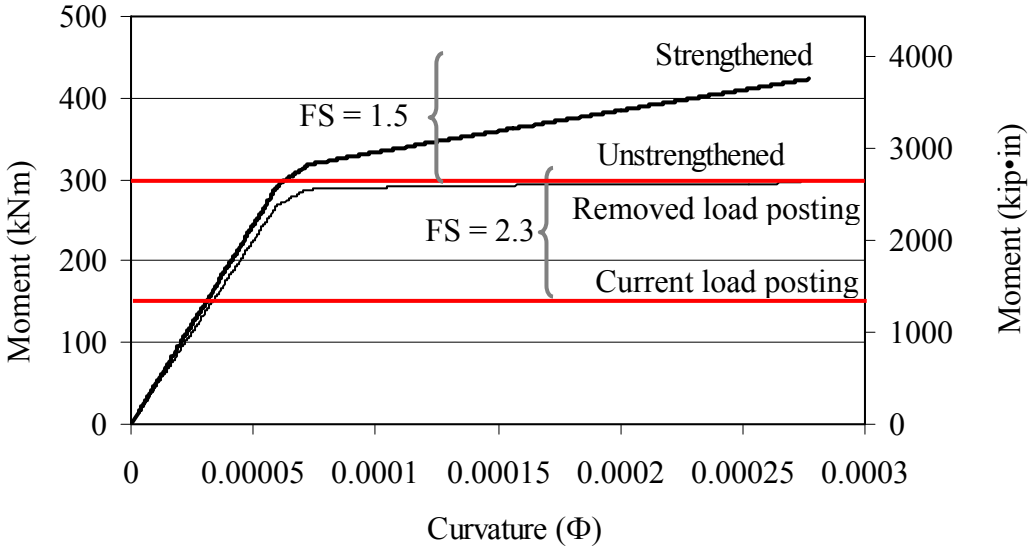

Figure 6.15 Moment-curvature relationship in the strengthened and unstrengthened systems.

After the strengthening with 2 layers of Sikawrap, an extra moment capacity of 127.40 kNm (1127.42 kip-in.) will be reached. The moment for the current load posting was 126.56 kNm (1120 kip-in). Comparing this moment with the moment capacity of the unstrengthened bridge, a factor of safety of 2.3 was reached. The HS44 truck load gives a moment of 278.432 kNm (2464 kip-in), which gives a factor of safety of 1.5. The obtained factor of safety is a normal value for current standards in construction in the US.

With this extra moment capacity and considering the results from the FE analysis for potential higher loads can be assured that the load posting can be removed.

6.4 Check of Shear Capacity

In order to assure the resistance of the bridge when the strengthened system were applied and the load posting removed, the shear capacity of the bridge was also checked by hand. Considering Beam 3 of the bridge and the slab corresponding to it as shown in Figure 5.11, the check of the shear capacity was carried out following the specifications given by ACI Committee 318 (2002). All the calculations can be seen in Appendix G. The maximum shear force in the beam was 116.72 kN (26240.83 lb). As the shear capacity of the concrete alone was found to be 178.13 kN (40047.47 lb), there was no need to calculate the contribution by the shear reinforcement.

7 Conclusions

In this chapter, general conclusions from the FE analysis are given. Following the general conclusions, recommendations for industry and future research are also given.

7.1 General Conclusions

The following conclusions can be drawn from the FE analysis conducted:

1) From all the cases analyzed, strengthening the bridge with two layers of SikaWrap presented the biggest reduction in deflection and stresses comparing to the unstrengthened bridge. The extra moment capacity along with the FE analysis on potential higher loads lead to the conclusion that the load posting can be removed after strengthening the bridge with two layers of SikaWrap.

2) As seen in Table 5.9, the maximum reduction in deflection is reached in the case of two layers of SikaWrap; reduction of 2.2 % in deflection with respect to the bridge without retrofitting, subjected to Type 3 Truck load. Although the values do not present a large reduction in the deflection, the bridge behavior has been improved.

3) Increasing the number of elements will provide a slightly more accurate solution, but also the computational time will increase considerably. Both variables should be taken into account to provide the most appropiate analysis.

7.2 Recommendations

The FE analysis was carried out on the basis of some assumptions, such as perfect bond behaviour between the FRP strip and the concrete. For a correct behaviour of the strengthened system it is recommended to give special attention to the end anchorage. End anchorage can prevent debonding failure, which is a brittle and catastrophic mechanism.

After the future strengthening of the bridge, the removal of the load posting is recommended.

7.3 Recommendations for Future Research

Concerning the future research in the strengthening of the White Bayou Bridge, the strengthened bridge should be loaded with the load cases exposed in this research and the strains and deflections should be verified with the results from the FE analysis.

8 References

ABAQUS online documentation. Version 6.4.

ACI Committee 318, (2002): *Building Code Requirements for Structural concrete and Coments*. American Concrete Institute, Farmington Hills, Mich., 2002, 441 pp.

ACI Committee 440, (2002): G*uide for the Design and Construction of Externally bonded FRP Systems for Strengthening Concrete Structures*. American Concrete Institute, Farmington Hills, Mich., 2002, 45 pp.

ACI Manual of Concrete Practice (1983): *Control of Cracking in Concrete Structures*. American Concrete Institute, Detroit, Michigan, 1983.

Alampalli, S., (2000): Modal analysis of a fiber-reinforced polymer composite highway bridge. *Proceedings of SPIE-the international society for optical engineering*. Vol. 4052, No. 1, 2000. pp. 21-25.

Alkhrdaji, T., Thomas, J., (2004): Techniques for successful structural repair and strengthening of concrete facilities. *Concrete Engineering International*. Vol. 8, No. 3, Autumn 2004. pp. 51-53.

American Association of State Transportation Highway Officials (AASHTO), (2004): *AASHTO LRFD Bridge Design Specifications*, 16th ed., Washington, DC, 2004.

Aprile, A., Spacone, E., Limkatanyu, S., (2001): Role of Bond in RC Beams Strengthened with Steel and FRP Plates. *Journal of Structural Engineering*, Vol. 127, No. 12, December, 2001. pp. 1445-1452.

Arduini, M., Nanni, A., (1997a): Parametric Study of Beams with Externally Bonded FRP Reinforcement. *ACI Structural Journal*, Vol. 94, No. 5, September – October 1997a, pp. 493-501.

Arduini, M., Di Tommaso, A., Nanni, A., (1997b): Brittle Failure in FRP Plate and Sheet Bonded Beams. *ACI Structural Journal*, Vol. 94, No. 4, July-August 1997b, pp. 363-370.

Ascione, l., Berardi, V.P., Feo, L., Mancusi, G., (2005): A numerical evaluation of the interlaminar stress state in externally FRP plated RC beams. *Composites. Part B*, Engineering. Vol. 36, No. 1, January 2005, pp. 83-90.

Bakis, C.E., Bank, L.C., Brown, V.L., Cosenza, E., Davalos, J.F., Lesko, J.J., Machida, A., Rizkalla, S.H., Triantafillou, T.C., (2002): Fiber Reinforced Polymer Composites for Construction – State-of-the-Art Review. *Journal for Composites for Construction*. May 2002. pp. 73-87.

Biggs, R.M., Barton, F.W., Gomez, J.P., Massarelli, P.J., Mckeel, W.T., (2000): *Finite Element Modeling and Analysis of Reinforced Concrete Bridge Decks*. Virginia Transportation Research Council. September 2000. VTRC 01-R4.

Bureau of Transportation Statistics (2004): *Transportation Statistics Annual Report*. U.S. Department of Transportation, Washington, DC, 2004

Buyukozturk, O., Hearing, B., (1998): Failure Behaviour of Precracked Concrete Beams Retrofitted with FRP. *Journal of Composites for Construction*. Vol. 2, No. 3, August 1998, pp. 138-144.

Carlin, B.P., (1998): *Investigation of the Strength and Ductility of Reinforced Concrete Beams Strengthed with CFRP Laminates*. Master's Thesis. Department of Civil Engineering. Virginia Polytechnic Institute and State University. Blacksburg, Virginia. March, 1998, 107 pp.

Carolin, A. (2003): *Carbon Fibre Reinforced Polymers for Strengthening of Structural Elements*. Ph.D. Thesis. Department of Civil and Mining Engineering. Division of Structural Engineering. Luleå University of Technology. Luleå, Sweden. June, 2003. 194 pp.

Chen, J.F., Teng, J.G., (2001): Anchorage Strength Models for FRP and Steel Plates Bonded to Concrete. *Journal of Structural Engineering*. Vol. 127, No. 7, July, 2001. pp. 784-791

Colotti, V., Spadea, G., (2005): An analytical model for crack control in reinforced concrete elements under combined forces. Cement & concrete composites. Vol. 27, No. 4, April 2005, pp. 503-514.

De Lorenzis, L., Miller, B., Nanni, A. (2001): Bond of Fiber-Reinforced Polymer Laminates to Concrete. *ACI Materials Journal*, Vol. 98, No. 3, May-June 2001, pp. 256-264

Galati N., Casadei P., Nanni A., (2004): *Strengthening of Martin Springs outer road bridge, Phelps County*. Center for Infrastructure and Engineering Studies. January, 2004, 90 pp.

Gose, S. C., Nanni, A., (2002): *Anchorage System For Externally Bonded FRP Laminates Using Near Surface Mounted FRP Rods*. Center for Infrastructure Engineering Studies. University of Missouri-Rolla. Rolla, Missouri, February 2002, 63 pp.

Grace, N.B., Abdel-Sayed, G., Ragheb, W.F., (2002): Strenthening of Concrete Beams Using Innovative Ductile Fiber-Reinforce Polymer Fabric. *ACI Structural Journal*. Vol. 99, No. 5, September-October 2002. pp. 692-700.

Hassan, T., Rizkalla, S., (2002): Flexural Strengthening of Prestressed Bridge Slabs with FRP Systems. *PCI Journal*, January - February 2002, Vol. 47, No. 1, pp. 76-93.

Hassan, T., Rizkalla, S., (2002): Effectiveness of FRP for Strengthening Concrete Bridges. *Journal of the International Association for Bridge and Structural Engineering (IABSE)*, SEI2, Vol. 12, No. 2, May 2002, pp. 89-95.

Hassan, T., Rizkalla, S., (2003): Investigation of Bond in Concrete Structures Strengthened with Near Surface Mounted Carbon Fiber Reinforced Polymer Strips.

Journal of Composites for Construction, Vol. 7, No. 3, August 1, 2003. pp. 248-257.

Hollaway, L.C., Head, P.R., (2001): *Advanced Polymer Composites And Polymers In The Civil Infrastructure*. Elsevier. 2001. 316 pp.

Hormann M., Menrath H., Ramm E., (2002): Numerical Investigation of Fiber Reinforced Polymers Poststrengthened Concrete Slabs. *Journal of engineering mechanics*. Vol. 128, No.5, May 2002. pp. 552-561.

Hu, H., Lin, F., Jan, Y. (2004): Nonlinear Finite Element Analysis of Reinforced Concrete Beams Strengthened by Fiber-Reinforced Plastics. *Composite Structures*. Vol. 63, 2004, pp. 271-281.

Kachalakev D.I., (2001): Experimental Results and Design Methods of Structural Strengthening of RC Beams Using Composite Laminates. *33rd International SAMPE Technical Conference*. November 5-8, 2001. pp. 792-807.

Karbhari, V.M., Mirmiran, A., Shahawy, M, Nanni, A., (2004): Constructions Specifications for Bonded Repair and Retrofit of Concrete Structures Using FRP Composites – Results of a NCHRP Study. *Composites 2004, Convention and Trade Show Composites Manufacturers Association*, October, 2004, Tampa, Florida, USA, pp. 1-10.

Khalifa, A., Alkhrdaji, T., Nanni, A., Lansburg, S., (1999): Anchorage of Surface Mounted FRP Reinforcement. *Concrete International: Design and Construction*, Vol. 21, No. 10, Oct. 1999, pp. 49-54.

Klaiber F.W., Dunker K.F., Wipf T.J., Sanders W.W., (1987): *Methods of Strengthening Existing Highway Bridges*. NCHRP Report 293. Transportation Research Board, National Research Council, Washington DC, 1987.

Kwak, H. G., Filippou, F. C., (1990): *Finite element analysis of reinforced concrete structures under monotonic loads*. Structural Engineering, Mechanics and Materials, Department of Civil Engineering, University of California, Berkeley. November 1990, 124 pp.

Lamanna, A. J., Bank, L. C., and Scott, D. W., (2001a): Flexural Strengthening of RC Beams Using Fasteners and FRP Strips. *ACI Structural Journal*, Vol. 98, No. 3, May-June 2001, pp. 368-376.

Lamanna, A. J., Bank, L. C., and Scott, D. W. (2001b): *Rapid Flexural Strengthening of Full Scale RC Beams Using Powder Actuated Fasteners and FRP Strips*. FRPRCS-5 Fiber Reinforced Plastics for Reinforced Concrete Structures, University of Cambridge, UK, Vol. 1, July 16 - 18, 2001, pp. 389-397.

Lamanna, A. J. (2002): *Flexural strengthening of reinforced concrete beams with mechanically fastened fiber reinforced strips*. Ph. D. Thesis. University of Wisconsin – Madison. 2002. 287 pp.

Leet, K.: *Conforms to 1989 ACI Codes. Reinforce Concrete Design Conforms*. Second Edition. McGraw-Hill, Inc.

Malek A.M., Saadatmanesh H., (1998): Analytical Study of Reinforced Concrete Beams Strengthened with Web-Bonded Fiber Reinforcel Plastic Plates or Fabrics". *Structural Journal*. ACI 1998; 95-S31: pp. 343-364.

Mallick, P.K., (1988): *Fiber-reinforced composites: materials, manufacturing, and design*. Marcel Dekker Inc, New York, New York, USA, 1988, 469 pp.

Macgregor, J.G., (1997): *Reinforced Concrete, Mechanics and Design.* Third Edition, Prentice Hall, New Jersey, USA, 939 pp.

Mckenna, J.K., Erki, M.A., (1994): Strengthening of Reinforced Concrete Flexural Members using externally applied steel plates and fibre composites sheets – a survey. *Canadian Journal of Civil Engineering*. Vol. 21, No. 1, February 1994, pp. 16-24.

Meier, U., (1992): Carbon fibre-reinforced polymers: Modern materials in bridge engineering. *Structural Engineering International*. IABSE, Zurich, Switzerland, Vol. 2, No. 1, February 1992, pp. 7-12.

Meyer, C., Okamura, H., (1985): Finite element analysis of reinforced concrete structures. *Proceedings of the seminar sponsored by the Japan Society for the Promotion of Science and the U.S. National Science Foundation*. American Society of Civil Engineers. New York, 1985, 685 pp.

Monti, G., Spoelstra, M. R. (1997): Fiber-section analysis of RC bridge piers retrofitted with FRP jackets. *Building to last; proceedings of Structures Congress XV*. Pt. 2, April 1997, Portland, Oregon, pp. 884-888.

Oehlers, D.J., (1990): Strengthening Reinforced Concrete Beams by Bonding Steel Plates to Their Soffits. *The Institution of Engineers Australia Structural Engineering Conference*. No. 90, 1990, Australia, pp. 346-350.

Oehlers, D.J., (2001): Development of design rules for retrofitting by adhesive bonding or bolting either FRP or steel plates to RC beams or slabs in bridges and buildings. *Composites, Part A: Applied science and manufacturing*. Vol. 32, 2001, pp. 1345-1355.

Oh, B. H., Cho, J. Y., Park, .D. G. (2003): Failure Behavior and Separation Criterion for Strengthened Concrete Members with Steel Plates. *Journal of Structural Engineering,* Vol. 129, No. 9, September, 2003, pp. 1191-1198.

Pham, H., Al-Mahaidi, R. (2004): Experimental investigation into flexural retrofitting of reinforced concrete bridge beams using FRP composites. *Composite structures*. Vol. 66, No. 1-4, October/December, 2004, pp. 617-625.

Plos, M., (200): Finite Element Analysis of Reinforced Concrete Structures. Compendium 96:14. Department of Structural Engineering. Chalmers University of Technology. Göteborg, Sweden, 2000, 48 pp.

Raithby, K. D., (1980): External Strengthening of Concrete Bridges with Bonded Steel Plates. *Suplementary Report. Transport and Research Laboratory*. No. 612, 1980, 22 pp.

Ritchie P.A., Thomas D.A., Lu L., Connelly G.M., (1991): External Reinforcement of Concrete Beams Using Fiber Reinforced Plastics. *ACI Structural Journal*. Vol. 88, No. 4, July-August 1991, 88 - S52. pp. 490 - 500.

Rizkalla, S., Hassan, T. and Hassan, N., (2003): Design Recommendations for the use of FRP for Reinforcement and Strengthening of Concrete Structures. *Journal of Progress in Structural Engineering and Materials*. Vol. 5, No. 1, November, 2003, pp. 16-28

Ross C.A., Jerome D.M., Tedesco J.W., Hughes M.L., (1999): Strengthening of Reinforced Concrete Beams with Externally Bonded Composite Laminates. *Struct. J. ACI* 1999; 96-S23: pp. 212-220.

Sena Cruz, J.M., Oliveira de Barros, J.A., (2004): Bond Between Near-Surface Mounted Carbon-Fiber-Reinforced Polymer Laminate Strips and Concrete. *Journal of Composites for Construction*. Vol. 8, No.6, December 2004, pp. 519-527.

Sheikh S.A., (2002): Performance of Concrete Structures Retrofitted with Fibre Reinforced Polymers. *Engineering Structures*, Vol. 24, No. 7, July 2002. pp. 869-879.

Sika Carbudur. Composite Strengthening Systems. Engineering Guidelines for Design and Application. Version 3.0.

Sirju, K., Sharma, A.K., (2001): Strengthening of Reinforced Concrete Members under Compresion and Bending. *Structures & Buildings*, Vol. 146, No. 2, May 2001, pp. 227-231.

Spadea, G., Swamy, R.N., Bencardino, F., (2001): Strength and Ductility of RC Beams Repaired with Bonded CFRP Laminates. *Journal of Bridge Engineering*, Vol. 6, No. 5, September/October, 2001. pp. 349-355.

State of Louisiana Department of Transportation and Development (2004): *Bridge Design Manual.* May 3, 2004, 493 pp.

Swamy, R. N., Mukhopadhyaya, P. (1999): Debonding of carbon-fibre-reinforced polymer plate from concrete beams. *Proceedings of the Institution of Civil Engineers. Structures and buildings*. Vol. 134, No. 4, November 1999, pp. 301-317.

Täljsten, B., Carolin, A., Nordin, H., (2003): Concrete structures strengthened with near surface mounted reinforcement of CFRP. *Advances in structural engineering*. Vol. 6, No. 3, August 2003, pp. 201-213.

Tedesco J.W., Stallings J.M., El-Mihilmy M., (1999): Finite Element Method analysis of a concrete bridge repaired with fiber reinforced plastic laminates. *Computer & Structures*. Vol. 72, No. 1-3, Jul-Aug 1999, pp. 379-407.

U.S. Department of Transportation, Bureau of Transportation Statistics, *Transportation Statistics Annual Report*. (Washington, DC: 2004)

Zhang, J. W., Teng, G. J., Wong, Y.L., Lu, Z.T. (2001): Behavior of Two-Way RC slabs Externally Bonded With Steel Plate. *Journal of Structural Engineering*, Vol. 127, No. 4, April 2001, pp. 390-397.

Appendix A: Current state of the bridge

Figure A.1 Lateral view of the White Bayou Bridge.

Figure A.2 Bottom view of the White Bayou Bridge (scour can be seen on the piles).

Figure A.3 Joint between spans.

Figure A.4 Bottom view of the bridge deck.

Figure A.5 Bottom view of the concrete spalling deck.

Figure A.6 Detail view of a deteriorated beam.

Figure A.7 Detail view of a deteriorated joint.

Appendix B: Crack Spacing Calculations

The average final crack spacing for members subjected principally to flexure or tension, srm (in mm), can be calculated from the equation:

$$srm = 50 + 0{,}25\ k1\ k2\ \phi / \rho r$$

where

ϕ is the bar size in mm. ϕ = 1.125 in. = 28 mm

k1 is a coefficient which takes account of the bond properties of the bar.
Values of k1 are:

k1 = 0.8 for high bond bars
k1 = 1.6 for plain bars

In this case k1 = 1.6

k2 is a coefficient which takes account of the form of the strain distribution.
Values of k2 are:

k2 = 0.5 for pure bending
k2 = 1.0 for pure tension

In this case k2 = 0.5

ρr is the effective reinforcement ratio

$$\rho r = As/Ac_{ef}$$

where

As is the area of reinforcement contained within the effective tension area,

Ac_{ef} is the area of concrete surrounding the tension reinforcement, of depth equal to 2,5 times the distance from the tension face of the section to the centroid of the reinforcement.

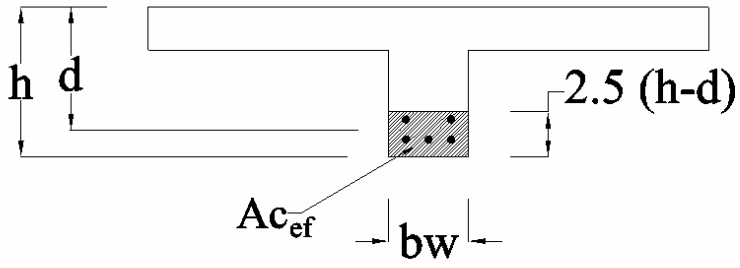

$As = 4.97\ in.^2 = 3206.44\ mm^2$

$Ac_{ef} = 2.5\ (h - d)\ bw$

$h = 22.5\ in. = 551.25\ mm$

$d = 18.675\ in. = 474.34\ mm$

$bw = 12\ in. = 304.8\ mm$

$\rho r = 0.055$

$Ac_{ef} = 5.861 \times 10^4\ in.^2$

$Ac_{ef} = 90.839\ mm^2$

Finally, the final crack spacing (srm) is:

$$srm := 50 + 0.25 \cdot k1 \cdot k2 \cdot \frac{\phi}{\rho r}$$

$srm = 152.353\ mm$

$srm = 5.998\ in.$

Appendix C: Analytical Study of Midspan Deflection

- Materials Properties

Ec = Concrete Elastic Modulus $Ec := 4230000 \cdot \frac{lbf}{in^2}$

fc = Concrete Ultimate Strength $fc := 5500 \cdot \frac{lbf}{in^2}$

Es = Steel Elastic Modulus $Es := 29000000 \cdot \frac{lbf}{in^2}$

- Section Properties

Gross Section

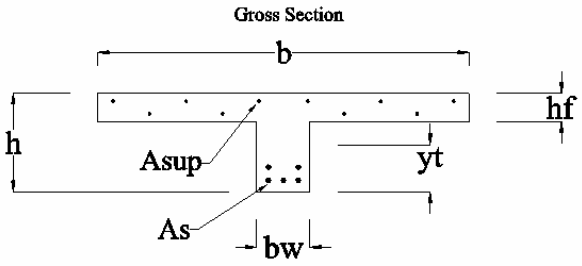

$b := 84 \cdot in$

$bw := 12 \cdot in$

$h := 22.5 \cdot in$

$hf := 6.5 \cdot in$

As = Beam reinforcement $As := 4.97 \cdot in^2$

Asup = Slab reinforcement $Asup := 1.9634 \cdot in^2$

Cracked Section

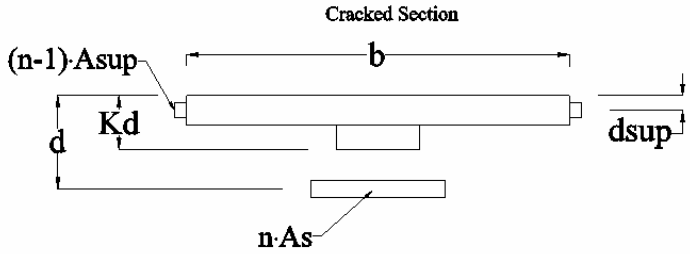

$d := 18.675 \cdot in$

$dsup := 3.25 \cdot in$

- Moments of Inertia

$n := \frac{Es}{Ec}$ $n = 6.856$

$C := \frac{bw}{n \cdot As}$ $C = 0.352 \frac{1}{in}$

$f := hf \cdot \frac{(b - bw)}{n \cdot As}$ $f = 13.735$

$yt := h - \left(\frac{1}{2}\right) \frac{\left[bw \cdot h^2 + (b - bw) \cdot hf^2\right]}{(b - bw) \cdot hf + bw \cdot h}$ $yt = 16.323\,in$

Ig = Gross Section Moment of Inertia

$$Ig := (b - bw)\cdot hf\cdot\left[\left(h - \frac{hf}{2}\right) - yt\right]^2 + bw\cdot h\cdot\left(yt - \frac{h}{2}\right)^2 + bw\cdot\frac{h^3}{12} + (b - bw)\cdot\frac{hf^3}{12}$$

$$Ig = 2.4 \times 10^4\,in^4$$

$$r := (n - 1)\cdot\frac{Asup}{n\cdot As} \qquad r = 0.337$$

$$kd := \frac{\sqrt{C\cdot(2\cdot d + hf\cdot f + 2\cdot r\cdot dsup) + (f + r + 1)^2} - (f + r + 1)}{C}$$

$$kd = 4.079\,in$$

Icr = Cracked Section Moment of Inertia

$$Icr = (b - bw)\cdot\frac{hf^3}{12} + bw\cdot\frac{kd^3}{3} + (b - bw)\cdot hf\cdot\left(kd - \frac{hf}{2}\right)^2 +$$

$$+ n\cdot As\cdot(d - kd)^2 + (n - 1)\cdot Asup\cdot(kd - dsup)^2$$

$$Icr = 9.508 \times 10^3\,in^4$$

- Maximum moment at beam number 2

Truck position

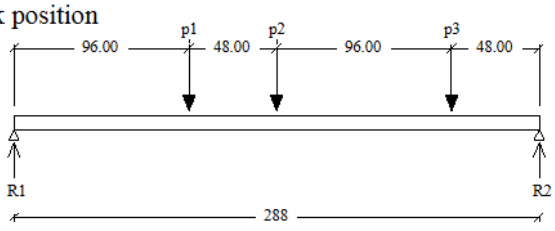

Moment law

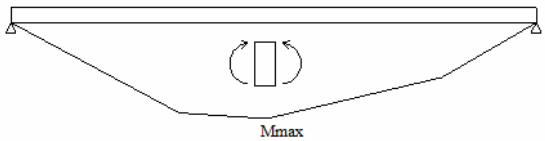

$p1 := 16000 \cdot lbf \qquad l := 288 \cdot in$

$p2 := 16000 \cdot lbf$

$p3 := 9000 \cdot lbf$

$kp := 0.30 \qquad kp = \text{Percentage of load carried by beam 2}$

$p1c := kp \cdot p1 \qquad p1c = 4.8 \times 10^3\ lbf$

$p2c := kp \cdot p2 \qquad p2c = 4.8 \times 10^3\ lbf$

$p3c := kp \cdot p3 \qquad p3c = 2.7 \times 10^3\ lbf$

$$R1 := \frac{(p1c \cdot 192 + p2c \cdot 144 + p3c \cdot 48)}{288} \qquad R1 = 6.05 \times 10^3\ lbf$$

$Mmax := R1 \cdot 144 \cdot in - p1c \cdot (144 \cdot in - 96 \cdot in) \qquad Mmax = 6.408 \times 10^5\ lbf \cdot in$

$$fr := 7.5 \cdot \left(\sqrt{fc}\right) \cdot \sqrt{\frac{lbf}{in^2}} \qquad fr = 556.215 \frac{lbf}{in^2}$$

$$Mcr := fr \cdot \frac{Ig}{yt} \qquad Mcr = 8.177 \times 10^5\ lbf \cdot in$$

$$Ie := \left(\frac{Mcr}{Mmax}\right)^3 \cdot Ig + \left[1 - \left(\frac{Mcr}{Mmax}\right)^3\right] \cdot Icr \qquad Ie = 3.961 \times 10^4\ in^4$$

$Ig = 2.4 \times 10^4\ in^4$

- Deflection computation

  As the moment applied (Mmax) is below the critical moment (Mcr), the concrete does not crack. Thus, gross section properties should be used in the computation of deflection. Following the elasticity theory, the deflections at a simple span beam, can be calculated from the following equations:

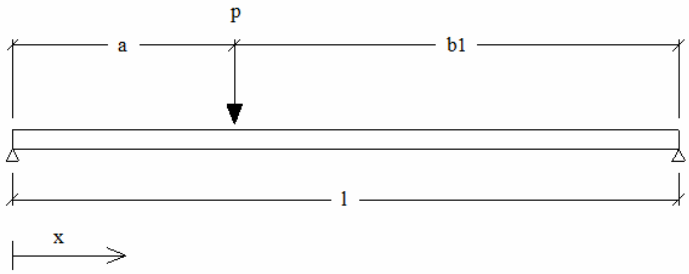

$$\text{Deflection } (x<a) = \frac{(p \cdot b1 \cdot x)}{6 \cdot Ec \cdot Ie \cdot l} \cdot \left(l^2 - b1^2 - x^2\right)$$

As $Ie \geq Ig$ then $Ie := Ig$

1. For p = p1c :

$b1 := 96 \cdot in \qquad x := \frac{l}{2}$

$$Deflection\_1 := \frac{(p1c \cdot b1 \cdot x)}{6 \cdot Ec \cdot Ie \cdot l} \cdot \left(l^2 - b1^2 - x^2\right) \qquad Deflection\_1 = 0.02\,in$$

2. For p = p2c :

$b2 := 144 \cdot in \qquad x := \frac{l}{2}$

$$Deflection\_2 := (p2c \cdot b2) \cdot x \cdot \frac{\left(l^2 - b2^2 - x^2\right)}{6 \cdot Ec \cdot Ie \cdot l} \qquad Deflection\_2 = 0.024\,in$$

3. For p = p3c :

$b3 := 48 \cdot in \qquad x := \frac{l}{2}$

$$Deflection\_3 := (p3c \cdot b3) \cdot x \cdot \frac{\left(l^2 - b3^2 - x^2\right)}{6 \cdot Ec \cdot Ie \cdot l} \qquad Deflection\_3 = 6.374 \times 10^{-3}\,in$$

Finally, adding all the different results for each load, the final deflection at midspan of the beam is:

$$Deflection\_final := (Deflection\_1 + Deflection\_2 + Deflection\_3)$$

$$Deflection\_final = 0.05\,in$$

Appendix D: Ultimate Moment Capacity

Section strengthened with two Sikawrap 103c sheets with Sikadur Hex 300 epoxy

Section properties:

$A_{s1} := 2.982\,in^2$ $A_{s2} := 1.988\,in^2$ $f_y := 29\ ksi$ $E_s := 29000\ ksi$ $f_{fu} := 104\ ksi$ $E_f := 9447\ ksi$

$d_1 := 19.875\ in$ $d_2 := 16.875\ in$ $d_f := 22.54\ in$

$t_f := 0.040\ in$ $b_f := 12\ in$ $A_f := t_f b_f 2$ $A_f = 0.96\ in^2$

$f_{cu} := 5.5$ $b := 84$ $\varepsilon_{cu} := 0.0028$

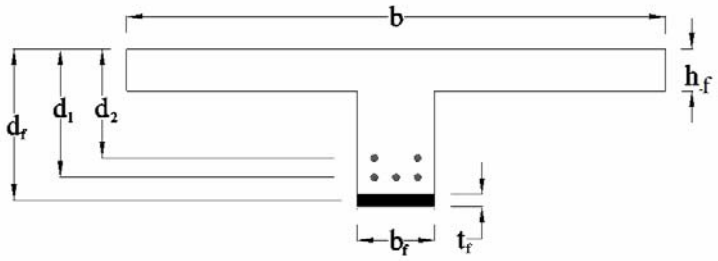

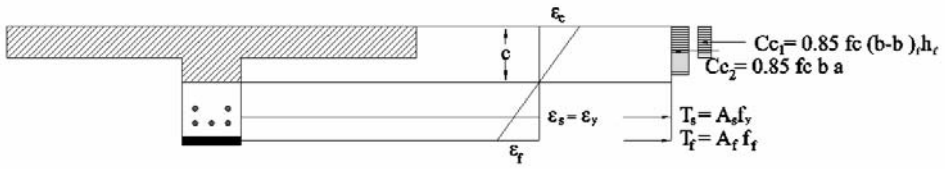

$$
\begin{aligned}
Q := \;& \varepsilon_c \leftarrow 0.00001 \\
& i \leftarrow 1 \\
& \text{while } \varepsilon_c \le 0.002 \\
& \quad \alpha \leftarrow -83333 \cdot \varepsilon_c^{\,2} + 500 \cdot \varepsilon_c \\
& \quad A \leftarrow \alpha \cdot b \cdot f_{cu} \\
& \quad B \leftarrow A_{s1} \cdot E_s \cdot \varepsilon_c + A_{s2} \cdot E_s \cdot \varepsilon_c + A_f E_f \varepsilon_c \\
& \quad C \leftarrow -\left(A_{s1} \cdot E_s \cdot \varepsilon_c \cdot d_1 + A_{s2} \cdot E_s \cdot \varepsilon_c \cdot d_2 + A_f E_f \varepsilon_c \cdot d_f\right) \\
& \quad c_1 \leftarrow \frac{-B + \sqrt{B^2 - 4C \cdot A}}{2A} \\
& \quad c_2 \leftarrow \frac{-B - \sqrt{B^2 - 4C \cdot A}}{2A} \\
& \quad c \leftarrow \begin{cases} c_1 & \text{if } c_1 \ge 0 \\ c_2 & \text{otherwise} \end{cases} \\
& \quad f_{s1} \leftarrow \varepsilon_c \cdot E_s \cdot \frac{d_1 - c}{c} \\
& \quad f_{s2} \leftarrow \varepsilon_c \cdot E_s \cdot \frac{d_2 - c}{c} \\
& \quad f_f \leftarrow \varepsilon_c \cdot E_f \frac{d_f - c}{c} \\
& \quad \gamma \leftarrow \frac{\left(\frac{1}{3} - 41.7 \cdot \varepsilon_c\right)}{1 - 166.7 \cdot \varepsilon_c} \\
& \quad M \leftarrow A_{s1} \cdot f_{s1} \cdot \left(d_1 - \gamma \cdot c\right) + A_{s2} \cdot f_{s2} \cdot \left(d_2 - \gamma \cdot c\right) + A_f f_f \left(d_f - \gamma \cdot c\right) \\
& \quad m_i \leftarrow A_{s1} \cdot f_{s1} \cdot \left(d_1 - \gamma \cdot c\right) + A_{s2} \cdot f_{s2} \cdot \left(d_2 - \gamma \cdot c\right) + A_f f_f \left(d_f - \gamma \cdot c\right) \\
& \quad \phi \leftarrow \frac{\varepsilon_c}{c} \\
& \quad \Phi_i \leftarrow \frac{\varepsilon_c}{c} \\
& \quad \varepsilon_c \leftarrow \varepsilon_c + 0.000001 \\
& \quad i \leftarrow i + 1 \\
& \quad \text{break if } f_{s1} \ge f_y
\end{aligned}
$$

$$\begin{pmatrix} f_{s1} \\ f_{s2} \\ f_f \\ M \\ \phi \\ \varepsilon_c \\ m \\ \Phi \\ c \end{pmatrix}$$

Values at first steel yield:

$f_{s1} := Q_1$ $\quad f_{s1} = 29.115 \quad ksi$

$f_{s2} := Q_2$ $\quad f_{s2} = 23.853 \quad ksi$

$f_f := Q_3$ $\quad f_f = 11.007 \quad ksi$

$M_y := \frac{Q_4}{12}$ $\quad M_y = 217.046 \quad ft - kip$

$\phi_y := Q_5$ $\quad \phi_y = 6.048 \times 10^{-5}$

$\varepsilon_c := Q_6$ $\quad \varepsilon_c = 1.99 \times 10^{-4}$

$c := Q_9$ $\quad c = 3.274$

$Q_u :=$ $\varepsilon_c \leftarrow Q_6 + 0.000001$

$i \leftarrow 1$

$\varepsilon_{s1} \leftarrow 0$

$\varepsilon_{s2} \leftarrow 0$

$f_{s1} \leftarrow 0$

$f_{s2} \leftarrow 0$

$f_f \leftarrow 0$

$M \leftarrow 0$

$\phi \leftarrow 0$

$\alpha \leftarrow 0$

$\gamma \leftarrow 0$

while $\varepsilon_c \le 0.002$

  while $f_{s2} < f_y$

    $\alpha \leftarrow -83333 \cdot \varepsilon_c^{\,2} + 500 \cdot \varepsilon_c$

    $A \leftarrow \alpha \cdot b \cdot f_{cu}$

    $B \leftarrow -\left(A_{s1} \cdot f_y - A_{s2} \cdot E_s \cdot \varepsilon_c - A_f E_f \varepsilon_c\right)$

    $C \leftarrow -\left(A_{s2} \cdot E_s \cdot \varepsilon_c \cdot d_2 + A_f E_f \varepsilon_c \cdot d_f\right)$

    $c_1 \leftarrow \dfrac{-B + \sqrt{B^2 - 4C \cdot A}}{2A}$

    $c_2 \leftarrow \dfrac{-B - \sqrt{B^2 - 4C \cdot A}}{2A}$

    $c \leftarrow \begin{cases} c_1 & \text{if } c_1 \ge 0 \\ c_2 & \text{otherwise} \end{cases}$

    $f_{s1} \leftarrow \varepsilon_c \cdot E_s \cdot \dfrac{d_1 - c}{c}$

    $f_{s2} \leftarrow \varepsilon_c \cdot E_s \cdot \dfrac{d_2 - c}{c}$

    $f_f \leftarrow \varepsilon_c \cdot E_f \dfrac{d_f - c}{c}$

    $\varepsilon_{s1} \leftarrow \varepsilon_c \cdot \dfrac{d_1 - c}{c}$

$$\varepsilon_{s2} \leftarrow \varepsilon_c \cdot \frac{d_2 - c}{c}$$

$$n_{i,1} \leftarrow f_f$$

$$n_{i,2} \leftarrow f_{s2}$$

$$\gamma \leftarrow \frac{\left(\frac{1}{3} - 41.7 \cdot \varepsilon_c\right)}{1 - 166.7 \cdot \varepsilon_c}$$

$$M \leftarrow A_{s1} \cdot f_y \cdot \left(d_1 - \gamma \cdot c\right) + A_{s2} \cdot f_{s2} \cdot \left(d_2 - \gamma \cdot c\right) + A_f f_f \left(d_f - \gamma \cdot c\right)$$

$$m_i \leftarrow A_{s1} \cdot f_y \cdot \left(d_1 - \gamma \cdot c\right) + A_{s2} \cdot f_{s2} \cdot \left(d_2 - \gamma \cdot c\right) + A_f f_f \left(d_f - \gamma \cdot c\right)$$

$$\phi \leftarrow \frac{\varepsilon_c}{c}$$

$$\Phi_i \leftarrow \frac{\varepsilon_c}{c}$$

break if $\varepsilon_{s1} \geq 0.005$

$$i \leftarrow i + 1$$

$$\varepsilon_c \leftarrow \varepsilon_c + 0.000001$$

while $f_f \leq f_{fu}$

$$\alpha \leftarrow -83333 \cdot \varepsilon_c^{\,2} + 500 \cdot \varepsilon_c$$

$$A \leftarrow \alpha \cdot b \cdot f_{cu}$$

$$B \leftarrow -\left(A_{s1} \cdot f_y + A_{s2} \cdot f_y - A_f E_f \varepsilon_c\right)$$

$$C \leftarrow -\left(A_f E_f \varepsilon_c \cdot d_f\right)$$

$$c_1 \leftarrow \frac{-B + \sqrt{B^2 - 4C \cdot A}}{2A}$$

$$c_2 \leftarrow \frac{-B - \sqrt{B^2 - 4C \cdot A}}{2A}$$

$$c \leftarrow \begin{cases} c_1 & \text{if } c_1 \geq 0 \\ c_2 & \text{otherwise} \end{cases}$$

$$f_{s1} \leftarrow \varepsilon_c \cdot E_s \cdot \frac{d_1 - c}{c}$$

$$f_{s2} \leftarrow \varepsilon_c \cdot E_s \cdot \frac{d_2 - c}{c}$$

$$d_f - c$$

$$f_f \leftarrow \varepsilon_c \cdot E_f \frac{\quad}{c}$$

$$\varepsilon_{s1} \leftarrow \varepsilon_c \cdot \frac{d_1 - c}{c}$$

$$\varepsilon_{s2} \leftarrow \varepsilon_c \cdot \frac{d_2 - c}{c}$$

$$\varepsilon_f \leftarrow \varepsilon_c \cdot \frac{d_f - c}{c}$$

$$k_i \leftarrow f_{s2}$$

$$\gamma \leftarrow \frac{\left(\frac{1}{3} - 41.7 \cdot \varepsilon_c\right)}{1 - 166.7 \cdot \varepsilon_c}$$

$$M \leftarrow A_{s1} \cdot f_y \cdot \left(d_1 - \gamma \cdot c\right) + A_{s2} \cdot f_y \cdot \left(d_2 - \gamma \cdot c\right) + A_f f_f \left(d_f - \gamma \cdot c\right)$$

$$m_i \leftarrow A_{s1} \cdot f_y \cdot \left(d_1 - \gamma \cdot c\right) + A_{s2} \cdot f_y \cdot \left(d_2 - \gamma \cdot c\right) + A_f f_f \left(d_f - \gamma \cdot c\right)$$

$$\phi \leftarrow \frac{\varepsilon_c}{c}$$

$$\Phi_i \leftarrow \frac{\varepsilon_c}{c}$$

break if $\varepsilon_{s1} \geq 0.005$

$$\varepsilon_c \leftarrow \varepsilon_c + 0.000001$$

$$i \leftarrow i + 1$$

break if $\varepsilon_{s1} \geq 0.005$

break if $f_f \geq f_{fu}$

$$\begin{pmatrix} \varepsilon_{s1} \\ \varepsilon_{s2} \\ \varepsilon_f \\ f_f \\ M \\ \phi \\ c \\ m \\ \Phi \\ \varepsilon_c \end{pmatrix}$$

Values at failure:

$\varepsilon_{s1} := Q_{u_1}$ $\quad \varepsilon_{s1} = 5 \times 10^{-3}$

$\varepsilon_{s2} := Q_{u_2}$ $\quad \varepsilon_{s2} = 4.169 \times 10^{-3}$

$\varepsilon_f := Q_{u_3}$ $\quad \varepsilon_f = 5.739 \times 10^{-3}$

$f_f := Q_{u_4}$ $\quad f_f = 54.215$ ksi

$M_u := \frac{Q_{u_5}}{12}$ $\quad M_u = 311.863$ ft – kip

$\phi_u := Q_{u_6}$ $\quad \phi_u = 2.771 \times 10^{-4}$

$\varepsilon_c := Q_{u_{10}}$ $\quad \varepsilon_c = 5.07 \times 10^{-4}$

$c := Q_{u_7}$ $\quad c = 3.274$

Ultimate moment (M_u):

$M_u := Q_{u_5}$ $\quad M_u = 3.742 \times 10^3$ kip·in

Contributions from the different materials in the ultimate moment:

- Reinforcing Steel :

$Ms := A_{s1} \cdot f_y \cdot (d_1 - c) + A_{s2} \cdot f_y \cdot (d_2 - c)$ $\quad Ms = 2.428 \times 10^3$ kip·in

- FRP strips :

$Mf := A_f f_f (d_f - c)$ $\quad Mf = 1.078 \times 10^3$ kip·in

- Concrete :

$Mc := 0.85\varepsilon_c \cdot Ec \cdot c \cdot b \cdot c$ $\quad Mc = 240.039$ kip·in

$Mtot := Ms + Mf + Mc$ $\quad Mtot = 3.746 \times 10^3$ kip·in

Appendix E: Loading Scenarios

Type 3 truck load

Case A

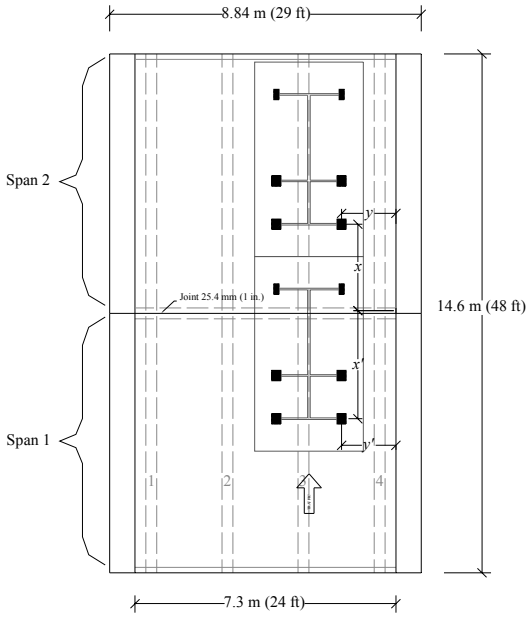

Case B

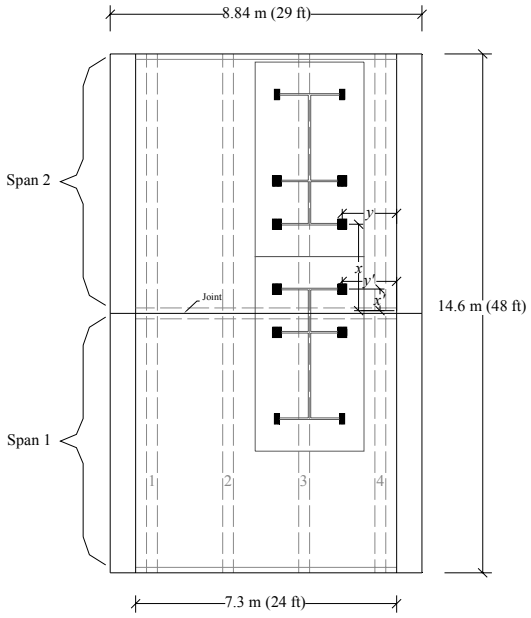

Case C

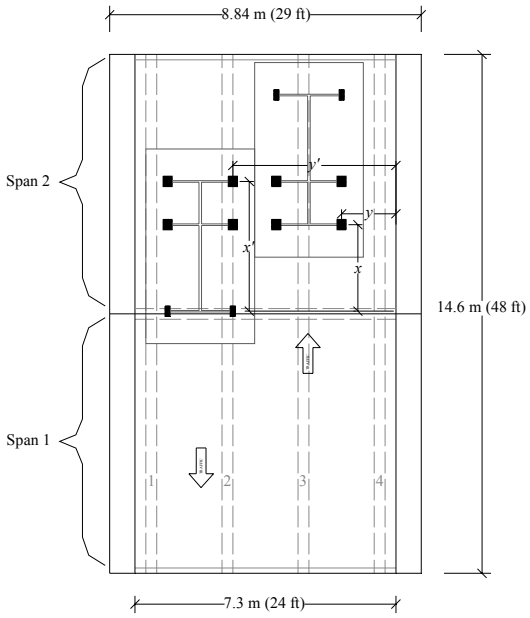

Case D

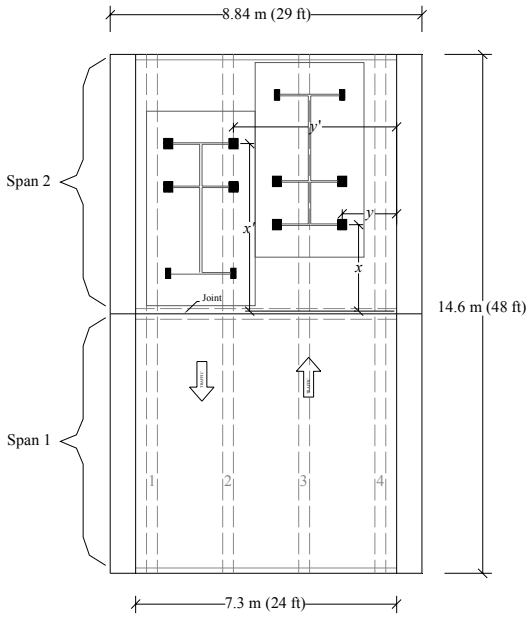

H20-44 truck load

Case A

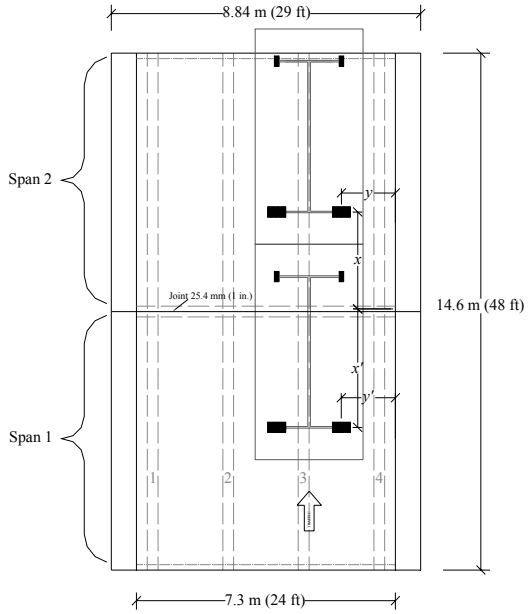

Case B

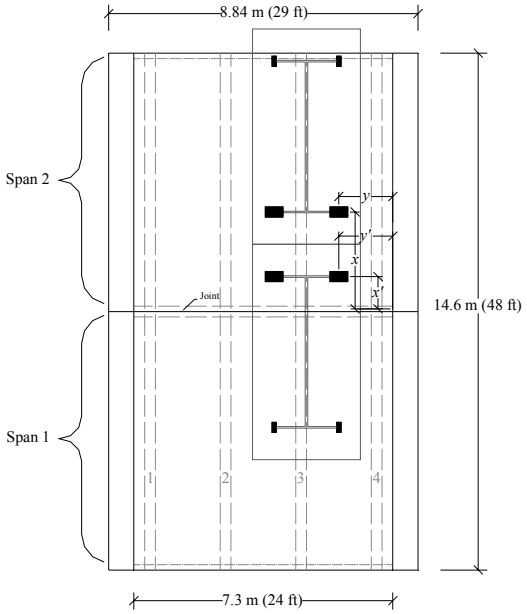

Case C

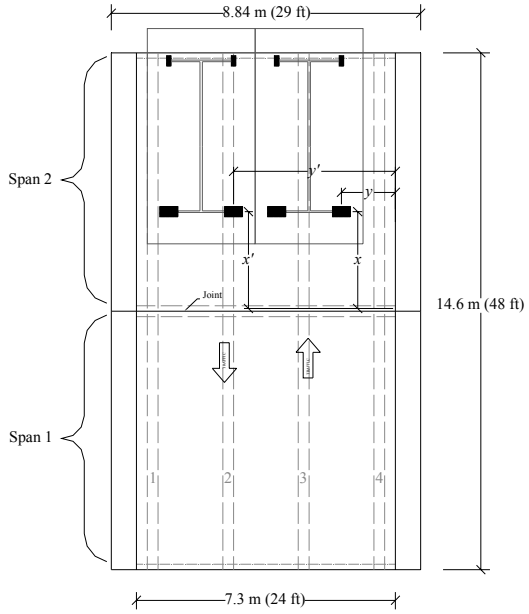

Case D

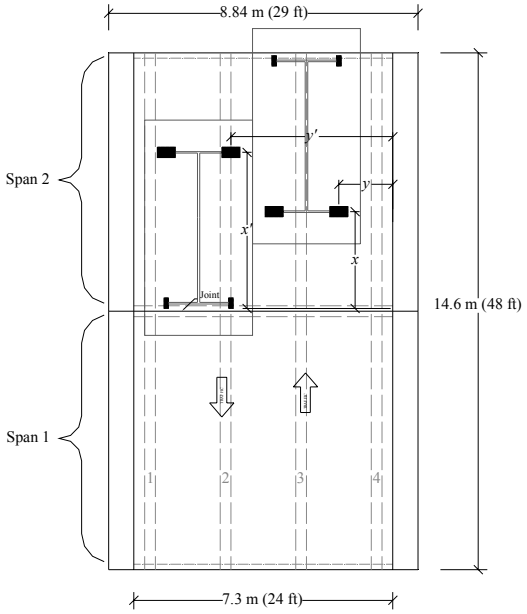

Case E

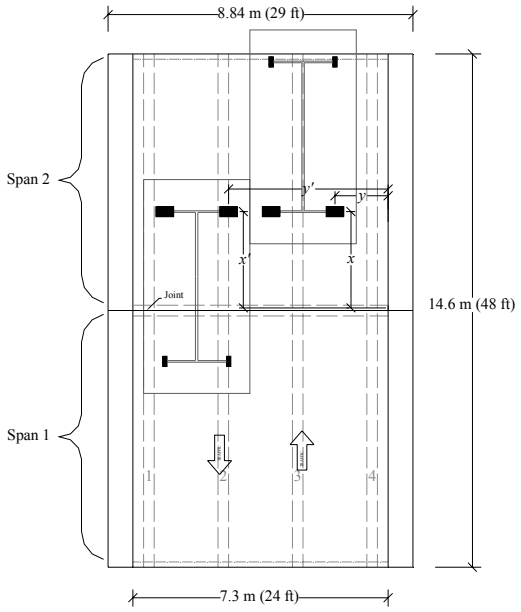

Table E.1 Load positions for Type 3 truck loads.

Type 3 Truck	Position 1st Truck		Position 2nd Truck	
	x m (in.)	*y* m (in.)	*x'* m (in.)	*y'* m (in.)
Case A	2.440 (96)	1.524 (60.00)	3.048 (120.00)	1.524 (60.00)
Case B	2.440 (96)	1.524 (60.00)	0.610 (24.00)	1.524 (60.00)
Case C	2.440 (96)	1.524 (60.00)	4.724 (186.00)	4.572 (180.00)
Case D	2.440 (96)	1.524 (60.00)	3.658 (144.00)	4.572 (180.00)

Table E.2 Load positions for H20-44 truck loads.

H20-44 Truck	Position 1st Truck		Position 2nd Truck	
	x m (in.)	*y* m (in.)	*x'* m (in.)	*y'* m (in.)
Case A	2.743 (108)	1.524 (60.00)	3.354 (132.05)	1.524 (60.00)
Case B	2.743 (108)	1.524 (60.00)	0.914 (36.00)	1.524 (60.00)
Case C	2.743 (108)	1.524 (60.00)	2.743 (108.00)	4.572 (180.00)
Case D	2.743 (108)	1.524 (60.00)	4.419 (174.00)	4.572 (180.00)
Case E	2.743 (108)	1.524 (60.00)	2.743 (108.00)	4.572 (180.00)

Appendix F: Load Posting

- Superimposed Dead loads

$l := 288 \cdot in$

$A1 := 72 \cdot in^2$

$A2 := 60 \cdot in^2$

$A3 := 108 \cdot in^2$

$A4 := 152.5 \cdot in^2$

$A5 := 69 \cdot in^2$

$A6 := 7.5 \cdot in^2$

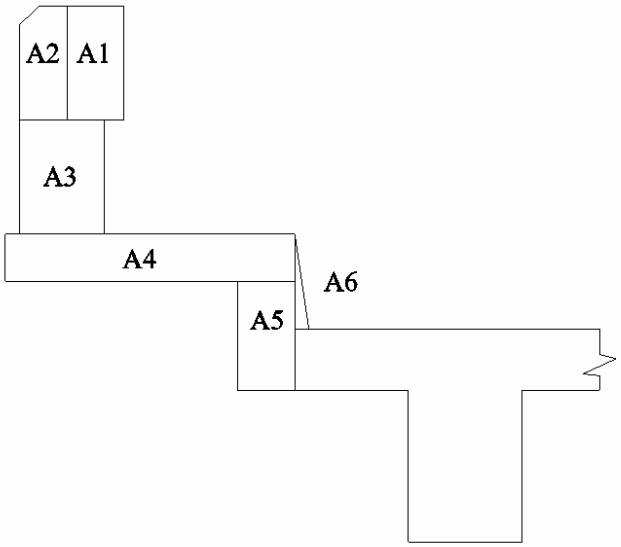

$wc := 0.083 \cdot \frac{lbf}{in^3}$ Weight of concrete = wc

- Weigth per post

$wp := (A2 + A3) \cdot 12 \cdot in \cdot wc$ $wp = 167.33\ lbf$

wpt = Load of the posts distruibuted alonf the span

$wpt := 4 \cdot \frac{wp}{l}$ $wpt = 2.32 \frac{lbf}{in}$

- Weigth of concrete railing

$wr := (A1 + A4 + A5 + A6) \cdot wc$ $wr = 24.98 \frac{lbf}{in}$

- Weigth of concrete railing and posts distributed through the width of the roadway (distributed to all the girders)

n = number of girders $n := 4$

$wrt := 2 \frac{(wr + wpt)}{n}$ $wrt = 13.65 \frac{lbf}{in}$

- Weigth of asphalt

$th := 5 \cdot in$ th = thickness of the asphalt layer

$wa := 0.0833 \cdot \frac{lbf}{in^3}$ wa = weight of asphalt

$wat := (th \cdot wa) \cdot 84in$ $wat = 34.99 \frac{lbf}{in}$

- Total superimposed dead load

$wsdl := wat + wrt$ $wsdl = 48.64 \frac{lbf}{in}$

- Dead load of member

$At := 738 \cdot in^2$

$wgdl := At \cdot wc$ $wgdl = 61.25 \frac{lbf}{in}$

- Total dead load

$wdl := wsdl + wgdl$ $wdl = 109.89 \frac{lbf}{in}$

- Dead load moment

$Mdl := \frac{wdl \cdot l^2}{8}$ Mdl = Dead load momemt

$Mdl = 1139375.808\, lbf \cdot in$

- Ultimate moment capacity

The calculations for the ultimate moment capacity are shown in Appendix D

$Mu := 3742355.388 \cdot lbf \cdot in$

- Impact

$I := \frac{50}{\frac{l}{12 \cdot in} + 125}$ $I = 0.34$ $I \le 0.3$

$I := 0.3$

- Live loads
  - Inventory H15 truck load:

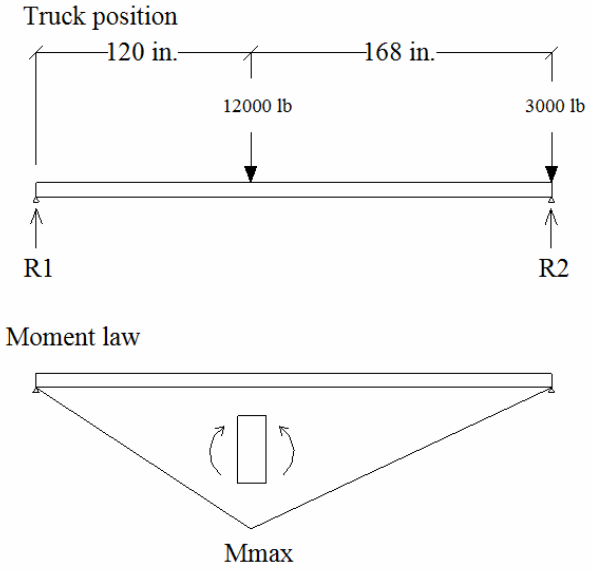

$p1 := 12000 \cdot lbf$ $l := 288 \cdot in$

$p2 := 3000 \cdot lbf$

$R1 := \frac{(p1 \cdot 168)}{288}$ $R1 = 7000\,lbf$

$R2 := p1 + p2 - R1$ $R2 = 8000\,lbf$

$Mmax := R1 \cdot 120 \cdot in$ $Mmax = 840000\,lbf \cdot in$

$Mll := Mmax$ $Mll = 840000\,lbf \cdot in$

$RFinv := \frac{\left(\frac{3}{5}\right) \cdot \left[\left(\frac{Mu}{1.3}\right) - Mdl\right]}{Mll \cdot (1 + I)}$ RFinv = Inventory Rating Factor

$RFinv = 0.96$

$IR := RFinv \cdot 15$ IR = Inventory rating

$IR = 14.34$

$IR := 14$ Decimal portion is truncated

Inventory = 114

- Operating H20-44 truck load

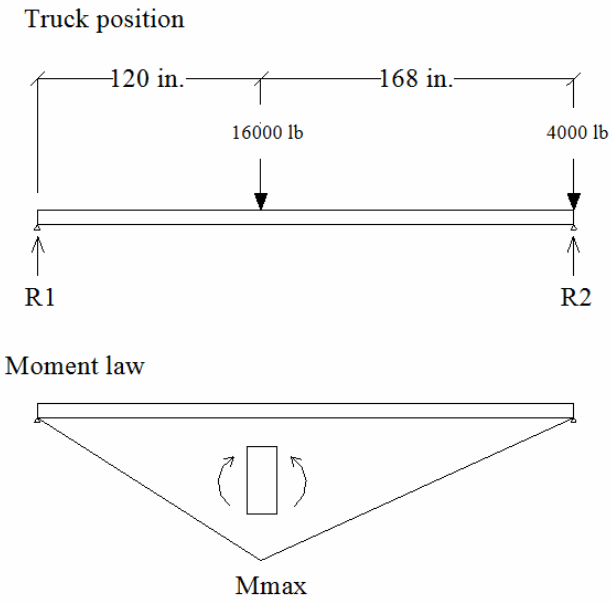

$p1 := 16000 \cdot lbf$

$p2 := 4000 \cdot lbf$

$R1 := \frac{(p1 \cdot 168)}{288}$ $\quad R1 = 9333.33\,lbf$

$R2 := p1 + p2 - R1$ $\quad R2 = 10666.67\,lbf$

$Mmax := R1 \cdot 120 \cdot in$ $\quad Mmax = 1120000\,lbf \cdot in$

$Mll := Mmax$ $\quad Mll = 1120000\,lbf \cdot in$

$RFopr := \frac{\left(\frac{Mu}{1.3}\right) - Mdl}{Mll \cdot (1 + I)}$ $\quad RFopr$ = Operating Rating Factor

$RFopr = 1.19$

$OR := RFopr \cdot 20$ $\quad OR$ = Operating rating

$OR = 23.89$

$OR := 23$ $\quad$ Decimal portion is truncated

Operating = 123 $\quad$ The digit 1 is added in front of the rating value

- Posting Type 3 truck load

Truck position

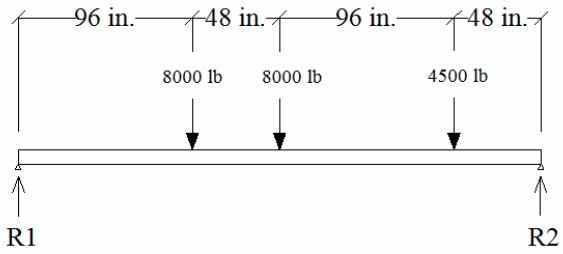

Moment law

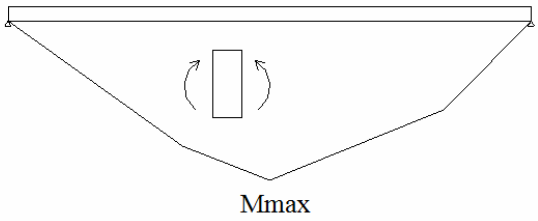

$p1 := 8000 \cdot lbf$

$p2 := 8000 \cdot lbf$

$p3 := 4500 \cdot lbf$

$R1 := \frac{(p1 \cdot 192 + p2 \cdot 144 + p3 \cdot 48)}{288}$ $\quad R1 = 10083.33\,lbf$

$R2 := p1 + p2 + p3 - R1$ $\quad R2 = 10416.67\,lbf$

$Mmax := R1 \cdot 144 \cdot in - p1 \cdot (144 \cdot in - 96 \cdot in)$ $\quad Mmax = 1068000\,lbf \cdot in$

$Mll := Mmax$ $\quad Mll = 1068000\,lbf \cdot in$

$RFopr := \frac{\left(\frac{Mu}{1.3}\right) - Mdl}{Mll \cdot (1 + I)}$ $\quad$ RFopr = Operating Rating Factor

$RFopr = 1.25$

$PR := RFopr \cdot 20.5$ $\quad$ PR = Posting rating

$PR = 25.68$

$PR := 25$ $\quad$ Decimal portion is truncated

Posting = 425 $\quad$ The digit 4 is added in front of the rating value

Appendix G: Check of Shear Capacity

- Superimposed Dead loads

$l := 288 \cdot in$

$A1 := 72 \cdot in^2$

$A2 := 60 \cdot in^2$

$A3 := 108 \cdot in^2$

$A4 := 152.5 \cdot in^2$

$A5 := 69 \cdot in^2$

$A6 := 7.5 \cdot in^2$

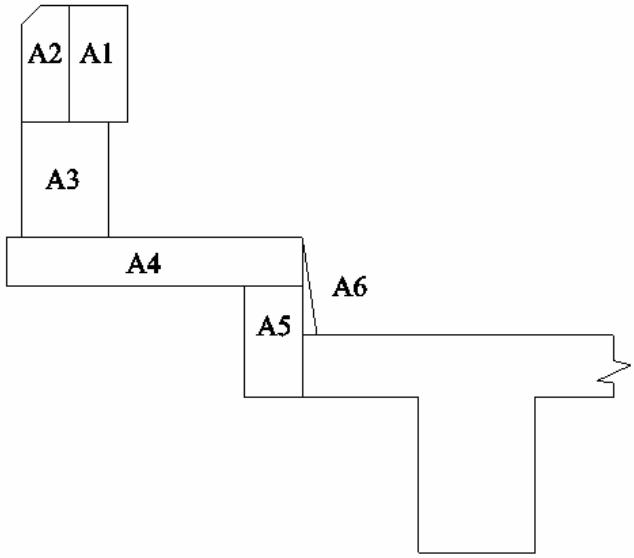

$wc := 0.083 \cdot \frac{lbf}{in^3}$ Weight of concrete = wc

- Weigth per post

$wp := (A2 + A3) \cdot 12 \cdot in \cdot wc$ $wp = 167.33\,lbf$

wpt = Load of the posts distruibuted alonf the span

$wpt := 4 \cdot \frac{wp}{l}$ $wpt = 2.32 \frac{lbf}{in}$

- Weigth of concrete railing

$wr := (A1 + A4 + A5 + A6) \cdot wc$ $wr = 24.98 \frac{lbf}{in}$

- Weigth of concrete railing and posts distributed through the width of the roadway (distributed to all the girders)

n = number of girders $n := 4$

$wrt := 2 \frac{(wr + wpt)}{n}$ $wrt = 13.65 \frac{lbf}{in}$

- Weigth of asphalt

$th := 5 \cdot in$ th = thickness of the asphalt layer

$wa := 0.0833 \cdot \frac{lbf}{in^3}$ wa = weight of asphalt

$wat := (th \cdot wa) \cdot 84in$ $wat = 34.99 \frac{lbf}{in}$

- Total superimposed dead load

$wsdl := wat + wrt$ $wsdl = 48.64 \frac{lbf}{in}$

- Dead load of member

$At := 738 \cdot in^2$

$wgdl := At \cdot wc$ $wgdl = 61.25 \frac{lbf}{in}$

- Total dead load

$wdl := wsdl + wgdl$ $wdl = 109.89 \frac{lbf}{in}$

- Shear law

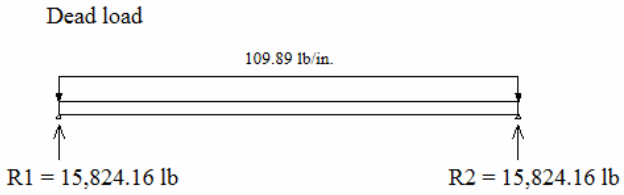

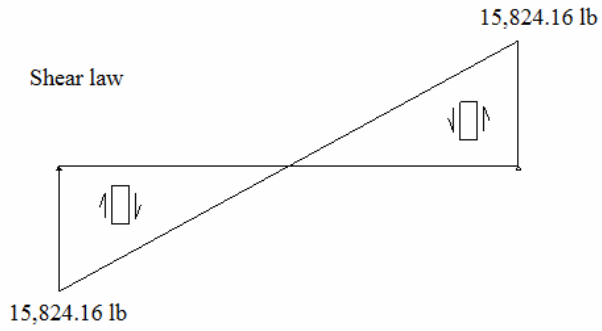

$R1 := \frac{wdl \cdot l}{2}$ $R1 = 15824.66\,lbf$

- Live loads
  - H20-44 truck load

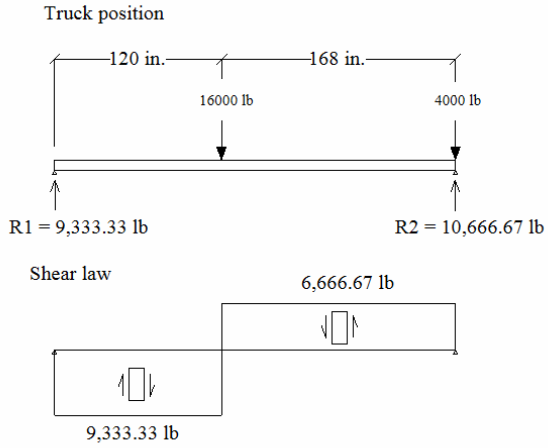

$p1 := 16000 \cdot lbf \qquad R1 := \frac{(p1 \cdot 168)}{288} \qquad R1 = 15824.66 lbf$

$p2 := 4000 \cdot lbf \qquad R2 := p1 + p2 - R1 \qquad R2 = 10666.67 lbf$

- Type 3 truck load

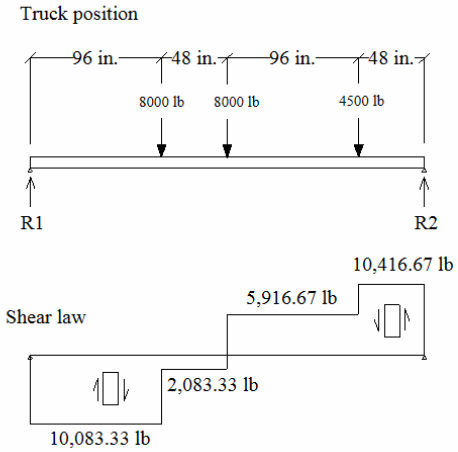

$p1 := 8000 \cdot lbf$

$p2 := 8000 \cdot lbf$

$p3 := 4500 \cdot lbf$

$R1 := \frac{(p1 \cdot 192 + p2 \cdot 144 + p3 \cdot 48)}{288} \qquad R1 = 10083.33 lbf$

$R2 := p1 + p2 + p3 - R1 \qquad R2 = 10416.67 lbf$

To compute the maximum shear force in the beam, the shear law from the dead loac and the shear law from the live load should be summarized:

- Dead load shear law + H20-44 shear law

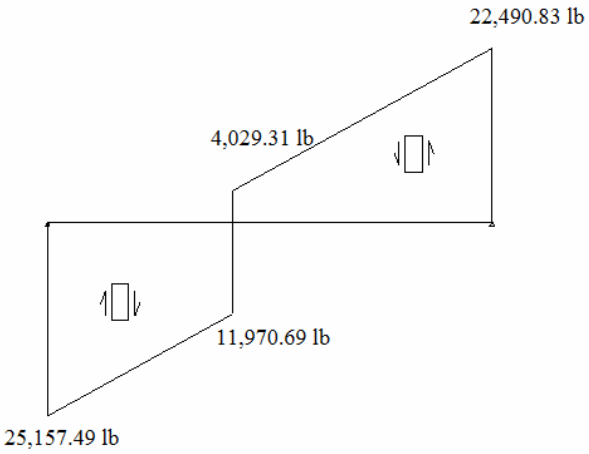

- Dead load shear law + Type 3 shear law

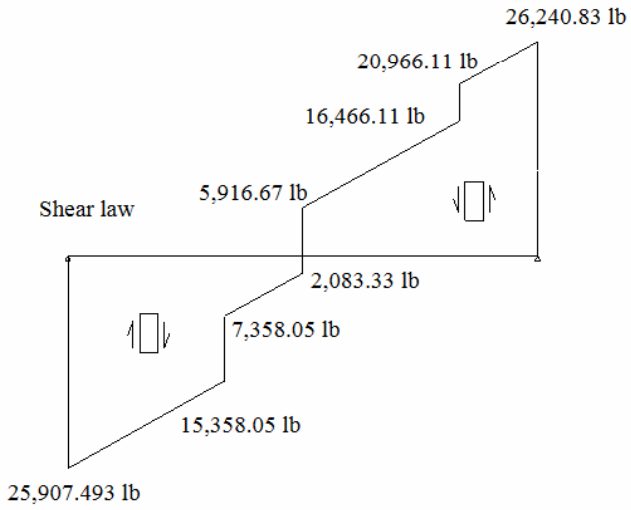

The maximum shear force is 26,240.83 lb when the Type 3 is the load applied. This value shoud be less than ϕ*Vn , (ϕ = reduction factor):

$V_u := 26240.83 \cdot lbf$

$V_n := V_c + V_s$

$Vu < \phi * Vn$

$\phi := 0.75$

Vu = Maximum shear force

Vc = Shear carried by the concrete

Vs = Shear carried by the stirrups

$b_w := 12\ in$

$h := 22.5\ in$

$f'_c := 5500\ \frac{lbf}{in^2}$

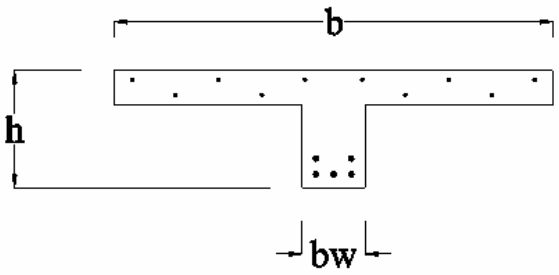

$V_c := 2 \cdot \sqrt{f'_c} \cdot b_w \cdot h$ $\qquad V_c = 40047.47\ lbf$

$V_{check} := \phi \cdot V_c$ $\qquad V_{check} = 30035.6\ lbf$

As Vu = 26,240.83 lb is less than Vcheck, it is not necessary to chec the shear capacity of the steel, because the concrete shear capacity is enough for the truck load